

7/1/13

Magnetospheric Science Objectives of the *Juno* Mission

1
2
3
4
5
6
7
8
9
10
11
12
13
14
15
16
17
18
19
20
21

F. Bagenal¹, A. Adriani², F. Allegrini^{3,13}, S. J. Bolton³, B. Bonfond⁴, E. J. Bunce⁵, J.E.P. Connerney⁶, S. W. H. Cowley⁵, R. W. Ebert³, G. R. Gladstone³, C. J. Hansen⁷, W. S. Kurth⁸, S. M. Levin⁹, B. H. Mauk¹⁰, D. J. McComas^{3,13}, C. P. Paranicas¹⁰, D. Santos-Costas³, R. M. Thorne¹¹, P. Valek^{3,13}, J. H. Waite³, P. Zarka¹²

- 1 – University of Colorado, Boulder, CO
- 2 – INAF-IAPS, Rome Italy
- 3 – Southwest Research Institute, San Antonio, TX
- 4 – Laboratory for Planetary and Atmospheric Physics, University of Liège, Belgium
- 5 – University of Leicester, UK
- 6 – Goddard Space Flight Center, Greenbelt, MD
- 7 – Planetary Science Institute, Tucson, AZ
- 8 – University of Iowa, Iowa City, IA
- 9 – Jet Propulsion Lab, Pasadena, CA
- 10 – Applied Physics Lab., The Johns Hopkins University, Laurel, MD
- 11 – Atmospheric Sciences, UCLA, Los Angeles, CA
- 12 – Observatoire de Paris, CNRS-LEISA, 92190 Meudon, France
- 13 – University of Texas, San Antonio, TX 78249

Abstract

22
23

24 In July 2016, NASA's *Juno* mission becomes the first spacecraft to enter polar orbit of
25 Jupiter and venture deep into unexplored polar territories of the magnetosphere. Focusing
26 on these polar regions, we review current understanding of the structure and dynamics of
27 the magnetosphere and summarize the outstanding issues. The *Juno* mission profile
28 involves (a) a several-week approach from the dawn side of Jupiter's magnetosphere, with
29 an orbit-insertion maneuver on July 6, 2016; (b) a 107-day capture orbit, also on the dawn
30 flank; and (c) a series of thirty 11-day science orbits with the spacecraft flying over
31 Jupiter's poles and ducking under the radiation belts. We show how *Juno's* view of the
32 magnetosphere evolves over the year of science orbits. The *Juno* spacecraft carries a range
33 of instruments that take particles and fields measurements, remote sensing observations of
34 auroral emissions at UV, visible, IR and radio wavelengths, and detect microwave emission
35 from Jupiter's radiation belts. We summarize how these *Juno* measurements address issues
36 of auroral processes, microphysical plasma physics, ionosphere-magnetosphere and
37 satellite-magnetosphere coupling, sources and sinks of plasma, the radiation belts, and the
38 dynamics of the outer magnetosphere. To reach Jupiter, the *Juno* spacecraft passes close to
39 the Earth on October 9, 2013, gaining the necessary gravity assist. The Earth flyby is an
40 opportunity to test *Juno's* instrumentation as well as take scientific data in the terrestrial
41 magnetosphere, in conjunction with ground-based and Earth-orbiting assets.

42

1. Introduction

43

1.1 OVERVIEW

44
45

46 The vast and complicated magnetosphere of Jupiter was first detected in 1954, before Van
47 Allen's *Explorer 1* discovery of the Earth's radiation belts, via bursts of radio emission at
48 decameter wavelengths (Burke & Franklin 1955). Subsequent radio observations at
49 decimeter wavelengths revealed synchrotron emission from trapped electrons (Field 1959;
50 Drake and Hvatum 1959). These early radio measurements showed that Jupiter has a
51 strong magnetic field (opposite in polarity to the Earth's) tilted about 10° from the spin axis
52 and that energetic ($>MeV$) electrons are trapped near the equator close to the planet (see

53 for example review by Carr et al. 1983). These very energetic particles pose a formidable
54 hazard for spacecraft exploring Jupiter's inner magnetosphere.

55 The peculiar role of Io was first pointed out in the observations by Bigg (1964) that
56 bursts of radio emission were modulated by the position of the moon along its orbit around
57 Jupiter. The magnetometers and particle detectors on *Pioneer 10* (1973) and *Pioneer 11*
58 (1974) exposed the vastness of Jupiter's magnetosphere and made in situ measurements of
59 energetic ions and electrons. The *Voyager 1* fly-by in 1979 revealed Io's prodigious volcanic
60 activity, thus explaining why this innermost Galilean moon plays such a strong role. Key
61 information about the Io plasma torus and Io-induced aurora came from a variety of Earth-
62 and space-based telescopes at wavelengths across the spectrum. Additional data came from
63 subsequent traversals of Jupiter's magnetosphere by the *Ulysses* (1992), *Cassini* (2000) and
64 *New Horizons* (2007) spacecraft, but it was the 33 orbits of *Galileo* (1995–2003) around
65 Jupiter that mapped out the equatorial magnetospheric structures and monitored their
66 temporal variability.

67 Jupiter's strong magnetic field makes the magnetosphere of Jupiter the largest
68 object within the heliosphere (**Figure 1**), stretching in the direction towards the Sun for
69 typical distances of 65-100 R_J (the radius of Jupiter, $R_J = 71492$ at the 1 bar level, see the
70 Appendix). Over a ton/second of Io's SO_2 atmosphere escapes the satellite. The escaping
71 neutrals are dissociated, ionized and trapped by the magnetic field. The resulting dense
72 (~ 2000 particles/cm³) torus of plasma, roughly corotates with Jupiter's ~ 10 hour spin
73 period. The ions of sulfur and oxygen ($T_i \sim 100$ eV) are excited by the ~ 5 eV thermal
74 electrons and radiate ~ 1.5 terawatts of UV emission. Rather than cooling on expansion, the
75 iogenic plasma is heated (by an as-yet-unknown process) to temperatures of ~ 10 s keV as it
76 is transported radially outwards (via flux tube interchange motions) on timescales of
77 weeks. Coupling of the magnetospheric plasma to Jupiter's rotating atmosphere dominates
78 the dynamics of the magnetosphere, the ensuing strong centrifugal forces producing an
79 extended, equatorially-confined plasmadisk. Associated with the electrical currents that
80 couple the magnetospheric and ionospheric plasmas are intense auroral emissions that
81 span the spectrum from X-rays to radio. The hot plasma in Jupiter's plasmadisk inflates the
82 magnetosphere, making it larger and more compressible than a magnetic dipole alone.
83 While the vast magnetosphere presents a substantial obstacle to the solar wind, the nature

84 of the interaction between the solar wind and magnetospheric plasma remains an issue of
85 debate.

86 **Figure 2** shows some current ideas of the global structure and dynamics of the
87 magnetosphere comprising: a rotation-dominated inner/middle plasmadisk, magnetic
88 coupling to Jupiter's atmosphere/ionosphere, slow diffusive radial transport, a sporadic x-
89 line across the magnetotail, plasmoids ejected down the tail and interaction regions in
90 boundary layers on the flanks. While the equatorial plane has been traversed multiple times and
91 is well mapped, the polar region has barely been explored and major questions remain.

92 The pre-*Galileo* understanding is presented in Dessler (1983)'s book *Physics of the*
93 *Jovian Magnetosphere* and the advances made by the *Ulysses* and *Galileo* missions are reviewed
94 in seven chapters of *Jupiter: The Planet, Satellites and Magnetosphere* (edited by Bagenal,
95 Dowling and McKinnon 2004). In this paper we summarize the current understanding of
96 Jupiter's magnetosphere, the outstanding issues and the methods *Juno* employs to address them.
97 An overview of the whole *Juno* mission is provided by Bolton et al. (*this issue*). The *Juno*
98 instruments that make in situ magnetospheric measurements are the magnetometer MAG
99 (Connerney et al. *this issue*), the electric and magnetic wave detectors Waves (Kurth et al. *this*
100 *issue*), the electron and ion detectors JADE (McComas et al. *this issue*), and the energetic
101 particle detectors JEDI (Mauk et al. *this issue*). Remote sensing measurements of the aurora are
102 carried out at UV wavelegths by UVS (Gladstone et al. *this issue*), in the IR by JIRAM (Adriani
103 et al. *this issue*) and at visible wavelengths by *JunoCam* (Hansen et al. *this issue*). Emissions
104 from the radiation belts are detected via emissions in the microwave region of the spectrum by
105 the MWR instrument (Janssen et al. *this issue*).

106

107 1.2 COMPARATIVE MAGNETOSPHERES

108

109 Reviews of planetary magnetospheres range in their approach to the subject from considering it a
110 topic in space plasma physics (exploiting the breadth of planetary environments as a laboratory
111 to explore space plasmas) to a branch of planetary science (presenting the space environment as
112 a component of planetary objects). Basic, qualitative introductions are given by Van Allen &
113 Bagenal (1999) and by Kivelson & Bagenal (2007). Deeper studies of comparative

114 magnetospheres span from the abstract to the specific (Siscoe 1979; Vasyliunas 2004, 2009;
 115 Kivelson 2007; Walker & Russell 1995; Bagenal 1992; Russell 2004, 2006; Bagenal 2009).

116 The interaction between a planetary object and the surrounding plasma depends on the
 117 properties of both the object and the plasma flow in which it is embedded. A planet with a
 118 significant internal magnetic field forms a magnetosphere that extends the planet's influence
 119 beyond its surface or cloud tops. The interaction of the supersonic solar wind with a planetary
 120 magnetic field (either generated by an internal dynamo or induced externally) produces a bow
 121 shock (BS) upstream of the planet. Behind the bow shock, the slowed, heated magnetosheath
 122 plasma is deflected around the magnetospheric obstacle. The magnetospheric boundary – the
 123 magnetopause (MP) – was usually regarded to first order as an impenetrable boundary. However,
 124 the amount of mass, momentum and magnetic flux exchanged across the magnetopause is an
 125 active area of research at Earth and other planets. The distance between the center of the planet
 126 and the magnetopause in the direction of the Sun, R_{MP} , is generally determined by a balance
 127 between the ram pressure of the solar wind and the internal pressure of the magnetosphere
 128 (combining both magnetic and plasma pressures). Whatever the details of the interaction, in all
 129 explored cases there is a “wake” or “tail” – the magnetotail – that can extend at least several
 130 hundred times R_{MP} downstream in the solar wind.

131 **Figure 3** illustrates the huge range in scale of planetary magnetospheres. The
 132 magnetospheres of the giant planets encompass most of their extensive moon systems, including
 133 the four Galilean moons of Jupiter, many icy satellites (importantly Enceladus), and Titan at
 134 Saturn. Earth's Moon, however, resides almost entirely outside the magnetosphere, spending less
 135 than 5% of its orbit crossing the magnetotail. The R_{MP} of Earth is about $10 R_E$ which is only a
 136 little larger than the radius of the planet Saturn. The R_{MP} of Saturn is about $20 R_S$ which is about
 137 $17 R_J$, a modest fraction of Jupiter's magnetopause distance (R_{MP} of Jupiter ranges between
 138 typical scales of 63 and $92 R_J$).

139 **Table 1** lists the basic parameters characterizing the magnetospheres of Earth, Jupiter,
 140 and Saturn. The classical scale of a planet's magnetosphere, R_{CF} , as derived by Chapman and
 141 Ferraro (1930), comes from balancing the ram pressure of the solar wind with the magnetic
 142 pressure of a dipole planetary field. A simple pressure balance between the ram pressure of the
 143 solar wind (ρV^2)_{sw} and the magnetic pressure of a dipole field ($B^2/2\mu_0$) produces a weak variation
 144 in the dayside magnetopause distance R_{MP} such that $R_{MP} \propto (\rho V^2)_{sw}^{-1/6}$ (for a solar wind mass

145 density $\rho_{sw} = m_p n_{sw}$ and speed V_{sw}). That is, a dipole magnetosphere is very “stiff” with modest
 146 response to large changes in the solar wind.

147 As shown in Table 1 and illustrated in Figure 3, this Chapman-Ferraro magnetopause
 148 distance works well for Earth but underestimates the sizes of the giant planet magnetospheres,
 149 particularly for Jupiter. If the pressure of the energetic particle populations P inside the
 150 magnetosphere, dominates over the local magnetic field pressure ($B^2/2\mu_0$), then $\beta = P/(B^2/2\mu_0) >$
 151 1 and the particle pressure inflates and stretches out the magnetic field, generating strong
 152 currents in the equatorial plasma disk. Figure 3 illustrates how the substantial internal plasma
 153 pressure at Jupiter (and to a lesser extent at Saturn) expands the magnetosphere well beyond that
 154 of a dipole internal field. At Jupiter, values of β greater than unity are found beyond $\sim 15 R_J$,
 155 increasing to $\beta > 100$ by $45 R_J$ (Mauk et al. 2004). Not only does the plasma pressure dominate
 156 the magnetic pressure, but the radial profile of plasma pressure is also considerably flatter than
 157 the $R^{-1/6}$ variation in magnetic pressure for a dipole field. It is the high plasma pressure in the
 158 plasma disk that doubles the scale of Jupiter’s magnetosphere from the dipolar stand-off distance
 159 of $\sim 42 R_J$ to over $90 R_J$. Careful statistical analysis (combined with modeling) of how the
 160 magnetopause standoff distance at Jupiter varies with solar wind conditions by Joy et al. (2002)
 161 revealed a bimodal distribution with high probabilities at 63 and 92 R_J . Furthermore, the
 162 observed magnetopause locations indicate a variation in R_{MP} with solar wind ram pressure $R_{MP} \propto$
 163 $(\rho V^2)_{sw}^{-1/4.5}$ that is much stronger than for a dipole (Slavin et al. 1985; Huddleston et al. 1998;
 164 Joy et al. 2002; Alexeev & Belenkaya 2005). Consequently, a factor 10 increase in ram pressure
 165 at Earth shrinks R_{MP} to 70% of the nominal value while at Jupiter the tenfold variations in solar
 166 wind pressure often observed at 5 AU cause the dayside magnetopause to move by a factor of ~ 2 .
 167 At Saturn the magnetospheric plasma pressures are less than Jupiter but the plasma β is still
 168 greater than unity beyond $8 R_S$ (e.g. Sergis et al. 2010) and has values of $\beta = 2-5$ in the plasma
 169 sheet. The more modest values of β at Saturn are consistent with the magnetopause stand-off
 170 distance varying as $(\rho V^2)_{sw}^{-1/5}$ (Kanani et al. 2010).

171 Saturn’s magnetosphere is similarly dominated by a satellite source of plasma
 172 (Enceladus) and rotational dynamics. The major difference, apart from scale, is that the material
 173 escaping Enceladus (mostly water products) remain largely neutral and forms an extended
 174 corona. The densities of plasma in the Enceladus torus remain relatively low. The modest size of
 175 Saturn’s magnetosphere also means that the solar wind has a stronger influence on

176 magnetospheric dynamics at Saturn. For reviews of the magnetosphere of Saturn see chapters by
177 Gombosi et al. (2009), Kurth et al. (2009), Mauk et al. (2009), Mitchell et al. (2009) in *Saturn*
178 *from Cassini-Huygens* (edited by Dougherty et al. 2009). These reviews summarize our
179 understanding after the primary phase of the *Cassini* mission to Saturn. In 2008 Cassini made the
180 only traversal by a spacecraft of an auroral radio source at a planet other than the Earth (Lamy et
181 al. 2010; Mutel et al. 2010; Schippers et al. 2011). The properties of the auroral plasma and
182 microphysical processes at a giant planet were uniquely documented. These studies serve as a
183 reference for comparisons with Juno in-situ measurements at Jupiter. The later phases of the
184 *Cassini* mission involve a series of polar orbits, similar to *Juno*'s orbits around Jupiter, that will
185 hopefully elucidate structures and processes in the polar magnetosphere.

186 As elaborated below, the giant, rotation-dominated magnetosphere of Jupiter is very
187 different from the small, solar-wind-dominated magnetosphere of Earth. Nevertheless, we expect
188 all magnetospheres to be governed by the same underlying plasma processes. Thus, as *Juno*
189 ventures into Jupiter's polar regions we are also guided by the experience derived from Earth
190 missions such as *IMP*, *ISEE*, *DE*, *POLAR* and particularly the *VIKING* and *FAST* missions (e.g.,
191 Bahnsen et al. 1989; Roux et al. 1993; McFadden et al. 1999) whose extensive measurements
192 have provided the basis of our understanding of the physical processes in polar regions.

193

194 1.3 POLAR REGIONS

195

196 Figure 1 (inset B) shows a UV image from the *Hubble Space Telescope* (Clarke et al. 2004) that
197 illustrates the complex structure of the jovian aurora. As discussed below, the auroral emissions
198 at X-ray to radio wavelengths suggest that a variety of physical processes are occurring in the
199 polar magnetosphere, including beams of ions and electrons carrying electrical currents, waves
200 generated locally as well as traveling through the region, stationary electrical potential structures
201 as well as many transient features (sketched in the top right inset C in Figure 1, loosely based on
202 *FAST* observations at Earth).

203 **Figure 4** shows the trajectories of the seven previous flyby missions (left) and the 33
204 orbits of *Galileo* (right) in the Jupiter system. Since the flyby missions used the orbital
205 momentum of Jupiter for a gravitational boost to their next target they all passed on the dusk (or
206 trailing) side of the planet except *Ulysses* that used Jupiter to get out of the ecliptic plane. (Aside:

7/1/13

207 note that *Pioneer 11* left the Jupiter system moving towards the Sun rather than away. The
208 spacecraft took 4½ years to traverse the solar system and encounter Saturn on the opposite side
209 of the Sun as Jupiter.) As illustrated in the lower plots in Figure 4, the only spacecraft that passed
210 close to Jupiter's polar region was *Pioneer 11*. However, when the *Pioneer 11* trajectory is
211 plotted in magnetic coordinates, it is clear that the spacecraft did not traverse the region of
212 auroral currents (**Figure 5**, from Trainor et al. 1975). Thus, *Juno* is the first spacecraft to explore
213 the regions where auroral currents flow, particles are accelerated, and radio emissions are
214 generated.

215

216 1.4 OUTSTANDING ISSUES

217

218 Above we have provided a brief description of the magnetosphere of Jupiter that is based
219 primarily on observations made in the equatorial regions. The lack of in situ measurements
220 over the poles raises many outstanding issues about the polar magnetosphere:

- 221 • What is the high latitude structure of the magnetosphere? Is it fundamentally
222 similar to the Earth or radically different?
- 223 • Where and how are the particles that excite the aurora accelerated?
- 224 • Where and how is auroral radio emission generated?
- 225 • What causes the very transient polar aurora?
- 226 • How much of the planetary field connects to the solar interplanetary magnetic field?
227 What is the size and variability of Jupiter's polar cap?
- 228 • How is the main aurora related to magnetospheric dynamics and/or changes in the
229 solar wind?
- 230 • What mechanisms accelerate particles to radiation belt energies? What processes
231 control the structure and dynamics of the radiation belts?
- 232 • How is the magnetosphere coupled to the solar wind? What are the mechanisms and
233 quantities of mass and momentum transfer across the magnetopause?
- 234 • What is the role of coupling of the solar wind to the magnetosphere in
235 magnetospheric dynamics? How deep does the influence penetrate or is the
236 interaction confined to a boundary layer?

- 237 • How do the polar regions couple to the long magnetotail observed by *Voyager 2* and
 238 *New Horizons*?

239 In the rest of this paper we first address the geometry of *Juno*'s orbits in the jovian
 240 magnetosphere and then describe how *Juno* addresses these scientific issues.

241

242 **2. *Juno*'s trajectory through the magnetosphere**

243

244 2.1 ORBIT OVERVIEW

245

246 The *Juno* spacecraft was launched on August 5, 2011 and, after an Earth flyby on October 9,
 247 2013, arrives at Jupiter on July 5, 2016 (Bolton et al. *this issue*). After orbit insertion, *Juno*
 248 spends the next 106 days on a capture orbit that takes *Juno* out to 180 R_J on the dawn flank of
 249 the magnetosphere (**Figure 6**).

250 After the second close pass of Jupiter on October 19, 2016, *Juno* starts a series of 33
 251 highly eccentric 11-day period science orbits (apojove distance of 38 R_J , perijove of 1.05 R_J) that
 252 last until October 2017. All orbits are close to polar, inclined less than a degree from the poles.
 253 Jupiter's motion around the Sun over the 1-year duration of the mission, results in the apojoves
 254 of the *Juno* orbits moving earlier in local time from close to 0600 (dawn) to 0400 LT. The
 255 rotational flattening (oblateness) of the planet Jupiter causes *Juno*'s orbit to precess, so that the
 256 semi-major axis tilt with respect to the equatorial plane shifts progressively southward from -4.6°
 257 to -33.5° , eventually bringing the spacecraft progressively farther into the hazardous radiation
 258 belts. After each perijove there is an orbit trim maneuver that is designed to bring *Juno* back to
 259 Jupiter at a precise time so that each successive pass is at a jovian longitude displaced by $180+12$
 260 $= 192^\circ$ (S3LH or 168° S3RH, see Appendix for description of coordinate systems) from the
 261 previous perijove. This allows instruments on the spacecraft to systematically map out longitude
 262 structures in the atmosphere and interior, as well as gravity and magnetic fields (see Connerney
 263 et al. *this issue*; Anderson et al. *this issue*; Janssen et al. *this issue*).

264 Labeling orbits by perijove (where orbit insertion is PJ0), we show the geometry of
 265 science orbits 3, 17 and 31 in **Figure 7** to illustrate typical early, middle and late orbits. A time
 266 for the start/stop of a numbered orbit is chosen about a day from perijove. The perijove distance
 267 of $\sim 1.05 R_J$ is ~ 5000 km above Jupiter's cloud deck. The black dots (at ± 4 hours of perijove)

268 illustrate how *Juno* passes very quickly from pole-to-pole (moving ~ 60 km/s around perijove,
269 ~ 20 km/s over the poles), gathering data at high rates. The high-rate data are stored on the
270 spacecraft and then transmitted to Earth over the remaining days of the ~ 11 -day orbit. The orbit
271 precession driven by Jupiter's oblateness not only produces a $\sim 1^\circ$ increased tilt per orbit but also
272 brings the (non-perijove) equatorial crossing distance closer to Jupiter by $\sim 0.9 R_J$ per orbit.
273 **Figure 8** shows how *Juno*'s northward crossing of Jupiter's geographic equator of (plane of
274 Galilean satellite orbits) moves inwards, crossing each satellite orbital distance only once over
275 the duration of the mission. *Juno* crosses the orbit of Callisto between orbits 11 and 12, the orbit
276 of Ganymede between orbits 23 and 24, and the orbit of Europa at the very end of the nominal
277 mission between orbits 33 and 34. The planned prime mission for *Juno* has the spacecraft
278 entering Jupiter on PJ34 with the result that *Juno* does not come close to the orbit of Io. Hansen
279 et al. (*this issue*) show when the Galilean satellites can be imaged by *JunoCam*.

280

281 2.2 BOUNDARY CROSSINGS

282

283 Figure 6 shows the locations of the magnetopause (MP) and bow shock (BS) derived by Joy et al.
284 (2002) based on combining previous spacecraft measurements and an MHD model. The average
285 MP and BS distances (close to the equator on the dawn flank) are $105 R_J$ and $165 R_J$ respectively
286 with the 10th to 90th percentile ranges shaded (85 - $145 R_J$ for the MP and 130 - $230 R_J$ for the BS).
287 Comparing these distances with *Juno*'s approach to Jupiter and capture orbit, we can expect the
288 spacecraft to spend ~ 80 days (~ 20 on approach and ~ 60 days during capture) in the boundary
289 regions of the magnetosphere and bow shock.

290 Typical solar wind conditions based on *Ulysses* data obtained near Jupiter's orbit during
291 the declining phase of the solar cycle, appropriate for *Juno*'s arrival at Jupiter in July 2016, are
292 summarized in **Table 2** (based on Ebert et al. 2010). Note that because the distributions of solar
293 wind and interplanetary magnetic field (IMF) properties are far from a simple Gaussian
294 distribution, we show the 10% and 90% percentiles, and median, as well as the mean (\pm standard
295 deviation). The presence of a tail at higher values is particularly noticeable for the solar wind
296 speed, density and temperature. Variability in density and flow speed produce more than a factor
297 of 10 variation in the dynamic pressure between 10% and 90% percentiles and correspondingly
298 strong variations in the compressible magnetosphere (discussed in section 1.2 above). By

299 contrast, the solar wind flow direction is very tightly constrained to within a few degrees of
300 radial. Of importance for the dynamics of Jupiter's magnetosphere is the direction of the IMF.
301 Table 2 shows that the angle of the IMF out of the ecliptic plane (meridional angle) has a
302 standard deviation of only 30° and 10/90% percentiles of $\pm 40^\circ$. Unlike at Earth, there are very
303 rare occasions when the IMF is anti-parallel to the internal (southward-pointing) field, likely
304 contributing to the low rates of steady, large-scale reconnection at Jupiter (Walker & Russell
305 1985; Desroche et al. 2012). Similarly, by 5.2 AU the Parker spiral of the IMF has wound up to
306 nearly azimuthal. That is, fields originally pointed away vs. towards the Sun have become wound
307 up so they are close to $\pm 90^\circ$ from radial at Jupiter. This means that the field changes direction a
308 few times per solar rotation, but remains within 45° of azimuthal for 80% of the time. Included
309 in Table 2 are a couple of parameters that are useful for characterizing the solar wind interaction
310 with the magnetosphere and is discussed further in Section 3.4: the plasma beta (ratio of thermal
311 pressure to magnetic field pressure) and the Alfvén Mach number (ratio of flow speed to Alfvén
312 speed).

313 Using the Joy et al. (2002) model of how these boundaries vary with solar wind dynamic
314 pressure and 1-hour averages of *Ulysses* SWOOPS solar wind data (Bame et al. 1992), we
315 predict that *Juno* will cross the BS 64 ± 9 times and the MP 42 ± 9 times. To illustrate the
316 frequent crossings of these boundaries that *Juno* might expect, we have plotted the MP and BS
317 distances based on 2500 hours of SWOOPS solar wind pressure data and superimposed a sample
318 trajectory of *Juno* over its capture orbit in **Figure 9**. The pattern of recurring compression
319 regions (responsible for sharp decreases in magnetospheric size shown in Figure 9) is
320 characteristic of the declining phase of the solar cycle experienced by *Cassini* at Saturn in 2004-
321 8 (Jackman et al. 2004) and by *Juno* a solar cycle later. Note that over the *Juno* capture orbit we
322 expect the polarity of the IMF to change dozens of times during this > 3 month period.

323 Observations of the solar wind, aurora and magnetospheric conditions during this phase
324 of the mission provides an excellent opportunity to explore the nature of the solar wind
325 interaction with Jupiter's dawn magnetosphere (see discussion in Section 3.4 below).

326

327 2.3 MAGNETOSPHERIC MODELS

328

329 In order to relate the *Juno* orbits to structures of the magnetosphere we need a magnetic field
330 model. The detailed history of models of Jupiter's magnetic field is reviewed by Connerney
331 (2007) and Connerney et al. (*this issue*). The VIP4 and VIT4 models of Connerney et al. (1998)
332 and Connerney (2007) combine spacecraft measurements of the in situ field with the location of
333 the localized auroral emission associated with Io (which must map along the magnetic field to
334 the known location of Io's orbit) to constrain up to 24 coefficients of the internal field. Grodent
335 et al. (2008) noted that both the Io and Ganymede auroral footprints required a region of
336 anomalously strong magnetic field. They add a small dipole field (~1% of primary field) located
337 about $\frac{3}{4}$ of the planet's radius from the planet's center in the northern hemisphere. Hess et al.
338 (2011) modified the VIP4 model to match both the latitude of the Io footprints as well as the
339 longitude, assuming a propagation lead angle from the Alfvén wing model of the Io interaction.
340 Hess et al. (2011)'s VIPAL model produces a good match to the measurements of Io-triggered
341 radio emission such as maximum frequency and arc shape (see discussion in Section 3.1).

342 **Figure 10** (from Hess et al. 2011) illustrates the magnetic field at Jupiter's cloud tops (~1
343 bar level of the atmosphere) from three magnetic field models (VIP4, Grodent, VIPAL) as well
344 as the predicted and observed location of the footprint that maps from Io to the planet. The
345 differences between these models are important for planning *Juno* observations of the auroral
346 regions (see Section 3.1 below). The close passage of *Juno* to the planet and extensive coverage
347 in both latitude and longitude allows the MAG team to determine the internal magnetic field of
348 Jupiter in greater detail and to much higher accuracy (Connerney et al. *this issue*).

349 Models of magnetospheric structure that include external currents as well as the internal
350 magnetic field, are generally of 3 types: empirical formulations based on matching in situ
351 magnetic field measurements; models that use observed distributions of particle pressure to
352 derive equilibrium solutions for the equatorial plasma sheet; and numerical MHD models. While
353 a global MHD model is desirable, the global models to date have tended to concentrate on the
354 outer magnetosphere, ignoring the dipole tilt and higher order moments. Furthermore, current
355 MHD models do not have the necessary heating of magnetospheric plasma and hence have not
356 managed to match the observed plasma pressures in the plasma sheet (Walker & Ogino 2003;
357 Fukazawa et al. 2005, 2006, 2010; Chane et al. 2013). Hence current global MHD models are not
358 very useful for predictions of what *Juno* measures in the plasma sheet. Models of the plasma
359 sheet that do fold in realistic pressure distributions either assume axisymmetry (Caudal 1986;

360 Caudal & Connerney 1989; Cowley et al. 2005, 2008b; Nichols 2011) or again concentrate on
 361 the outer magnetosphere (Belenkaya 2004; Alexeev & Belenkaya 2005; Belenkaya et al. 2005,
 362 2006). A useful model for global magnetic field structure has been that of Khurana (1997) and
 363 Khurana & Schwarzl (2005), which combines internal magnetic field components (e.g., VIP4 of
 364 Connerney et al. 1998), an equatorial current sheet that varies with local time, plus currents in
 365 the magnetotail and on the magnetopause. The parameters of the model have been derived by
 366 matching magnetic field data, primarily from *Galileo*.

367 **Figure 11** shows examples of the magnetic field structures in the extended
 368 magnetosphere of Jupiter. The top panel shows a sketch of the current and field configurations.
 369 The equatorially stretched magnetic flux tubes are associated with the strong azimuthal currents
 370 (j_ϕ) that flow in the plasma sheet. Radial currents through the plasma sheet (j_r) are closed into/out
 371 of the ionosphere via field-aligned currents (j_\parallel). It is the upward (or outward) currents that are
 372 likely carried by the downward-precipitating electrons that excite the main auroral oval
 373 (reviewed by Clarke et al. 2004). The true locations of the necessary downward (or inward)
 374 currents that close the current system are not known. Some argue that they flow at least partly at
 375 the magnetopause (Cowley & Bunce 2001; Bunce et al. 2004; Kivelson et al. 2002; Cowley et al.
 376 2005), while others suggest that the downward currents are interspersed with the upward currents
 377 in the interior of the plasma sheet (Mauk & Saur 2007). The middle two panels of Figure 11
 378 shows the currents and magnetic fields from the axisymmetric model of Cowley et al. (2008b)
 379 for the coupling of Jupiter's plasma disk to the ionosphere. The model field is the sum of the
 380 planetary dipole and the field from a $5-R_J$ -thick equatorial current sheet (following Connerney
 381 1981). The magnetic field lines that map to the ionosphere at co-latitudes of $5\text{--}25^\circ$ relative to the
 382 northern and southern magnetic poles, are shown at steps of 5° . In both panels the green lines,
 383 also magnetic field lines, show the regions of upward-directed field-aligned current, the solid
 384 lines show the central field line of the current layer and the dashed lines the approximate
 385 boundaries on either side. Specifically, the current regions shown by the outer pair of green solid
 386 lines in the northern and southern hemispheres map to the model open-closed field line
 387 boundaries at 10.7° with respect to both poles with the dashed green lines showing the $\sim 0.4^\circ$
 388 expected width of these currents. Similarly the green lines in the equatorial region correspond to
 389 the center and range of the upward currents that couple the ionosphere and plasma sheet. The left
 390 panel shows positive and negative contours ($\pm 2, \pm 5, \pm 10, \pm 20$, and ± 50 nT) of the azimuthal B

391 field produced by the magnetosphere-ionosphere coupling current system. In the right panel the
392 contours show the tilt angle of the field out of magnetic meridian plane.

393 Extensive analysis of the *Galileo* magnetometer data show that there are strong
394 asymmetries in the magnetic field with local time (Khurana & Kivelson 1989; Khurana 2001).
395 The effects of local asymmetries in the magnetic field (illustrated in the bottom two plots of
396 Figure 11) are included in the model of Khurana & Schwarzl (2005). They show that the bend-
397 back (i.e. deviation from the meridian plane) is much stronger on the dawn side than the dusk
398 side. This local time variation in field bend-back must be due to non-axisymmetry of the radial
399 currents, as illustrated in Figure 11B.

400

401 2.4 SCIENCE ORBITS

402

403 To illustrate the effect of Jupiter's tilted magnetic field, **Figure 12** shows orbit 3 at two
404 different phases of Jupiter's rotation ~5 hours apart. Around apojove (when the spacecraft
405 moves slowest), the plasma sheet flaps every 5 hours over the spacecraft. As the spacecraft
406 passes over the poles, the phase of the tilt is critical for predicting when the spacecraft crosses
407 the field-aligned currents that couple the plasma sheet to the planet.

408 To further illustrate the effect of the tilt, **Figure 13** shows the orbits of perijoves 3, 17
409 and 31 in a magnetic coordinate system that is aligned with a 9.515° tilt of the dipole
410 approximation to Jupiter's internal field. The magnetic field model, equatorial current sheet and
411 field-aligned current systems are derived from the azimuthally symmetric model of Cowley et al.
412 (2008b) illustrated in the center panel of Figure 11. Note how these "wiggly plots" illustrate how
413 the spacecraft trajectory crosses the current systems, both in the equator and over the poles. In
414 the early orbits the inbound and outbound trajectories each cross both equatorial and polar
415 regions. But as the orbit precesses the inbound segment crosses the north polar currents very
416 close to the planet while the outbound segment makes multiple crossings of the southern polar
417 currents. This evolution of the orbit means that *Juno* traverses the important polar regions at a
418 range of heights above Jupiter's atmosphere. Sometimes, the spacecraft seems to move parallel
419 to a magnetic L-shell for several hours which allows *Juno*'s instruments to map structure along
420 the field (e.g. locate potential structures such as double-layers, the radio emission generation
421 region, etc; discussed in Section 3.1.4). At other times, the spacecraft rapidly crosses a range of

7/1/13

422 magnetic latitudes providing an opportunity to measure latitudinal structures. For example, note
423 that the inbound trajectory on orbit 3 makes multiple crossings of the (upward) current structures
424 that couple the planet to the magnetospheric plasma sheet and the outbound trajectory on orbit 17
425 makes multiple crossings of the (downward) currents that couple to the outer magnetosphere.

426

427 2.5 POLAR REGION COVERAGE

428

429 In Figures 7 and 12 the red dots on the trajectory illustrate the location of *Juno* \pm 4 hours of
430 perijove. Considering each of these points as examples, one can see that at any moment in time
431 (or location) along the *Juno* trajectory, a magnetic field model allows one to extrapolate along
432 the magnetic field (say from the approaching, northern red dot 4 hours out) and project down
433 onto the planet the instantaneous magnetic footprint of the spacecraft. For the same instant, it is
434 possible to calculate, using the same magnetic field model, where the conjugate field line
435 intersects the planet at the opposite hemisphere of the planet. We have carried out this exercise
436 using the VIP4+Khurana magnetic field for each of the orbits and **Figure 14** shows orbits 3, 17
437 and 31. Since we are not confident in the models beyond 80 R_J we cut off the conjugate mapping
438 if the field line goes beyond 80 R_J . The left projections are the shortest path for the
439 inbound/northern hemisphere (above) and outbound/southern hemisphere (below). On the right
440 we show the footprint path mapped to the corresponding conjugate hemispheres. The fact that
441 the planet rotates (every 9.925 hours) under the spacecraft produces a curled path in the System
442 III coordinate system rotating with Jupiter (see Appendix for description of coordinate systems).
443 This means that *Juno* is likely to make multiple crossings of the region mapping to the main
444 auroral oval during a single orbit. Mapping the magnetic field to the outer magnetosphere
445 becomes increasingly unreliable at larger distances and gaps in the conjugate footprint path
446 reflect times when the field line from the spacecraft maps to distances beyond 80 R_J . Note that as
447 the orbit precesses, the inbound footprint spends increasingly more time outside the main oval
448 (for both north/local and south/conjugate hemispheres) while the outbound footprint spends an
449 increasingly more time in tighter curls well inside the main auroral oval (as also illustrated in
450 magnetic coordinates of Figure 13).

451 We are not only interested in where a field line being traversed by the *Juno* spacecraft
452 maps to the planet, but also how far the field maps out into the magnetosphere. **Figure 15** shows

453 the mapping along the field line from the spacecraft to the point that is farthest from Jupiter.
454 Note that the 10° tilt of the magnetic dipole from the rotation axis means that the farthest
455 crossing point oscillates twice per ~ 10 hour rotation period. Also note that because the magnetic
456 field models are not able to reliably map to large distances from Jupiter, we have cut off the plots
457 at $80 R_J$ from Jupiter. As the orbits precess to greater southern latitudes, an increasing fraction of
458 the orbit maps to such large distances. Since the ratio of magnetic field strength between the
459 equator and poles is very large ($>10^5$), the loss cone for particles originating at the distant
460 equatorial regions is very small ($<10^{-3}$ degrees). Therefore, the only particles that can reach high
461 latitudes (and the *Juno* spacecraft as it traverses the polar region) must be very closely aligned
462 with the magnetic field at the equator, unless they are accelerated by strong electric fields along
463 the magnetic field relatively close to the planet.

464

465 2.6 SYNCHROTRON BELT COVERAGE

466

467 The first two flyby missions, *Pioneer 10* and *11*, passed relatively close to Jupiter and the
468 energetic particle detectors on board measured intense fluxes of both ions and electrons (Figure 5
469 and **Figure 16**). Ground-based and space-based radio receivers have mapped and monitored the
470 associated synchrotron emission (see reviews by Schardt & Goertz 1983; Bolton et al. 2004).
471 The subsequent *Voyager* flybys and the *Galileo* orbits largely avoided the intense radiation belts
472 close to the planet because of the hazard they pose to instrumentation. Similarly, *Juno*'s orbit is
473 designed to avoid the regions with the most intense fluxes for as much of the mission as possible.
474 The orbit precession, however, eventually brings the spacecraft into the hazardous regions later
475 in the mission (as illustrated by orbit 31 in Figure 16). Meanwhile, on each of *Juno*'s orbits, the
476 MWR instrument detects emissions from these radiation belts at 6 microwave wavelengths,
477 mapping out the radiation belt structure over the duration of the mission (Janssen et al. *this issue*).

478

479 **3. How *Juno* addresses the scientific issues**

480

481 In Section 1.4 above, we listed the outstanding issues of Jupiter's magnetosphere, particularly of
482 the unexplored polar regions. Having described the *Juno* trajectory, we next delve further into
483 these science issues and discuss how *Juno* addresses them.

484

485 3.1 AURORAL PROCESSES

486

487 Auroral processes at Jupiter generate emissions at wavelengths across the spectrum – from radio
488 to x-rays – that are reviewed by Clarke et al. (2004) and in nine chapters of *Auroral*
489 *Phenomenology and Magnetospheric Processes* edited by Keiling et al. (2012). Remote
490 observations of radio emissions and in situ measurements of plasma waves are indications of the
491 processes that accelerate electrons and, less often, ions (reviewed by Carr et al. 1983; Zarka 1998,
492 2000). When these accelerated particles bombard the atmosphere they excite the atmospheric
493 constituents (mostly hydrogen) that then re-radiate their energy. While visible auroral emissions
494 were observed by the Galileo spacecraft (Vasavada et al. 1999), and New Horizons (Gladstone et
495 al. 2007), most of the emissions are in the UV (H and H₂ Lyman & Werner bands) or IR (H₃⁺
496 emissions). X-rays have also been observed (see reviews by Elsner et al. 2005a,b; Branduardi-
497 Raymond et al. 2007a,b, 2008; Hui et al. 2010; Cravens & Ozak 2012) and are thought to be
498 excited when very energetic (10 MeV) oxygen and sulfur ions bombard the atmosphere (Ozak et
499 al. 2010). A model based on the intense field-aligned currents expected on Jupiter’s dayside cusp
500 has been discussed by Bunce et al. (2004).

501 **Figure 17** presents an overview of Jupiter’s auroral emissions at different wavelengths.
502 Most of the emission remains within ~15° of the magnetic poles, and while much more powerful
503 than the terrestrial aurora (see Table 1), the main emissions are far less variable in size and
504 strength. The steady, narrow (~1° or ~1500 km wide) main aurora comprises ~70% of the
505 emission and is a signature of Jupiter trying to spin the magnetospheric plasma up to corotation
506 with the planet’s 10-hour rotation period. Equatorward of the main auroral emission are three
507 small regions of emissions that are associated with the moons Io, Europa and Ganymede. No
508 emission has been detected associated with Callisto, but this may be because such emission
509 would be hard to separate from the main auroral emissions. Poleward of the main aurora is the
510 remaining ~30% of the emission that is highly variable both in time and space.

511 Auroral emissions are often described as providing the television screen that reveals
512 magnetospheric structures and processes. But, in practice, without in situ measurements at high
513 latitudes it is hard to directly relate what is seen in the aurora to magnetospheric dynamics,
514 especially in the polar regions where the magnetic field mapping from the planet to the (outer)

515 magnetosphere is very uncertain. Spectroscopic studies of emissions, combined with
516 measurements of brightness above the planet's limb have been modeled to diagnose the energy
517 of precipitating particles as well as atmospheric composition and structure (Bonfond et al. 2009;
518 Tao et al. 2011, 2012; Gustin et al. 2013). The mean electron energy is ~ 100 keV for the main
519 emissions. However this energy varies both with time and location. For example, the Io footprint
520 occurs at a higher altitude than the main emissions and is generated by electrons with a broad
521 energy distribution and a mean energy of ~ 1 keV. On the other hand, during dawn storms, the
522 mean electron energy could reach ~ 460 keV (Gustin et al., 2006). Nevertheless, lacking in situ
523 measurements at high latitudes, ideas about processes that generate aurora are largely based on
524 experience at Earth and are untested at Jupiter.

525 **Figure 18** shows an example of the view of the aurora on a sample *Juno* pass over the
526 north pole. Since the spacecraft is spinning at 2 rpm, the UVS and JIRAM slit-shaped fields-of-
527 view scan swaths over the planet. In this case, the UVS slit passes over the Io footprint (IFP),
528 roughly half of the main aurora. The location of the spacecraft footprint (S/C FP) for the VIP4
529 and VIPAL magnetic field models are shown about $\sim 5^\circ$ apart. JIRAM will make observations of
530 the aurora on the planet and at its limb. The instrument will be able to map the aurora and take
531 spectral measurements and possibly retrieve the temperatures at which the H_3^+ is emitting as well
532 as provide an estimate of the column density of the H_3^+ . For further discussion of the JIRAM
533 observations see Adriani et al. (*this issue*).

534 **Figure 19** illustrates the morphology of various radio emissions that have been detected
535 coming from Jupiter (reviewed by Zarka 1998, 2000, 2004). The Io decametric emission is Io-
536 DAM, while Io-independent emission (non-Io-DAM) merges with the hectometer component
537 (HOM). The auroral broadband kilometric component (bKOM) is associated with the main
538 aurora while the narrowband kilometric emission (nKOM) is generated by unidentified torus
539 inhomogeneities at the outer regions of Io's torus. The cones emphasize the radiation pattern of
540 the high-latitude emission sources (via the Cyclotron Maser Instability, largely accepted as the
541 generation mechanism of high latitude radio emissions), which exist in both northern and
542 southern hemispheres. Radio emissions labeled bKOM, HOM and DAM are generated near the
543 local electron gyrofrequency f_{ce} and are beamed in widely opened hollow cones aligned on
544 magnetic field lines with $L \sim 6$ (Io-DAM, see e.g; Zarka et al. 2001), $L = 7-9$ (HOM), $L > 10$
545 (bKOM, Ladreiter et al. 1994), and $L > 7$ (non-Io-DAM) where L refers to the radial distance of

546 the farthest point along the magnetic flux tube that is emitting the radio emission. The inset
547 shows the correspondence of these radio sources with UV emissions: main aurora with non-Io-
548 DAM and bKOM, and Io's spots and trail with Io-DAM. Quasi-periodic emissions (QP) may
549 originate from auroral latitudes (Hospodarsky et al. 2004; Kimura et al. 2010), while non-
550 thermal-continuum (NTC) was thought to be produced at density gradients near the
551 magnetopause (Kurth 1992), or alternately may be the low frequency end of QP bursts having
552 been reflected by magnetospheric density gradients.

553 At the same time that the remote sensing instruments are making these measurements, the
554 MAG instrument measures the planet's magnetic field and small-scale perturbations due to the
555 auroral currents that couple the planet to the magnetosphere. The JADE instrument suite includes
556 three electron sensors (JADE-E) arrayed to instantaneously observe essentially all pitch angles
557 and one ion composition sensor (JADE-I) (McComas et al. *this issue*). JADE-E provides
558 complete electron distribution measurements from ~ 0.1 to 100 keV with detailed electron pitch-
559 angle distributions at a 1 s cadence. JADE-I measures ions from ~ 0.005 to ~ 50 keV over an
560 instantaneous field of view of $270^\circ \times 90^\circ$ each 4 seconds, with observations over all directions in
561 space each 30-second rotation of the *Juno* spacecraft. JADE-I also provides ion composition
562 measurements from 1 to 50 amu with $m/\Delta m \sim 2.5$, which is sufficient to separate the heavy and
563 light ions, as well as oxygen vs. sulfur ions, in the Jovian magnetosphere. The JEDI instruments
564 cover wide fields of view to allow them to measure the electrons and ions moving along the
565 magnetic field. For further discussion of the *Juno* JADE experiment see Mauk et al. (*this issue*).

566 Figures 13, 14 illustrates how the $\sim 9.5^\circ$ tilt of the magnetic dipole axis and ~ 10 hour spin
567 of the planet produces multiple crossings of auroral structures. Figure 7 shows that the altitude at
568 which *Juno* crosses the polar regions varies as the orbit precesses over the mission. This means
569 that *Juno* likely passes directly through the regions where auroral particles are accelerated and
570 allow the MAG and Waves instruments to measure the local magnetic and electric field
571 perturbations. Waves will measure the electric and magnetic components of waves in the
572 frequency range from 50 Hz to 20 kHz and the electric component, only, from 20 kHz to ~ 40
573 MHz. In survey mode, Waves acquires a complete spectrum from both electric and magnetic
574 sensors at a nominal rate of once per second within a few hours of perijove. Burst data
575 comprising waveforms from 50 Hz through 150 kHz and a 1 MHz band including the local
576 electron cyclotron frequency are also acquired for a limited number of \sim minute-long intervals

7/1/13

577 triggered by large amplitudes in the band below 150 kHz. For further discussion of the *Juno*
578 Waves experiment see Kurth et al. (*this issue*).

579 While the location of the auroral features are relatively well known, the different
580 magnetic field models (as illustrated in Figure 10) produce slightly different mappings of the
581 instantaneous footprint of the field line passing through the *Juno* spacecraft. Such uncertainties
582 in field have to be considered for planning *Juno* observations but also for analysis of the data
583 returned, at least for the initial orbits, until the magnetic field is updated using *Juno* MAG data.
584 This uncertainty is what drives the need for Waves onboard event detection to retain the most
585 interesting (most intense) time periods.

586 Below we look at the three source regions of aurora, summarize current understanding of
587 how they are generated and describe the issues that *Juno* addresses.

588

589 3.1.1 Main Aurora

590 **Figure 20 (A, B)** show the location of the main aurora obtained by averaging images from the
591 Hubble Space Telescope and mapping them onto Jupiter's rotating coordinates. The shows
592 averages of HST STIS images from Dec. 2000 – Jan. 2001 projected to views from above the
593 (A) north and (B) south hemispheres from Grodent et al. (2003a). This main emission remains
594 fairly stable in both location (variations of <few degrees) and intensity (variations of factor
595 ~few) with limited response to variations in the solar wind (Nichols et al. 2009b). Note that
596 because the northern magnetic pole is tilted farther towards the equator than the south, more of
597 the northern auroral region can be imaged than the south. The “kidney-bean” shape of the
598 northern emission (Pallier and Prangé 2001) is thought to be due to a region of weak magnetic
599 field – a magnetic anomaly – that is located at about 75°N and 115° System III longitude that
600 pushes the main aurora poleward and the tail of the Io-related emission equatorward. Figure 20C
601 compares the dayside UV emissions (observed from Earth orbit by HST, Grodent et al. 2008)
602 with the nightside optical emissions (observed by Galileo, Vasavada et al. 1999). The persistence
603 of the kink shows that it is internal rather than a feature of local time. Figure 10 illustrates
604 different attempts to model this high-order structure in Jupiter's magnetic field. The fact that
605 Ganymede's auroral emission usually lies outside the main auroral oval tells us that these auroral
606 field lines (and the associated currents) map to distances beyond Ganymede's 15 R_J orbit, though
607 an exceptional occasion in 2007 is noted by Bonfond et al. (2012).

608 The idea that Jupiter's auroral current system is driven by rotational energy combined
609 with the production and outward transport of iogenic plasma was first proposed by Hill (1979)
610 and further developed by many authors (Pontius & Hill 1982; Huang & Hill 1989; Hill 2001;
611 Cowley & Bunce 2001, 2003; Nichols & Cowley 2004; Ray et al. 2010, 2013; Nichols 2011). A
612 consequence of the current closure is that the rotation of the ionosphere is coupled to the rotation
613 of the equatorial plasmas, and the equatorial plasmas are accelerated to a substantial fraction of
614 the rigid rotation speed. Hill (1979) pointed out that these coupling-currents (and corresponding
615 aurora) are stronger where the plasma begins to slip behind rigid corotation. *Voyager*
616 measurements showed the plasma departing significantly from corotation around $\sim 17\text{-}20 R_J$
617 (McNutt et al. 1979). Models gained greater sophistication with improved current sheet models
618 but the primary differences between the various studies cited above are whether the coupling
619 between the planet's rotation and the magnetospheric plasma is limited by the transfer of angular
620 momentum from the deep atmosphere to the ionosphere (e.g. Huang & Hill 1989); the
621 ionospheric conductance (e.g. Nichols & Cowley 2004); or the lack of current-carrying electrons
622 at high latitudes between the ionosphere and plasma sheet, modifying the relation between
623 current and the voltage along the magnetic field (e.g. Ray et al. 2010). Resolving this issue
624 requires measurements of particles and fields at high latitudes.

625 Experience at Earth, however, cautions us not to take the sketch in Figure 20, nor the
626 plots in Figures 13 and 14, too literally and that auroral currents are likely much more structured
627 and variable than suggested. Mauk & Saur (2007)'s analysis of data in the plasma sheet indicates
628 there are multiple pairs of upward and downward currents. Saur et al. (2003) suggested that the
629 structuring is so pervasive on multiple scales that turbulent processes may be the prime energy
630 conversion mechanism for the generation of Jupiter's aurora and argue that there is sufficient
631 energy in the magnetic turbulence to power Jupiter's main aurora. This is perhaps similar
632 to Earth's "Alfvenic aurora". *Juno* not only takes field and plasma measurements at high
633 cadence at polar latitudes but also makes multiple passes through the equatorial plasma
634 sheet (illustrated by Figures 12 and 13 in Section 2.4 above) to test such ideas.

635 Figure 19 illustrates the wide variety of wave phenomena (non-Io-DAM, HOM, b-KOM)
636 expected on main auroral field lines based on our understanding of Earth's auroral region along
637 with auroral hiss which should highlight these field lines that connect to the main auroral
638 emissions from Jupiter's atmosphere. These are the types of emissions that were in mind when

7/1/13

639 the Waves instrument was designed. For example the electron solitary waves, or phase space
640 holes, were identified in the near-equatorial middle magnetosphere by Barbosa et al. (1981) on
641 field lines directed nearly parallel to the equator. In 1981 this phenomena was known as
642 broadband electrostatic noise as the Fourier-transformed appearance of the solitary waves before
643 the detailed waveforms were identified. Based on the occurrence of broadband electrostatic
644 noise at Earth, Barbosa et al. (1981) used this phenomenon as a connection from the plasmashet
645 boundary layer to the auroral region. This was the first identification of the mapping of the
646 middle magnetosphere back to the main auroral which was confirmed by the subsequent
647 identification of the H_3^+ Io footprint auroral located well equatorward of the main oval
648 (Connerney et al. 1993). At higher frequencies we expect *Juno* to traverse the DAM and/or
649 HOM source regions, hence, we target the Waves experiment at a 1-MHz band including the
650 local electron cyclotron frequency in order to make high spectral resolutions of the cyclotron
651 maser instability emissions.

652 A correlation of the auroral emitted power with the solar wind pressure has been reported
653 by Nichols et al. (2007); Clarke et al. (2009); Nichols et al. (2009a). Southwood and Kivelson
654 (2001) predicted that solar wind compressions would increase the angular velocity of the
655 equatorial plasma, decrease the currents related to the corotation lag, and thus result in a dimmer
656 aurora. Contrary to these expectations, Nichols et al. (2007) reported a brightening of the main
657 emission corresponding to a period when the magnetosphere first modestly shrunk and then
658 expanded, based on images acquired in 2000 while Cassini was upstream of Jupiter. Clarke et al.
659 (2009) compared the brightness of the whole Jovian aurora with the solar wind conditions during
660 the large 2007 HST campaign and came to a similar conclusion, i.e. a correlation of the auroral
661 brightness with the solar wind pressure. Using the same 2007 data set, Nichols et al. (2009a)
662 separated the auroral into distinct regions: the low latitude emissions, the main emissions, the
663 high latitude emissions, in order to identify the component of the aurora which responded the
664 most to the solar wind input. The outer region does not appear to be correlated with the solar
665 wind condition, but enhancements of the main emissions and, to a lesser extent, of parts of the
666 polar emissions were associated to solar wind compressions, as in Nichols et al. (2007). It should
667 be noted that estimates of the solar wind condition at Jupiter relying on Earth-based
668 measurements have always been challenging; the trickiest part being the accurate prediction of
669 the arrival time of the shocks. The delay between the arrival of a compression region at the

670 dayside front of the magnetopause and the auroral response is thus unclear with the current
671 dataset. While there exists some evidence for a solar wind connection in nonthermal radio
672 emissions (Prange et al. 1993; Zarka 1998; Echer et al. 2010; Hess et al. 2012;), the emission
673 region of the main aurora is buried deep in the magnetosphere and is generally agreed to be
674 primarily associated with field-aligned currents that couple the 20-30 R_J plasma disk to the
675 ionosphere.

676 As illustrated in Figures 13 and 14, Juno crosses regions of these main auroral currents
677 many times and at a range of altitudes. The MAG, Waves, JEDI and JADE instruments make in
678 situ measurements of fields and particles (measuring currents, electric fields, particle fluxes, etc.)
679 at the same time that UVS, JIRAM and JunoCAM measures auroral emissions on the planet
680 (characterizing the location, altitude profile and spectra of the auroral emissions). Moving at ~ 20
681 km/s over the poles of Jupiter, Juno takes only a few minutes to cross the narrow width of the
682 main aurora. The opportunity to observe the whole aurora for various orientations of the dipole
683 will help disentangling local time effects from System III longitude effects, in term of brightness
684 and location of the main emissions. Juno will also reveal the relative importance of the internal
685 parameters, such as the variations plasma sheet density, versus the external parameters, such as
686 the solar wind dynamic pressure, for morphology and brightness of the main aurora.

687 Without an upstream monitor of the solar wind, Juno will have to rely on extrapolation
688 from Earth of solar wind properties to Jupiter. Nevertheless, Waves, UVS, JIRAM and JunoCam
689 will measure the auroral emissions as MAG, JEDI and JADE measure particle fluxes as the Juno
690 spacecraft makes multiple traversals through magnetic flux tubes connected to the main auroral
691 regions (e.g. see Figures 14 and 18).

692

693 3.1.2 Polar Aurora

694 **Figure 21** shows observations of UV, x-ray and IR emissions from the polar regions of
695 Jupiter. The major issues with interpreting the polar data include (a) variations in space and time
696 on a range of scales, and (b) difficulties in mapping to regions of the magnetosphere. Moreover,
697 these polar regions map to the outer magnetosphere where there is debate about the
698 magnetospheric dynamics (discussed in Section 3.4 below).

699 Perhaps the most comprehensive study of the polar aurora was completed by Grodent et
700 al. (2003b) who showed that the polar emissions contribute $\sim 30\%$ of the total auroral brightness

7/1/13

701 and show bursts lasting ~100 seconds. Combining these UV images with IR spectroscopy of H_3^+
702 emissions (Stallard et al. 2001, 2003), defines three main regions: a dark region on the dawn side,
703 polarward of the main aurora that may be connected to regions of magnetospheric flow in the
704 middle to outer magnetosphere where plasma is moving inward and sunward; an active region
705 around noon and into the dusk side where there are bright flares and arc-like structures (Nichols
706 et al. 2009a) and a “swirl” region of variable emission with slow/stagnant flows which may be
707 the region of magnetic flux that connects to the solar wind. Mapping observed magnetic flux at
708 the equator to the polar regions supports the idea that the swirl region contains flux tubes that are
709 connected to the planet at one end and are open to the solar wind at the other (Vogt et al. 2011).
710 Deep in the magnetotail (50-100 R_J), blobs of plasma – plasmoids – have been observed to
711 disconnect from the plasma sheet and leave down the magnetotail (Woch et al., 2002; Kronberg
712 et al. 2007; Vogt et al. 2010; Kasahara et al. 2013). Grodent et al. (2003b, 2004) and Radioti et al.
713 (2008, 2010, 2011) have associated small bursts of polar emission on the dusk and nightside with
714 these plasma ejections. On the dayside, a bright auroral spot has often been seen around noon in
715 a region that may map to the magnetospheric cusp (Pallier & Prange 2001, 2004; Waite et al.
716 2001; Bonfond et al. 2011).

717 X-ray emissions from Jupiter have been observed since 1979. Most recent observations
718 are by the Chandra and XMM-Newton telescopes in Earth orbit (reviewed by Elsner et al. 2005;
719 Branduardi-Raymont et al. 2010). Careful modeling of the interaction of energetic (10 MeV)
720 oxygen and sulfur ions with Jupiter's atmosphere suggest that these x-rays are produced by high-
721 charge-state ions – such as O^{6+} and O^{7+} – that are stripped of electrons as they bombard the
722 atmosphere (Hui et al., 2010; Ozak et al. 2010). This begs the question of where the 10 MeV ions
723 come from. Cravens et al. (2003) suggest high voltage (million volt) potential drops in regions of
724 downward currents. Bunce et al. (2004) suggest such accelerations could be produced via
725 reconnection at the dayside magnetopause in regions of intense downward field-aligned current.

726 Again, *Juno*'s MAG, Waves, JEDI and JADE instruments makes in situ measurements of
727 fields and particles (measuring currents, electric fields, particle fluxes, etc;) at the same time that
728 UVS, JIRAM and *Juno*CAM measure the rapidly varying locations and spectra of polar auroral
729 emissions on the planet. But the transient and small-scale nature of these polar emissions likely
730 makes such structures harder to resolve. However, the unique point of view offered by *Juno* will
731 allow observations of the whole polar region, including midnight emissions poorly visible from

732 Earth, for a complete range of sub-solar longitudes. Waves will cover the polar auroral region
733 with 1-s cadence full spectra coupled with burst mode observations as described for the main
734 auroral oval, above.

735

736 3.1.3 Satellite Aurora

737

738 The interaction of magnetospheric plasma with Io, Europa and Ganymede all excite Alfvén
739 waves that travel along Jupiter’s magnetic field towards the planet (see reviews by Kivelson et al.
740 2004; Saur et al. 2004; Jia et al. 2009). Because of the dense plasma between the moons and
741 Jupiter, the travel time between these moons and the planet is longer than the time it takes the
742 corotating plasma to flow past the moon. This means that there is not a fixed current system
743 connecting the moon to the planet (sometimes described as a “unipolar inductor”) but rather
744 there is a stream of Alfvén waves that are reflected at the edges of the Io plasma torus or
745 Jupiter’s ionosphere. We have known for many decades that moons, particularly Io, trigger radio
746 emissions (see Io-DAM in Figure 19). There are theories proposed for how disturbances
747 generated by the moons accelerate radio-emitting electrons (reviewed by Hess et al. 2010a,b).
748 Furthermore, the bright auroral spots (Figure 17) tell us that fluxes of these electrons bombard
749 the atmosphere. Specifically, Hess et al. (2007) calculated a typical energy of ~4 keV for
750 electrons producing Io-induced fast radio bursts, whereas Bonfond et al. (2008, 2009) showed
751 that the vertical distribution of aurora above Jupiter’s limb suggests a mean energy of the
752 electrons of ~1 keV and that the spacing of multiple auroral spots indicates that electron beams
753 reflect between hemispheres, which is also consistent with the time-frequency drift of radio
754 bursts.

755 **Figure 22** shows the characteristic frequency-time arcs of Io-triggered radio emissions
756 that have been observed with Earth-based radio telescopes since 1964. Such shapes are well-
757 matched by the recent model of Hess et al. (2007) that uses current magnetic field models and
758 assumes that electrons with unstable loss-cone distributions generate the emission via the
759 cyclotron maser instability. **Figure 23** illustrates some of the auroral process associated with Io,
760 but similar processes are expected to be responsible for auroral spots produced by Europa and
761 Ganymede. There may be a weak interaction at Callisto but any auroral emission is probably
762 swamped by the main aurora. Bonfond et al. (2008) used combinations of electron beams and

763 Alfvén waves to explain the spacing of Iogenic auroral spots. While the Io spots and associated
764 radio bursts are associated with electrons accelerated by Alfvén waves (such as modelled by Su
765 et al. 2003; Hess et al. 2007; Jones & Su 2008), Ergun et al. (2009) argues that the auroral
766 emission produced downstream of Io (an auroral “wake” sometimes stretching half the way
767 around the planet) is produced by a steady system of upward and downward currents. Hill and
768 Vasyliunas (2002) argue that the Pedersen conductivity of the ionosphere limits the currents and
769 dictates the length of the wake. Ergun et al (2009) suggest that the wake extends far behind Io
770 because the lack of current-carrying electrons at high latitudes limits the currents that can flow
771 between the mass-loaded plasma behind Io and Jupiter’s ionosphere, implying that potential
772 structures develop at high latitudes (similar to the impedance regions sketched in Figure 20).
773 Bonfond et al. (2009) questions these two hypotheses since the altitude profile of the main Io
774 spot and the tail are very similar, suggesting that a similar process (Alfvén waves electron
775 acceleration) generated both features.

776 The *Juno* orbits have been designed to systematically map the planet, so it is unlikely that
777 the spacecraft passes directly through the flux tubes connected to the satellites (e.g. Figure 18).
778 But *Juno* likely crosses at least the wake of the Io auroral emission. We expect that the UVS and
779 JIRAM instruments will make multiple observations of the satellite auroral emissions. The
780 location of the different spots, their relative distance as well as the altitudinal profiles will be
781 observed. Moreover, spectral measurements will provide further information about the energy of
782 the precipitating electrons and the atmospheric response to this localized energy input.

783 As with the main aurora and polar aurora, Waves will use 1-s spectral cadence and its
784 burst mode to collect detailed waveforms to acquire information on plasma waves contributing to
785 the presumably Alfvénic-driven aurora and how they compare to the other types of auroras. The
786 variety of phenomena summarized in Figure 23 represents the differences one would expect from
787 our understanding of Earth’s auroras, hence, we will have an opportunity to see if a similar menu
788 of phenomena can be attributed to the various Jovian auroras.

789

790 *3.1.4 Auroral Physics*

791

792 The obvious advantage of studying auroral processes at Earth comes from both the long and
793 extensive coverage of observations from the ground from several decades of spacecraft

794 observations from a range of altitudes, including inside the Earth's AKR sources (Viking, FAST).
795 As in many areas of science, detailed knowledge tends to change basic questions into more
796 complex questions. Studies of aurorae at other planets, such as Jupiter, requires us to return to
797 the more basic issues (what are the driving forces, how do the processes work, what factors
798 modulate auroral behaviors, etc;) and test our understanding of the underlying physics under
799 rather different conditions. In their introductory chapter to Keiling et al. (2012)'s recent
800 monograph of auroral studies, Mauk & Bagenal (2012) ask, "A central question of planetary
801 space science in general and auroral physics in particular is: What aspects are universal and what
802 aspects are specific to the conditions that prevail at any one planet?" The current understanding
803 of auroral processes at Earth are summarized in Paschmann et al. (2002) as well as in Keiling et
804 al. (2012) where several chapters compare Earth with other planets.

805 A traditional view of the generation of auroral phenomena consists of (1) the generation
806 of electrical currents and voltages within the magnetized plasma of the magnetosphere, (2) the
807 diversion of those electrical currents along magnetic field lines toward the polar auroral regions,
808 (3) the generation of impedances and parallel electric fields along the magnetic field lines close
809 to the planet as a result of the low density of charge carriers in the regions just above the
810 ionosphere, (4) the acceleration of charged particles out of the regions of parallel impedance onto
811 the upper atmosphere as well as out into the distant magnetosphere, (5) the excitation and
812 ionization of atoms and molecules within the upper atmosphere by the accelerated electrons
813 resulting in strong auroral emissions and enhancements in the electrical conductivity of the
814 ionosphere, (6) the closure of the up-going and down-going electric current through the partially
815 conducting ionosphere, and (7) the associated heating through ohmic dissipation in the upper
816 atmosphere through the collision of current-carrying ions and neutral atmospheric constituents.
817 These are all general processes that Earth and Jupiter probably share. The differences are likely
818 found in the relative importance of each process and in the local properties of the plasma where
819 these processes are operating.

820 Based on experience at Earth, **Figure 24** (from Carlson et al. 1998) outlines the electric
821 current structures for different types of auroral zones: upward current regions, downward current
822 regions and regions of time-varying current. The goal of the FAST satellite was to gather
823 particles and fields data at a rate fast enough to be able to resolve these auroral structures as it
824 flew through them (Carlson et al. 1998). **Figure 25** (from Paschmann et al. 2002) shows example

7/1/13

825 data obtained by the FAST satellite. At the bottom of Figure 23 there is an image from the Polar
826 satellite that shows ultraviolet aurora (measured by the UVI instrument) and the projected
827 trajectory footprint of the FAST satellite. While FAST took the data in Figure 25, it was moving
828 northward across the nightside auroral oval. The top panel of data shows the magnetic field
829 perturbation relative to Earth's reference field, with the inferred field-aligned currents indicated
830 in green (downward), blue (upward) and the Alfvénic currents in red. The DC electric field
831 fluctuations in the second panel show the electrostatic shock structures associated with the
832 auroral acceleration region. The next four panels show ion and electron spectrograms versus
833 energy and pitch-angle. The bottom three panels show integrated ion outflow, and wave activity
834 ranging from near-DC to MHz frequencies.

835 Note that the whole of Figure 25 covers a duration of only seven minutes during which
836 the spacecraft traverses at least five different regions. Terrestrial auroral structures are observed
837 from ~1000 km in scale down to <1 km and probably extend to smaller scales, below current
838 observational limits. To observe small scale structures, the FAST mission included instruments
839 that operated at very high cadence for short-durations – in burst mode. Specifically, ion and
840 electron spectra were sampled every 78 ms while electron fluxes could be sampled as fast as
841 once every 1.6 ms (Carlson et al. 2001). The FAST spacecraft, over its >50,000 orbits of Earth,
842 could gather data at rates of 8 Mbits/sec, store and process data onboard and deliver data to the
843 ground at rates of 2 Mbits/sec (few Gbits/day).

844 At Jupiter, pre-*Juno* observations of the auroral structures are limited to remote sensing
845 either from Earth or from distant spacecraft. In radio at decameter wavelengths the very high
846 temporal and spectral resolutions achieved from the ground allow to study the source
847 microphysics (see e.g. Hess et al. 2007, 2009; Ryabov et al 2007), but this is not the case for
848 other waves and particles measurements. Typical width-scales of auroral structures are on the
849 order of 1° or 1500 km in Jupiter's atmosphere. To scale such widths to the location of *Juno* at
850 distance R from the center of Jupiter we use a relationship of $R^{3/2}$ corresponding to a dipole field.
851 For example, we find that when *Juno* is at an altitude of $2 R_J$ it crosses a distance of ~4000 km
852 corresponding to the width of the main auroral. Since *Juno* is moving at ~20 km/s over the poles
853 and ~60 km/s around perijove, this distance is covered in a few minutes, a couple of *Juno* spin
854 periods. Thus, the JADE highest resolution (burst-mode) data rate of 1 sec for electrons and 4 sec

7/1/13

855 for ions (further detailed in McComas et al. *this issue*) resolves the main auroral and possible
856 sub-structures that are to be expected if Jupiter's aurora follows our experience at Earth.

857 At 10s keV to MeV energies the JEDI instrument (further detailed in Mauk et al. *this*
858 *issue*) resolves these structures with ~second sampling rates. JEDI detects energetic electrons
859 (above 40 keV to over 500 keV) and energetic ions (about 20 keV to > 1 MeV for protons, and
860 50 keV to > 1 MeV for oxygen) with high energy, time, and angular resolution. It is three nearly
861 identical sensors, two fans covering 12°x160° and one that is 12x148°. They are mounted on the
862 spinning spacecraft with no moving parts. Two of the sensors view almost entirely in the plane
863 perpendicular to the high-gain antenna. The third fan is perpendicular to this plane so that, with
864 the spacecraft spin rate of about 2 RPM, nearly the whole sky is sampled every 30 s. Within
865 each sensor there are six look directions to provide angular coverage. At high enough energies,
866 ions and electrons will pass into the collimator, through a series of foils, and into solid-state
867 detectors. Secondary electrons liberated in the foils by the passage of the ions also provide a
868 time-of-flight measurement. Together with the energy detection in the SSD, the ion energy and
869 species can be calculated.

870 In the polar regions, JEDI will have excellent coverage of precipitating and upwardly
871 moving energetic particles. Dense, heavy plasma is centrifugally confined at Jupiter, but
872 particles at the JEDI energies can mirror at high latitudes and even reach the planetary
873 atmosphere. It is expected that fluxes of particles that generate the planetary aurora and heat and
874 ionize Jupiter's upper atmosphere will be obtained with very high time and spatial resolution.
875 Outward of the polar regions, JEDI will make in situ detections of the electron and ionic
876 radiation belts of Jupiter. Furthermore, by shielding some detectors on one of the sensors, JEDI
877 is able to measure the flux of > 1 MeV electrons hitting the detector.

878 At high latitudes along the Juno orbit, JEDI will make very coarse measurements of
879 energetic neutral atoms (ENAs) emitted from the inner regions. These are neutrals created when
880 energetic ions undergo collisions with neutral populations. The ENA created has approximately
881 the same energy as its parent ion. ENAs in Saturn's magnetosphere have been invaluable in
882 understanding some polar processes and magnetospheric activity in general. They are a tool for
883 inferring the presence of neutral distributions and also for illuminating temporal magnetospheric
884 processes.

885 The MAG investigation measures the vector magnetic field throughout periapsis at a rate
886 of 64 vector samples per second, with a vector accuracy of 100 parts per million and attitude
887 referenced in inertial space (via the ASC star cameras co-located with the MAG sensors) to some
888 tens of arcseconds. This should allow us to resolve auroral current sheets with a characteristic
889 dimension of about a km (further detailed in Connerney et al. *this issue*).

890 Associated with the main aurora are broadband kilometric (bKOM) and hectometric
891 (HOM), and decametric (DAM) radio emissions (Figure 19, Zarka 2000). The *Juno* Waves
892 experiment measures AC electric fields between frequencies of 50 Hz and > 40 MHz not only
893 detecting radio emissions along much of the orbit but also directly measuring the electric fields
894 in high latitude regions where these emissions are thought to be generated (further detailed in
895 Kurth et al. *this issue*). These measurements will allow to study the microphysics of the radio
896 sources in situ, as done at Saturn with Cassini (Lamy et al. 2010; Mutel et al. 2010). But the
897 Waves experiment will also detect the Jovian radio emissions along much of the orbit. Modeling
898 the time-frequency morphology of these emissions has proved to provide efficient remote
899 sensing of their source region (Hess et al. 2008, 2010). Although DAM emissions are not
900 detected above 40 MHz by a near-equatorial observer, today's magnetic field model permit an
901 emission at slightly higher frequencies, that could be beamed only toward high latitudes. *Juno*
902 will settle this question.

903 Just as Figure 25 shows an Earth auroral image taken by Polar as FAST gathered in situ
904 data, the *Juno* UVS, JIRAM and *Juno*Cam instruments images the jovian aurora in UV, IR and
905 visible wavelengths as *Juno*'s in situ detectors measure the local particles and fields. The
906 cadence of the remote sensing data are largely dictated by the 30 second spin period of the
907 spacecraft. As with FAST, it is key to arrange the *Juno* data sets together to allow identification
908 of the types of auroral regions from combined plots such as shown in Figure 25.

909

910 3.2 SYNCHROTRON/RADIATION BELTS

911

912 The radio emissions at decimeter wavelengths (DIM, see Figure 19) are known to be synchrotron
913 emission from energetic (10s MeV) electrons that are trapped in Jupiter's strong magnetic field
914 within a few jovian radii (see reviews by Carr et al. 1983; Bolton et al. 2004). Spacecraft
915 traversals of the jovian magnetosphere have also measured strong fluxes of energetic particles

916 much farther from Jupiter in an outer radiation region (6-20 R_J) is be discussed in Section 3.3
917 below.

918 **Figure 26** presents synthetic images of Jupiter's inner radiation belts obtained via remote
919 sensing of electromagnetic radiation via high frequency (DIM) radio emission and models of
920 electron fluxes based on these emissions plus a few in situ measurements obtained when Pioneer
921 11 and Galileo passed through this region. Santos-Costa et al. (2008) show less than factor of ~ 2
922 variation in total radio flux between 1962 and 2002. The bottom of Figure 24 shows a sketch of
923 the processes that affect the radiation belt particles as they diffuse inwards toward Jupiter,
924 interact with moons and dust, and lose energy via radiating synchrotron emission (Santos-Costa
925 & Bolton 2008).

926 Synchrotron emission from Jupiter's inner radiation belt is a foreground "noise" source
927 for microwave observations of the atmosphere, but also provides valuable information about the
928 distribution of high-energy electrons trapped in Jupiter's inner magnetosphere. Ground-based
929 measurements have been used to adjust models of the radiation belts (Garrett et al. 2005), but the
930 spatial resolution is limited. Furthermore, synchrotron emission is beamed in the direction of
931 electron motion, which is inextricably linked to the Jovian magnetic field, and the strength of
932 synchrotron emission is dependent on both the energy of the electrons and the strength of the
933 magnetic field. From Earth, we can only observe Jupiter from a limited range of angles, all
934 within ~ 10 degrees of the magnetic equator. As an electron spirals up and down the magnetic
935 field, it spends most of its time near the "mirror point", where it reverses direction with a pitch
936 angle of 90 degrees. The synchrotron emission taps the perpendicular energy of the electrons and
937 the bulk of the Jovian synchrotron emission seen from Earth comes from electrons mirroring on
938 magnetic field lines that are perpendicular to the line of sight. Thus, information about the
939 energy distribution of the electrons is entangled with information about their pitch-angle
940 distribution, and complicated by the structure of Jupiter's magnetic field. The MWR on *Juno*
941 (Janssen et al. *this issue*) does not suffer from this limitation.

942 With each spin of the spacecraft, MWR observes the synchrotron emission at each of six
943 frequencies, over a wide range of angles, from a unique vantage point. Furthermore, the
944 magnetometer experiment on *Juno* will be making a greatly improved map of the Jovian
945 magnetic field (B). The different frequencies pick out different electron energies (ϵ) because the
946 peak frequency of the synchrotron spectrum is proportional to $\epsilon^2 B$. As shown in Figure 24,

947 observations with the Very Large Array (VLA) show strong emission near the equator, implying
948 a "pancake" distribution of electrons with equatorial pitch angle close to 90 degrees, plus high-
949 latitude lobes which require a component with a more isotropic distribution of pitch angles near
950 $L=2$. The relative absence of emission at intermediate latitudes adds complexity, requiring either
951 a more complicated pitch-angle distribution or an energy distribution that depends on both pitch
952 angle and L-shell. *Juno's* trajectory takes it over the poles, and close to the planet at the equator,
953 allowing both the high latitude and the equatorial regions to be observed at a wide range of
954 angles with respect to the magnetic field, including both parallel and perpendicular to the field
955 lines. Observations at multiple frequencies from this wide range of vantage points, combined
956 with a precise map of the magnetic field, allows us to disentangle the energy and pitch angle
957 distributions from the line-of-sight effects. This is because the source is optically thin, allowing
958 tomographic reconstruction.

959 The JEDI instrument (Mauk et al. *this issue*) makes in situ measurements of the radiation
960 belts, characterizing electron spectra up to 0.5 MeV. However, there is information about
961 electron intensities at higher energies that is provided in two different forms. (1) JEDI includes
962 "witness detectors" that reside within the FOV of JEDI that are covered with enough shielding to
963 prevent <1 MeV electrons from hitting them. By comparing the response of these witness
964 detectors to the identical detectors within the JEDI FOV that do not have the shielding, JEDI
965 measures the integrated flux of >1 MeV electrons. (2) The overall shielding to the JEDI SSD
966 detectors is sufficient to keep penetrating electrons with energies greater than a threshold value
967 (~ 12 MeV) of electrons from reaching the detectors. This means that all of the solid-state
968 detectors could be impacted by electrons with energy >12 MeV. Since both the >1 MeV and the
969 >12 MeV electrons that reach the detectors also penetrate the detectors, modeling these
970 responses should be able to provide a measure of the in situ fluxes of electrons in this energy
971 range.

972 In addition to the inner electron radiation belts mentioned above, there is also an inner
973 radiation belt of energetic protons. The source of these ions is likely the CRAND process
974 (cosmic ray albedo neutron decay). Here cosmic rays impact Jupiter or its ring; the cosmic rays
975 are able to liberate neutrons from material and these decay in a very short time. If this decay
976 occurs close enough to the planet, the proton becomes trapped by the magnetic field. From
977 studying the proton radiation belts of Saturn, *Cassini* has clarified the pathway from cosmic rays

978 to the intense proton belts. Roussos et al. (2011) correlated the protons in the Saturn belts with
979 the solar cycle phase. The pathway shows that during times of high solar intensity, the cosmic
980 rays are impeded from entering the solar system and the proton belts are weaker.

981

982 3.3 PLASMA SHEET

983

984 The magnetosphere of Jupiter extends well beyond the orbits of the Galilean satellite
985 system. These moons provide most of the plasma that forms a disk around the planet (see list of
986 properties in **Table 3** and reviews by Thomas et al. 2004; Khurana et al. 2004; Krupp et al.
987 2004). In particular, Io loses about one ton per second of atmospheric material (mostly SO₂ and
988 dissociation products), which, when ionized to sulfur and oxygen ions, becomes trapped in
989 Jupiter's magnetic field (Figure 1D). Compared with the local plasma, which is corotating with
990 Jupiter at 74 km/s, the neutral atoms are moving slowly, close to Io's orbital speed of 17 km/s.
991 When a neutral atom becomes ionized (via electron impact) it experiences an electric field,
992 resulting in a gyromotion of 57 km/s. Thus, new S⁺ and O⁺ ions gain 540 eV and 270 eV in gyro-
993 energy, respectively. The new "pick-up" ion is also accelerated up to the bulk speed of the
994 surrounding plasma. The necessary momentum comes from the torus plasma, which is in turn
995 coupled, via field-aligned currents, to Jupiter – the jovian rotation being the ultimate source of
996 momentum and energy for most processes in the magnetosphere. About one-third to one-half of
997 the neutral atoms are ionized to produce additional fresh plasma while the rest are lost via
998 reactions in which a neutral atom exchanges an electron with a torus ion. When neutralized, the
999 previously charged, corotating particle is no longer confined by the magnetic field and, since the
1000 corotation speed is well above the gravitational escape speed of Jupiter, flies off as an energetic
1001 neutral atom. This charge-exchange process adds gyro-energy to the ions and extracts
1002 momentum from the surrounding plasma, but it does not add more plasma to the system.

1003 Strong centrifugal forces confine the plasma towards the equator. Thus, the densest
1004 plasma forms a torus around Jupiter at the orbit of Io. A lighter population of H⁺ ions (with a
1005 concentration of a few % and a temperature of a few 10s eV), less confined near the equator, has
1006 been inferred from radio (DAM) measurements (Zarka et al. 2001). The Io plasma torus has a
1007 total mass of ~2 megaton, which would be replenished by a source of ~1 ton/s in ~40 days.
1008 Multiplying by a typical energy ($T_i \approx 60$ eV, $T_e \approx 5$ eV) we obtain $\sim 6 \times 10^{17}$ J for the total
1009 thermal energy of the torus. The observed UV power is about 1.5 TW, emitted via more than 50
1010 ion spectral lines, most of which are in the EUV. This emission would drain all the energy of the
1011 torus electrons in ~7 hours. Ion pickup replenishes the energy, and Coulomb collisions feed the

1012 energy from ions to electrons, but not at a sufficient rate to maintain the observed emissions. A
1013 source of additional energy, perhaps mediated via plasma waves, seems to be supplying hot
1014 electrons and a comparable amount of energy as ion pickup. The ~ 40 day time scale (equivalent
1015 to ~ 100 rotations) for the replacement of the torus indicates surprisingly slow radial transport
1016 that maintains a relatively strong radial density gradient. Flux tubes laden with denser, cooler,
1017 plasma move outwards while relatively empty flux tubes containing hotter plasma from the outer
1018 magnetosphere move inwards – a process called flux tube interchange (reviewed in Thomas et al.
1019 2004).

1020 *Voyager*, *Galileo*, and, particularly, *Cassini* observations of UV emissions from the torus
1021 show temporal variability (by about a factor of a few) in torus properties (see review by Thomas
1022 et al. 2004 for earlier papers and more recent work with *Cassini* data by Steffl et al. 2004a,b,
1023 2006). Models of the physical chemistry of the torus match the observed properties in regard to
1024 the production of neutral O and S atoms, radial transport time, and source of hot electrons
1025 (Delamere & Bagenal 2003). A population of supra-thermal electrons is essential for producing
1026 both ionization states (the average ionization state of ions in the torus is between 1.6 and 1.9) and
1027 the terrawatts of UV emissions. Steffl et al. (2008) showed that a small ($<1\%$) hot electron
1028 population that varies with longitude and drifts by a few percent with respect to corotation could
1029 explain modulations in ionization state and emissions. This is supported by the subcorotating
1030 nKOM sources identified as plasma inhomogeneities in Io's torus (Reiner et al. 1993; Zarka
1031 1998). Rotation dominates the plasma flows observed in the jovian magnetosphere out to
1032 distances of $\sim 70 R_J$. Yet, the presence of sulfur and oxygen ions in the middle magnetosphere,
1033 far from Io, indicates that plasma is transported outwards, in directions transverse to the
1034 magnetic field. The net radial transport is thought to be slowest near Io's orbit (~ 15 m/s) and to
1035 speed up farther out (~ 50 m/s beyond $10 R_J$). Plasma from the Io torus spreads out from Jupiter
1036 as a $\sim 5R_J$ -thick plasma sheet throughout the magnetosphere.

1037 **Figure 27** shows an overview of conditions in the jovian plasma sheet and Table 3 lists
1038 estimates of the mass, energy and flows of these quantities through the jovian system. The
1039 distribution of plasma is based on *Voyager* and *Galileo* data, combined with simple models for
1040 the distribution of plasma along magnetic field lines (see discussion in Bagenal & Delamere
1041 2011). While the total plasma density (Figure 27A) is fairly well measured in the jovian plasma
1042 sheet, measurement of the temperature of the ions (Figure 27B) is complicated by (a) the mixture
1043 of ions of O and S at a range of ionization states, dominated at the $\sim 80\%$ level by O^+ and S^{++} ions
1044 which both have an mass/charge ratio of $16 \text{ amu}/q$; (b) ion distributions with non-Maxwellian
1045 tails; and (c) plasma instruments with different upper limits to their measurement range in E/q

1046 (~6 keV for *Voyager*, ~50 keV for *Galileo*). For example, as illustrated in Figure 27B, there are
1047 clearly times when the *Voyager* PLS instrument measured pockets of plasma containing a cold
1048 population of ~10 eV ions in the plasma sheet out to >40 R_J (Belcher 1983). At the same time,
1049 the *Galileo* PLS instrument showed that the high energy tail to the ion distribution suggests that
1050 more typical ion energies average between ~200 eV at 10 R_J to up to 1000 eV beyond 20 R_J. The
1051 smooth curve in Figure 27B is consistent with the latitudinal distribution of density measured as
1052 the plasma sheet flapped over the spacecraft (see discussion in Bagenal & Delamere 2011).

1053 The important conclusion, however, is that as the plasma moves radially outwards
1054 through the plasma sheet, it heats up. This is contrary to expectations that the plasma would cool
1055 on expansion into a larger volume. The nature of the heating mechanism has remained a puzzle
1056 since the first *Pioneer* flybys of Jupiter in the 1970s (Dessler 1983). Figure 27C shows plasma
1057 pressure (directly proportional to energy density) as a function of distance from Jupiter in the
1058 plasma sheet. The green line shows the thermal pressure of the bulk of the plasma (the thermal
1059 core of the ion distribution), the blue dotted curve shows the supra-thermal population of ions
1060 (10s keV energies), while the brown long-dashed line shows the ratio of these pressures. The
1061 pressure of the energetic ions dominates over the torus plasma except very close to the orbit of Io
1062 where the profile drops precipitously. This drop is due to the inward-diffusing energetic ions
1063 charge exchanging with the cloud of neutral particles that surround the orbit of Io and, to a lesser
1064 extent, Europa. Apart from the region close to Io, the energetic particles not only dominate over
1065 the pressure of the thermal plasma but beyond about 15 R_J the ratio of particle pressure to the
1066 pressure of the magnetic field (characterized by the parameter β) is greater than unity, rising to
1067 over a hundred beyond 40 R_J. The consequence of this high- β plasma is the stretching of the
1068 plasma sheet (Section 2.3) and compressibility of the magnetosphere, as discussed in Section 2.2
1069 above.

1070 As first noted by Northrup & Birmingham (1982) and reminded by Vogt et al. (2013),
1071 there is plenty of rotational energy in the atmosphere of Jupiter. Estimates of the power
1072 transferred from the thermosphere/ionosphere to the magnetosphere are on the order of 200 -300
1073 TW (Cowley et al. 2005; Yates et al. 2012). The issue is how to transfer the bulk motion of
1074 rotation into heating the plasma. Kivelson & Southwood (2005) proposed that the expansion of
1075 fluxtubes on the dusk side of Jupiter's magnetosphere could be sufficiently rapid to violate the
1076 second adiabatic invariant, leading to ion heating. Preliminary studies by Vogt et al. (2013)
1077 suggest this could be a viable mechanism.

1078 Combining the plasma mass density with a magnetic field model, in this case the
1079 Connerney (1992) O6-plus-current sheet model, we get an estimate of the local Alfvén speed
1080 (Figure 27E). Note that the speeds are quite slow in the plasma sheet (<300 km/s) but approach

1081 the speed of light off the magnetic equator, closer to the planet where the magnetic field is very
1082 strong and the density very low. Since Alfvén waves are how stresses are conveyed between the
1083 magnetospheric plasma and Jupiter’s ionosphere, it is these high Alfvén speeds that make
1084 numerical models of the jovian magnetosphere so demanding. At the same time, the very large
1085 scales of the jovian magnetosphere, produce large timescales for Alfvén waves to travel between
1086 the equator and ionosphere. For example, at 100 R_J the one-way Alfvén travel time is about 100
1087 minutes, during which time Jupiter’s ionosphere has rotated 60° and the plasma sheet has rotated
1088 about 30° . Thus, as the plasma moves radially away from the planet we expect it to be
1089 increasingly de-coupled from the rotating ionosphere.

1090 Table 3 lists quantities that illustrate the flow of mass and energy through the system. The
1091 distribution of mass for typical conditions in the plasma sheet is shown in **Figure 28**. Variation
1092 in torus emissions observed over several months by *Cassini* reflect the observed changes in the
1093 output of Io’s volcanic plumes of about a factor of 5 (between 600 kg/s and 2600 kg/s of neutral
1094 material). Note that these are sources of neutral material. Physical chemistry models matching
1095 the *Voyager* and *Cassini* data suggest that between 1/2 to 2/3 of this material is lost through
1096 charge exchange reactions as neutrals that escape the jovian system. This means that only 1/3 to
1097 1/2 of the neutral production rate (260 to 1400 kg/s) becomes plasma that is transported radially
1098 outwards through the plasma disk. Taking these values of plasma production/transport (\dot{M}) and
1099 the observed density profile, gives radial transport speeds of ~ 50 to ~ 200 km/s (Figure 28B). The
1100 corresponding range in torus residence time varies inversely with the source strength, from 14 to
1101 64 days (Delamere et al. 2004; Bagenal & Delamere 2011). This produces relatively minor
1102 (factor ~ 2) variations in density with time. The lower two plots in Figure 26 are alternative ways
1103 of quantifying the distribution of plasma in the system, either as in (C) via the total number of
1104 ions per magnetic flux shell (NL^2) or as in (D) via the total number of charges per unit magnetic
1105 flux (kg/Wb).

1106 The status of understanding of the structure and dynamics of the jovian magnetosphere at
1107 the end of the *Galileo* mission are summarized by Khurana et al. (2004) and Krupp et al. (2004)
1108 respectively. More recent studies can be categorized as those which concentrate on the structure
1109 of the magnetodisk with simplified assumptions about the coupling to the
1110 thermosphere/ionosphere (Nichols & Cowley 2004, 2005; Cowley et al., 2005, 2007; Nichols
1111 2011), vs. models which simplify the magnetospheric structure and concentrate on the
1112 thermosphere-ionosphere structure and dynamics (Smith & Aylward 2009; Tao et al. 2009, 2010;
1113 Yates et al. 2012). **Figure 29** provides an example, from Nichols (2011), of the magnetic field
1114 and current sheet structures for a steady-state axisymmetric model. They assume the plasma
1115 sheet content has a constant value of 8×10^{21} ions per Weber (c.f. observed values in Figure 28)

1116 for three values of the quantity (Σ_p^*/\dot{M}) where Σ_p^* is the effective conductivity of the ionosphere
1117 and \dot{M} is the mass flux through the plasma sheet.

1118 Estimates of the potential power supply from the thermosphere/ionosphere to the
1119 magnetosphere for model of Cowley et al. (2005) are about 200 to 300 TW (Table 3). Yates et al.
1120 (2012) find similar numbers with a similar model with more sophisticated treatment of the
1121 atmosphere/ionosphere. Studies by Ergun et al. (2009) and Ray et al. (2010, 2012) point out that
1122 the lack of plasma between the plasma sheet and the ionosphere leads to potential structures and
1123 saturation of currents flowing between the two regions, modifying the coupling between the
1124 magnetosphere and ionosphere. There is clearly plenty of energy in the atmosphere/ionosphere to
1125 both accelerate and heat the jovian plasma sheet (see power estimates in Table 3). The
1126 outstanding questions are (a) what specific processes control the momentum transfer from the
1127 planet to the magnetosphere – as well as the how/when these processes fail to transfer
1128 momentum – and (b) how processes convert rotational momentum into heat in the plasma sheet.
1129 A major scientific goal of the *Juno* mission is to explore the key high latitude regions for the first
1130 time as well as make multiple traversals of the plasma sheet to quantify the conditions and
1131 discriminate between different theories of how the magnetosphere couples to the planet's angular
1132 momentum to the plasma sheet.

1133 The trajectories shown in Figures 12 and 13 illustrate that *Juno* traverses the plasma sheet
1134 many times during the outer sections of the science orbits, making many passes through the
1135 region on the left-hand half of the plots in Figure 27. The JADE instrument makes extensive
1136 measurements (density, temperature, flows, composition) in the energy range of ~ 0.1 to 100 keV
1137 for electrons and ~ 0.005 to ~ 50 keV for ions; electron pitch angle distributions can be returned
1138 as rapidly as a 1s cadence and complete ion measurements are made over the 30s spacecraft
1139 rotation (for details see McComas et al. *this issue*). At the same time, the JEDI detectors measure
1140 the 10s-100s keV ions and electrons (for details see Mauk et al. *this issue*). The MAG instrument
1141 provides measurements of the magnetic field, both the internal field and perturbations due to
1142 currents flowing in the plasma sheet and also derive an estimate of the coupling currents between
1143 the planet and the magnetosphere. The Waves instrument provides measurements of plasma
1144 waves that could be heating the plasma as well as provide an estimate of the net electron density.
1145 For specific plasma sheet crossings selected by the MWG, Waves will increase its cadence from
1146 the nominal 1 spectrum per 30 seconds to one per 10 seconds. Presently, no burst data are
1147 planned for these, but such observations are possible if deemed to be important. These combined
1148 particles and fields measurements allows us to characterize the plasma properties and their

1149 variations with radial distance, latitude and longitude. Over the ~12 months that *Juno* is in the
1150 Jupiter system we will improve the estimates of mass and energy flow through the system (e.g.
1151 the quantities in Table 3) as well as describe any variations with time due to either volcanic
1152 output of Io or solar wind disturbances passing the jovian magnetosphere. We will also monitor
1153 the location of the main emissions and the Ganymede footprint, since they also vary as a function
1154 of the mass outflow rate and the plasma sheet density (Grodent et al. 2008; Bonfond et al. 2012).

1155 Furthermore, key for our understanding of atmosphere-ionosphere-magnetosphere
1156 coupling is the region of low plasma density between the plasma sheet and ionosphere (Figure
1157 13). *Juno* makes in situ measurements of the thermal plasma (JADE) and energetic particle
1158 populations (JEDI) as well as detect perturbations in the electric (Waves) and magnetic (MAG)
1159 fields in these regions where, if experience at Earth applies, we expect to see potential structures
1160 – transient or steady-state – as illustrated in Figures 20, 23 and 24.

1161

1162 3.4 OUTER MAGNETOSPHERIC DYNAMICS

1163

1164 As plasma moves radially outwards in the plasma sheet the coupling to the rotating ionosphere
1165 weakens, and the influence of the solar wind increases (see Figure 2). The high-beta plasma
1166 sheet (Figure 27D) is very compressible as manifested by the observed weaker power law
1167 dependence of the magnetopause standoff distance on solar wind ram pressure ($R_{MP} \propto$
1168 $(\rho V^2)_{sw}^{-1/4.5}$) than the -1/6 power law that one expects for a magnetic dipole alone (discussed in
1169 Section 1.2 above). On the dayside of the magnetosphere the ram pressure of the solar wind
1170 compresses the magnetosphere. Inward motion on the dawn side reduces the load on the
1171 ionosphere, producing a correspondingly dark region in the dawn polar aurora (Figure 21A). On
1172 the dusk side the plasma expands outwards and strong currents try to keep the magnetospheric
1173 plasma corotating. These strong currents produce the active dusk polar aurora. Kivelson &
1174 Southwood (2005) argued that the rapid expansion of flux tubes in the afternoon to dusk sector
1175 means that the second adiabatic invariant is not conserved, which results in the heating and
1176 thickening of the plasma sheet (Vogt et al. 2013).

1177 As pointed out in his seminal article (in which the dynamics of the outer magnetosphere
1178 was first addressed in a substantial fashion) Vasyliunas (1983) argued that at some point
1179 centrifugal forces take over from rotational coupling to the planet, stretching out the plasma
1180 sheet and magnetic field to the point where the plasma disconnects from the planet as blobs of

1181 plasma – plasmoids – that are ejected down the tail. Vasyliunas (1983) presented a sketch of
1182 magnetospheric structure that looks similar to the left hand of Figure 2 except that the line of
1183 plasmoid disconnections – the x-line – is tilted away from the sun on the dawn side rather than
1184 sunward. Analysis of plasma and magnetic field data led several authors to conclude that the x-
1185 line is sporadic and is tilted sunward on the dawnside (Woch et al. 2002; Kronberg et al. 2005,
1186 2008; Vogt et al. 2010; Ge et al. 2010; Kasahara et al. 2013).

1187 Pursuing evidence for Vasyliunas' argument that plasmoids are ejected down the jovian
1188 magnetotail, Grodent et al. (2003b, 2004) found spots of auroral emission poleward of the main
1189 aurora connected to the nightside magnetosphere that lasted for a few 10s of minutes. Such
1190 events appear to reoccur every 2 to 3 days (Radioti et al., 2008). These flashes seemed to occur
1191 from the dusk sector to the dawn sector, and they are probably coupled to a region of the
1192 magnetotail that was about $5 R_J$ to $50 R_J$ across and located further than $100 R_J$ down the tail
1193 (Grodent et al. 2004, Radioti et al. 2010, 2011). Studies of in situ measurements (Russell et al.
1194 2000; Woch et al. 2002; Kronberg et al. 2005; Vogt et al. 2010; Ge et al. 2010; Kasahara et al.
1195 2013) led to the conclusion that plasmoids on the order of $\sim 2.5 R_J$ in scale were being ejected
1196 every 4 hours to 3 days, with a predominance for the post-midnight sector at distances of $70 R_J$ to
1197 $120 R_J$. Could such plasmoids account for most of the plasma loss down the magnetotail?
1198 Bagenal (2007) approximated a plasmoid as a disk of plasma sheet $2 R_J$ thick having diameter 25
1199 R_J and density of 0.01 cm^{-3} , so that each plasmoid has a mass of about 500 ton. Ejecting one such
1200 plasmoid per day is equivalent to losing 0.006 ton/s. Increasing the frequency to once per hour
1201 raises the loss rate to 0.15 ton/s. Thus, on the one hand, even with optimistic numbers the loss of
1202 plasma from the magnetosphere due to such plasmoid ejections cannot match the canonical
1203 plasma production rate of 0.5 ton/s. On the other hand, a steady flow of plasma of density 0.01
1204 cm^{-3} , in a conduit that is $5 R_J$ thick and $100 R_J$ wide, moving at a speed of 200 km/s would
1205 provide a loss of 0.5 ton/s. Such numbers suggest that a quasi-steady loss rate is feasible. The
1206 question of the mechanism remains unanswered. Bagenal (2007) proposes a diffusive “drizzle”
1207 across weak, highly stretched, magnetotail fields, or perhaps a quasi-steady reconnection of
1208 small plasmoids, below the scale detectable via auroral emissions and limited spacecraft
1209 measurements.

1210 An overview sketch of the dynamics of the magnetosphere as proposed by Delamere &
1211 Bagenal (2010) is presented in Figure 2. Alternative views (e.g. Cowley et al. 2007; Kivelson &
1212 Southwood 2005; Badman and Cowley 2007) combine the Vasyliunas rotationally-driven
1213 ejection of plasmoids with a cycle of large-scale opening reconnection on the dayside and
1214 closing reconnection in the tail driving magnetospheric convection, as first proposed for the
1215 Earth by Dungey (1961). The problem with invoking a substantial role for a Dungey-style

1216 reconnection-driven convection system is that there is very little evidence of much dayside
1217 reconnection, making the Dungey reconnection potential is small compared with the
1218 planetary corotation potential (Walker and Russell 1985; Badman and Cowley 2007).

1219 In the spring of 2007 the *New Horizons* spacecraft flew past Jupiter, getting a
1220 gravitational boost on its way to Pluto, and made an unprecedented passage down the core of the
1221 jovian magnetotail, exiting on the northern dusk flank. For over three months, while covering a
1222 distance of $2000 R_J$, the spacecraft measured a combination of iogenic ions and ionospheric
1223 plasma (indicated by H^+ and H^{3+} ions) flowing down the tail (McComas et al. 2007; McNutt et al.
1224 2007). The fluxes of both thermal and energetic particles were highly variable on time scales of
1225 minutes to days. The tailward fluxes of internally generated plasma led McComas & Bagenal
1226 (2007) to argue that perhaps Jupiter does not have a complete Dungey cycle but that the large
1227 time scale for any reconnection flow suggests that magnetic flux that is opened near the sub-solar
1228 magnetopause re-closes on the magnetopause before it has traveled very far down the tail. They
1229 suggested that the magnetotail comprises a pipe of internally generated plasma that disconnects
1230 from the planetary field and flows away from Jupiter in intermittent surges or bubbles, with little
1231 or no planetward Dungey return flow. Cowley et al. (2008a) argue otherwise. At issue is not so
1232 much “Vasyliunas vs. Dungey” cycles (Cowley et al. (2003) showed they are not
1233 incompatible), but rather how much steady-state reconnection opens flux on the dayside,
1234 how much open flux is closed within the magnetotail, and whether there is significant
1235 sunward flow driven by this flux closure.

1236 While the magnetosphere of Saturn is much smaller than that of Jupiter and there is
1237 stronger evidence of the solar wind influencing magnetospheric dynamics (see reviews by Zarka,
1238 1998; Gombosi et al. 2009; Mitchell et al. 2009; Kurth et al. 2009; Mauk et al. 2009), the
1239 substantial data gathered by the *Cassini* spacecraft in the Saturn system have stimulated ideas
1240 about processes at Jupiter. Specifically, observations as the *Cassini* spacecraft traversed the
1241 boundary regions of the dayside magnetopause suggest that velocity shears drive Kelvin-
1242 Helmholtz instabilities (KHI), as first proposed based on *Voyager* data by Goertz (1983),
1243 pursued by Galopeau et al. (1995) and substantiated by Masters et al. (2009, 2010, 2011a,b,
1244 2012), and Delamere et al. (2011, 2013). Such observations are consistent with large-scale
1245 reconnection being suppressed due to the high Alfvén Mach number of the incoming solar wind
1246 in the outer heliosphere and a large change in plasma beta across the magnetopauses of Jupiter
1247 and Saturn (Masters et al. 2012; Desroche et al. 2012; 2013).

1248 Delamere & Bagenal (2010) argue that, due to such KHI – effectively viscous processes –
1249 on the magnetopause boundary, there is a substantial mixing of solar wind and magnetospheric

7/1/13

1250 plasmas. Simple estimates (Table 3) show that it is quite possible to lose much of the iogenic
1251 ~ton/sec of plasma across the magnetopause on the flanks of the magnetosphere and an
1252 equivalent amount of wind plasma (primarily protons with a few percent alpha particles) could
1253 enter and mix with the iogenic plasma (primarily sulfur and oxygen ions). The transfer of
1254 momentum from the solar wind to the magnetospheric plasma through such viscous processes
1255 slows down the magnetosheath plasma, draping the interplanetary magnetic field (IMF) around
1256 the magnetotail. Desroche et al. (2012) shows that if the magnetosphere of Jupiter is flattened
1257 due to the extended equatorial plasma disk, then the IMF is carried over the polar regions and
1258 draped vertically on the sides, enhancing KHI activity.

1259 In reality, we have very little information about the polar regions of Jupiter's
1260 magnetosphere and the sketch on the right of Figure 2 is guesswork. In particular, a primary
1261 issue is how large, if at all, is the polar cap region where magnetic flux tubes are connected to the
1262 planet on one end and extend out into the solar wind. Some argue that the magnetosphere is
1263 nearly closed (McComas & Bagenal 2007) while others suggest there is a substantial and
1264 changing polar cap (Vogt et al. 2010). Studies of the aurora plus conditions in the upstream solar
1265 wind suggest a relatively modest (~15-20 GWb/day) rate of flux opening and closing (Nichols et
1266 al. 2006).

1267 While *Juno*'s orbits are limited in their coverage of local time (largely confined to dusk at
1268 perijove and dawn at apojoive), they take the spacecraft over the polar regions where the particles
1269 and fields instruments are gathering a wide range of data that will be tested against the ideas
1270 discussed above for the dynamics of the outer magnetosphere. Since this is the first time
1271 measurements are made in these regions the approach is to keep the operations simple for
1272 observation of any eventuality. A major opportunity for *Juno* to explore the dynamics of the
1273 outer magnetosphere is on approach to Jupiter and the capture orbit (Figure 6) when the
1274 spacecraft spends several months in the dawn flank of the magnetosphere and is expected to
1275 make many crossings of the magnetopause and bow shock as the fluctuating solar wind buffets
1276 the compressible magnetosphere (Section 2.2, Figure 9). During the science orbits, while
1277 remaining within 38 R_J of Jupiter, the spacecraft crosses magnetic field lines that connect to the
1278 outer magnetosphere (Figure 15). The absence of energetic electrons has often been used as an
1279 indicator of whether such field lines have recently been – or continue to be – open to the solar
1280 wind (Goertz et al. 1976; Krimigis et al. 1979; Krupp et al. 2004; Delamere & Bagenal 2010).
1281 Finally, as *Juno* flies over the poles it looks down on the polar aurora (Figures 14, 18) and

1282 observes polar emissions in UV, IR and optical wavelengths. While Figure 18 illustrates that
1283 *Juno* is probably rarely connected to the very magnetic field lines in the locations of these small-
1284 scale, transient polar emissions, the chances are reasonable that over the whole mission *Juno*
1285 passes several times through a few such polar auroral structures and may be able too map out, in
1286 a statistical sense at least, the environment above the planet that maps to the distant, dynamic
1287 regions of the outer magnetosphere.

1288

1289

4. Earth Flyby

1290

1291 The original launch by an Atlas V rocket on August 5, 2011 was not able to carry the *Juno*
1292 spacecraft directly out to Jupiter. Consequently, on October 9, 2013 *Juno* returns to the Earth and
1293 make a close flyby in order to gain sufficient additional velocity to carry the spacecraft to the
1294 orbit of Jupiter. Several of the science instruments operate during the flyby, and the *Juno* mission
1295 takes advantage of this flyby to simulate operations on the spacecraft. For example, *Juno* is
1296 programed to make similar changes in the instrument data rate as those that are used during
1297 subsequent perijove passes once *Juno* is inserted into orbit around Jupiter. Other Earth-orbiting
1298 spacecraft are operational during the time of the flyby, and coordinated measurements are
1299 planned, which enable calibration of the *Juno* instruments.

1300 The orbit of *Juno* mapped onto the surface of the Earth is shown in panel A **Figure 30**.
1301 Closest approach occurs on the nightside around 19:22 UT at an altitude of 559 km. The orbit of
1302 *Juno* through the Earth's magnetosphere, shown in panels B and C, approaches the Earth in the
1303 early afternoon local time sector and passes through the nominal magnetopause just before 18:00
1304 UT. The exact time of entry depends on ambient solar wind dynamic pressure. An average
1305 location of the sub-solar magnetopause ($\sim 10 R_E$) has been plotted, but this may vary between 6
1306 and $14 R_E$ for extremely high or low solar wind pressure respectively. *Juno* only spends about 4
1307 hours within the Earth's magnetosphere before exiting on the dawn side on its way to Jupiter.

1308 During the flyby *Juno* passes directly through the most intense regions of the Earth's
1309 radiation belts, offering a unique opportunity to test the sensitivity of some of the *Juno*
1310 instruments (especially UVS, JIRAM, and the ACS star trackers cameras) to energetic
1311 penetrating particles. The passage through the energetic electron belts is illustrated in **Figure 31**,
1312 based on the AE8 statistical model for electrons with $E > 3$ MeV. The most intense relativistic
1313 electron flux is found in the outer radiation belts near $L \sim 4$. *Juno* passes through the outer belt on
1314 both the inbound and outbound orbits. However, the flux of energetic electrons in the outer

1315 radiation belt can vary by up to three orders of magnitude over timescales less than a day, so the
1316 model distributions shown in Figure 29 may not be appropriate for the time of the flyby.

1317 Fortunately, the two Earth-orbiting *Van Allen Probes* (**Figure 31**) makes observations of
1318 the radiation environment during the time of the *Juno* flyby and we coordinate the measurements
1319 made with the Relativistic Electron and Proton Telescope (REPT) with simultaneous
1320 observations of penetrating particles on *Juno*. The lower energy MagEIS instrument on each of
1321 the Van Allen Probes covers a similar range as the JEDI instrument on *Juno*, so we intend to use
1322 the coordinated observations to calibrate JEDI. *Juno* also passes through the inner electron
1323 radiation belt and the more intense energetic (> 30 MeV) ion belt near $L \sim 1.5$ soon after closest
1324 approach. This offers another opportunity to test the sensitivity of various *Juno* instrument to
1325 energetic penetrating ions, which are simultaneously measured by the REPT and RPS
1326 instruments on the *Van Allen Probes*.

1327 In addition to coordinated observations on the two *Van Allen Probes*, there are several
1328 other spacecraft that are expected to be operational during the time of the flyby, including three
1329 *THEMIS* spacecraft and the four *Cluster* spacecraft. These spacecraft are all equipped with
1330 instruments similar to the particles and fields instruments on *Juno*, and *Juno* makes
1331 measurements and performs additional instrument cross-calibration during the flyby. During
1332 October 2013 the main science targets of these missions are likely to be related to the
1333 magnetotail (*THEMIS*) and both the magnetotail and the auroral acceleration regions (*Cluster*)
1334 due to the respective spacecraft geometries during this epoch. In addition to the spacecraft
1335 measurements discussed above, it will also be of interest to use the ground-based facilities such
1336 as the SuperDARN global network of high latitude HF radars (located in both the northern and
1337 southern hemisphere). This radar network provides global-scale observations across the polar
1338 ionosphere, and as such can offer a global picture of magnetospheric dynamics.

1339 Once in the magnetosphere, *Juno* will be on magnetic field lines that map into the
1340 SuperDARN network's field of view in both hemispheres, while the *THEMIS* and *Cluster*
1341 spacecraft are likely to be situated in the magnetotail/inner magnetosphere. Science opportunities
1342 on the inbound portion of the *Juno* trajectory may include observations of dayside processes e.g.
1343 reconnection/flux transfer events. The SuperDARN observations of the ionospheric flows during
1344 this interval can be used to determine the global electric field and global reconnection rate. After
1345 the passage through the radiation belts (discussed above) the *Juno* trajectory leaves the ecliptic
1346 plane and takes the spacecraft through the northern magnetosphere lobe, and across the lobe
1347 magnetopause at high latitudes at $\sim 22:00$ UT. This region of the magnetopause has not been
1348 observed by recent magnetosphere missions (such as *Cluster*/*THEMIS*) and may offer the
1349 opportunity to observe signatures of lobe reconnection under northwards IMF conditions. Such

1350 signatures are also readily observed in the corresponding ionospheric flow measurements in the
1351 SuperDARN field-of-view.

1352 Furthermore, it is also possible to coordinate the flyby with other ground-based
1353 instrumentation such as magnetometer arrays (e.g. Image [Europe], Charisma [Canada]),
1354 incoherent scatter radars (e.g. EISCAT/Millstone Hill) and radio observatories (Nancay [France],
1355 UTR-2 [Ukraine], LOFAR [Netherlands]). Applications for dedicated radar time are part of a
1356 wider coordination effort in preparation for the *Juno* flyby.

1357

1358

5. Conclusions

1359 *Juno* is the first spacecraft to fly over the polar regions of Jupiter's magnetosphere. The
1360 spacecraft trajectory and instrument complement make *Juno* an excellent mission to tackle the
1361 key issues of the jovian aurora (spatial and temporal structure, generation processes, relationship
1362 to magnetospheric processes), the synchrotron radiation belt (spatial and temporal structure,
1363 source and loss processes) and plasma sheet (spatial and temporal structure, relationship to
1364 aurora, particle acceleration processes). Moreover, the approach and capture orbit provide
1365 valuable opportunities for *Juno* to quantify the solar wind interaction with boundary layers on the
1366 dawn side. Finally, the gravity assist flyby of Earth in October 2013 is an opportunity to test
1367 some of the *Juno* instruments in the Earth's magnetosphere as well as compare *Juno*
1368 observations with those taken from the ground and many spacecraft in Earth orbit.

1369

1370

1371 Appendix: Jovian Magnetospheric Coordinate Systems

1372

1373 Below we describe the five main coordinate systems of potential use by the *Juno* MWG. But
1374 first we need to clarify the fiducial value of the radius of Jupiter. Dessler (1983) declared
1375 use of the value $R_J = 71400$ km in the appendix of *Physics of the Jovian Magnetosphere*. A
1376 full description of the planetary parameters and coordinate systems is provided in
1377 Appendix 2 of *Jupiter: Planet, Satellites, Magnetosphere* (Bagenal, Dowling, McKinnon, (eds),
1378 2004) where the equatorial radius at the 1-bar level is given as $R_J = 71492 \pm 4$ km (Lindel et
1379 al. 1981). The JPL navigation team that provides *Juno* trajectory information uses $R_J =$
1380 **71492 km, the value we propose for all *Juno* MWG activities throughout the mission.**
1381 Note that because of the rapid rotation of the planet, the polar radius of Jupiter is much less
1382 (66854 km).

1383

1384 (1) Jupiter System III (S3LH, S3RH)

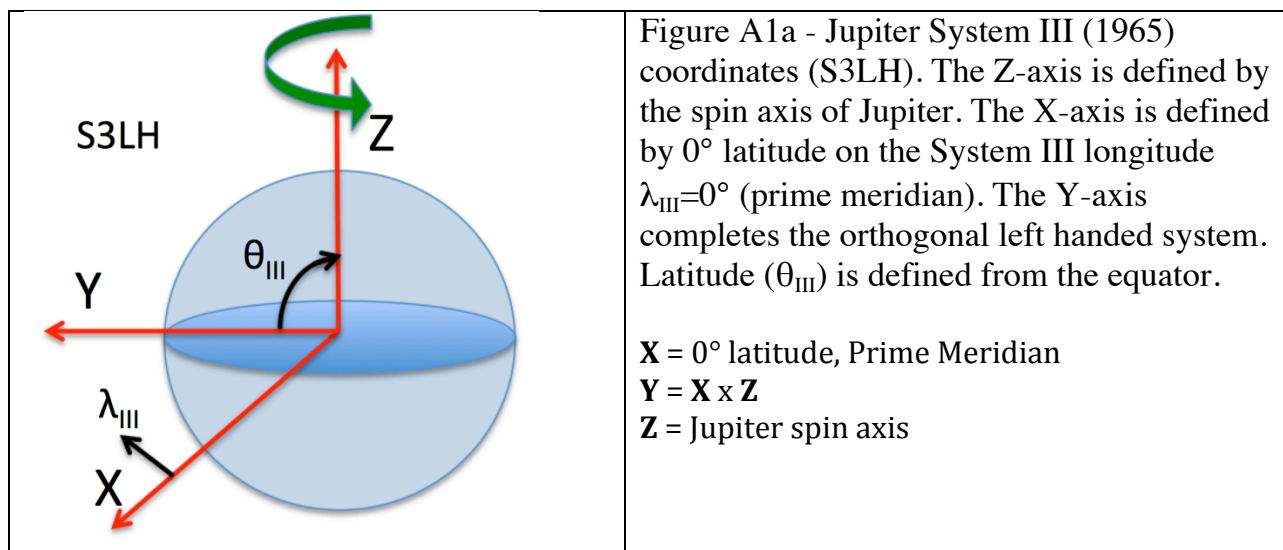
1385 This system rotates with the planet at the sidereal System III (1965) spin period of 9h 55m
1386 $29.1s = 9.925$ hours (or angular velocity of 1.76×10^{-4} rad/s = 870.536° /day). This spin

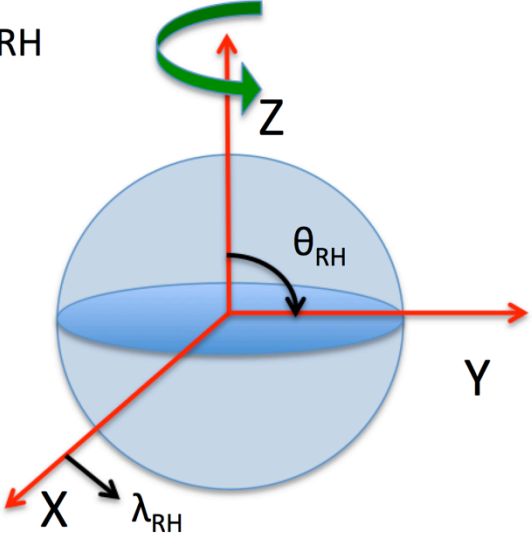
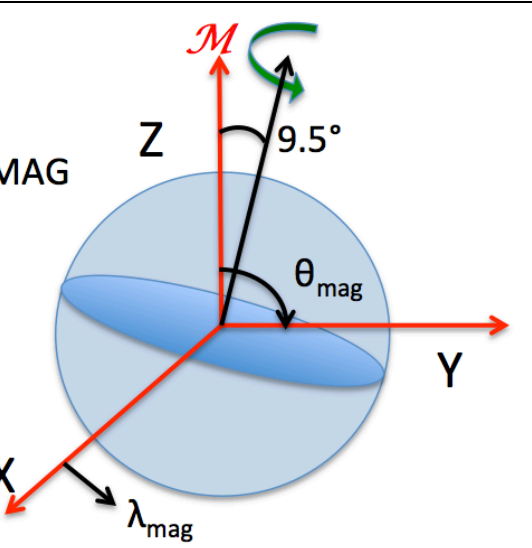
1387 period was originally based on ground-based radio observations and the longitude (λ_{III})
 1388 was defined to increase with time, as observed from Earth. The problem with this system is
 1389 that it is a left-handed coordinate system (which we label S3LH). Since many prefer right-
 1390 hand coordinate systems, we also define a RH system (S3RH) where the longitude
 1391 ($\lambda_{\text{RH}}=360^\circ-\lambda_{\text{III}}$) decreases with time as viewed from Earth. These two variations on jovian
 1392 System III are shown in Figure A1. The location of the Prime Meridian (the meridian plane
 1393 in both systems and where both longitudes are zero) is defined in terms of the Central
 1394 Meridian Longitude (i.e. Earth-Jupiter vector) on a specific date in 1965. S3LH uses latitude
 1395 (θ_{III}) while S3RH uses colatitude (θ_{RH}).

1396
 1397 Note that Higgins et al. (1996, 1997) proposed, based on 35 years of radio observations
 1398 of Jupiter, that the rotation rate of the planet interior maybe ~ 25 ms shorter than the
 1399 System III (1965) rotation rate (see also discussion in relation to magnetic field models
 1400 by Russell et al. 2001; Yu & Russell, 2009; Hess et al. 2011). A 25 ms shorter spin
 1401 period amounts to just $0.2^\circ/\text{yr}$ which is negligible over the duration of the *Juno* mission
 1402 but is significant for comparing *Voyager* and *Juno* epochs. Since this is a minimal change
 1403 in the rotation rate the IAU and the *Juno* project have decided not to change the official
 1404 System III rotation rate to limit confusion between systems and to allow easy comparison
 1405 of data sets from different epochs.

1406 (2) Jupiter Magnetic (JMAG)

1407 This system is the System III (RH) but is tilted by the 9.5° of the dipole approximation to
 1408 the magnetic field of Jupiter, tilted towards $\lambda_{\text{III}}=200.8^\circ$ or $\lambda_{\text{RH}}=159.2^\circ$. This tilt is based
 1409 on the VIP4 model (Connerney et al. 1998, *this issue*). The magnetic longitude is defined
 1410 with respect to the meridian where the magnetic and geographic equators cross (where
 1411 $\theta_{\text{III}}=0^\circ$ and $\theta_{\text{RH}}=\theta_{\text{MAG}}=90^\circ$) at $\lambda_{\text{III}}=290.8^\circ$ or $\lambda_{\text{RH}}=69.2^\circ$. Since most models tend to
 1412 work in right-handed coordinates, we only have a right-handed magnetic system.
 1413
 1414



<p>S3RH</p> 	<p>Figure A1b – Right-handed System III. This coordinate system has the same basis as the left-handed System III except that longitude is (λ_{RH}) decreases with time and co-latitude (θ_{RH}) is used.</p> <p>$X = 90^\circ$ colatitude, Prime Meridian $Y = Z \times X$ $Z =$ Jupiter spin axis</p>
<p>JMAG</p> 	<p>Figure A2 – Jupiter magnetic coordinates. This system rotates with Jupiter but has the Z-axis aligned with the magnetic dipole, M. The X-axis is aligned with the intersection of the magnetic and geographic equators at $\lambda_{III}=290.8^\circ$ or $\lambda_{RH}=69.2^\circ$</p> <p>$X = 69.2^\circ$ from Prime Meridian (where $\lambda_{III}=\lambda_{RH}=0$) $Y = Z \times X$ $Z =$ Jupiter dipole axis</p>

1415

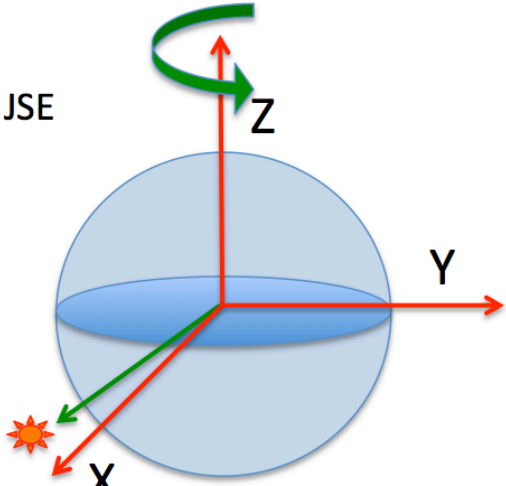
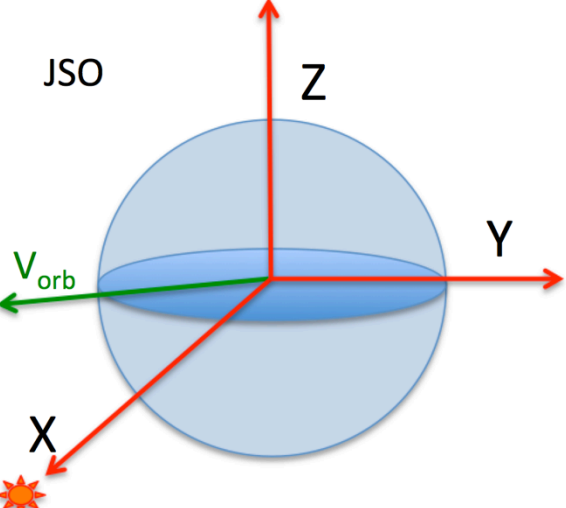
1416 **(3) Jupiter-Sun-Equator (JSE)**

1417 This system is Jupiter-centered, with the Z-axis aligned with the planet's spin axis but
 1418 does not spin with the planet. The X-axis is in the half-plane containing the spin axis and
 1419 the Jupiter-Sun vector.

1420

1421 **(4) Jupiter-Sun-Orbit (JSO)**

1422 This system aligns the X-axis with the Jupiter-Sun vector. The Y-axis is in the plane
 1423 containing the Jupiter-Sun vector and the orbital vector of Jupiter.

 <p>JSE</p>	<p>Figure A3 – This system has the Z-axis aligned with Jupiter’s spin axis but does not spin with the planet. Instead the X-axis is fixed in the plane containing the spin axis and the Jupiter-Sun vector (S).</p> <p>$\mathbf{X} = \mathbf{Y} \times \mathbf{Z}$ $\mathbf{Y} = \mathbf{S} \times \mathbf{Z}$ (i.e. in the equator) \mathbf{Z} = Jupiter’s spin axis</p>
 <p>JSO</p>	<p>Figure A4 – This system has the X-axis towards the Sun (S) and the Z-axis perpendicular to Jupiter’s orbital vector (V_{orb}). This puts Z normal to Jupiter’s orbital plane.</p> <p>$\mathbf{X} = \mathbf{S}$ $\mathbf{Y} = \mathbf{Z} \times \mathbf{X}$ $\mathbf{Z} = \mathbf{V}_{orb} \times \mathbf{X}$</p>

1424 **(5) Jupiter Heliospheric (JH)**

1425 Since *Juno* measures solar wind conditions surrounding Jupiter’s magnetosphere we need a
 1426 coordinate system that is based on heliospheric properties. This system is Jupiter-centered
 1427 and the X-axis is the Jupiter-Sun vector, the Y-axis is the solar equator, and the Z-axis
 1428 completes the system. This is the heliocentric system centered on Jupiter.

1429

1430 **Acknowledgements:**

1431

1432 We acknowledge all the outstanding contributions from the many people who made the *Juno*
 1433 mission a reality. FB would like to acknowledge the assistance of Steve Bartlett for making
 1434 several of the graphics, plus others at the University of Colorado for their help with producing
 1435 materials: Laura Brower, Adam Shinn, Dinesh Costlow, Emma Bunnell, Christopher Fowler,
 1436 Rob Wilson, Frank Crary and Drake Ranquist. Further information and plots for *Juno* orbits can
 1437 be found at <http://lasp.colorado.edu/mop/resources/juno/>

7/1/13

1438 Table 1: Comparison of Magnetospheres of Earth, Jupiter and Saturn
 1439

	Earth	Jupiter	Saturn
Radius, R_P (km)	6,373	71,492 ^(a)	60,268
Distance from Sun ^(b) (AU)	1	5.2	9.5
Spin period (hours)	24	9.924	10.656 ^(c)
Solar wind density, n_{sw} (cm^{-3})	7	0.2	0.07
Magnetic moment ^(d) (M_E)	1	20,000	600
Equatorial magnetic field, B_o (nT)	30,600	430,000	21,400
Plasma source (kg/s)	5	260-1400 ^(e)	12-250 ^(e)
Plasma source (ions/s)	2×10^{26}	$> 10^{28}$	$3-5 \times 10^{26}$
Dipole R_{CF} ^(f) (R_P)	10 R_E	46 R_J	20 R_S
Observed R_{MP} (R_P)	8-12 R_E	63-92 R_J	22-27 R_S
Plasma Transport Time ^(g)	hours-days	20-80 days	30-50 days
Auroral Emission Power (W)	10^{10}	10^{12}	10^{11}
Auroral Emission Power (W) in Radio Cf. Zarka, Treumann, Ryabov, ASS 2001 Zarka, Cecconi, Kurth, JGR 2004	$\sim 4e7$	8e10 DAM 4e10 HOM 5e8 bKOM 2e8 nKOM 5e9 QP b.	4e8

1440 ^(a) We define $1R_J = 71,492$ km (see discussion in the Appendix)

1441 ^(b) Semi-major axis of orbit. $1 \text{ A.U.} = 1.5 \times 10^8$ km

1442 ^(c) Based on Voyager observations of SKR emission. The rotation rate of Saturn is an
 1443 important issue of scientific debate (as reviewed by Carbary & Mitchell 2013).

1444 ^(d) $M_{\text{Earth}} = 7.9 \times 10^{25} \text{ Gauss cm}^3 = 7.9 \times 10^{15} \text{ Tesla m}^3$

1445 ^(e) Summarized by Bagenal and Delamere (2011)

1446 ^(f) R_{CF} is calculated using $R_{CF} = \xi (B_o^2 / 2\mu_o \rho_{sw} V_{SW}^2)^{1/6}$ for typical solar wind conditions of ρ_{sw}
 1447 $= m_p n_{sw}$ given above and $V_{SW} \sim 400 \text{ km s}^{-1}$ and ξ an empirical factor of ~ 1.4 to match Earth
 1448 observations (Walker and Russell 1995).

1449 ^(g) Typical residence time in the magnetosphere. Plasma stays inside the Earth's
 1450 plasmasphere for days but is convected through the outer magnetosphere in hours.

1451

1452

7/1/13

1453 Table 2 – Statistical properties of the interplanetary medium around the orbit of Jupiter^(a)
 1454

	10%^(b)	Mean^(c)	Standard Deviation^(c)	Median	90%^(b)
Proton speed (km/s)	369	451	±71	438	557
Solar wind azimuthal deflection (deg)	-3.1	-0.3	±2.1	-0.2	2.0
Solar wind meridional deflection (deg)	-2.6	-0.16	±2.1	-0.16	2.1
Proton temperature (eV)	0.55	2.8	±3.8	1.4	6.8
Proton density (cm ⁻³)	0.036	0.22	±0.27	0.13	0.50
Alpha particle composition (% by density)	2.6	3.1	±3.3	3.1	3.1
Dynamic pressure (nPa)	0.014	0.084	±0.11	0.045	0.20
B-field strength (nT)	0.18	0.69	±0.63	0.45	1.5
B-field azimuthal angle, B _t > 0 (deg)	46	95	±35	98	137
B-field azimuthal angle, B _t < 0 (deg)	-134	-81	±38	-79	-31
B-field meridional angle (deg)	-40.4	0.37	±31.1	0.49	40.8
Plasma β ^(d)	0.12	0.66	± 1.6	0.38	1.2
Alfvén Mach Number ^(e)	7.4	17.7	± 11.5	16	29

1455 (a) These values are based on 1-hour averages of *Ulysses* data obtained between 2003 (Day
 1456 Of Year 340) to 2005 (Day Of Year 008) at heliocentric distances of 5.273 to 5.403 AU
 1457 within 10° of Jupiter’s inclination at the time. These data were obtained around the phase
 1458 of the solar cycle (descending from maximum) that Juno is expected to arrive at Jupiter.
 1459 Based on Ebert et al. (2010)

1460 (b) 10th and 90th percentiles of the solar wind distribution

1461 (c) Mean and standard deviation of the distribution.

1462 (d) Ratio of proton thermal pressure to magnetic field pressure.

1463 (e) Ratio of solar wind speed to Alfvén speed.

1464

7/1/13

1465 Table 3 – Flow of mass and energy through the magnetosphere of Jupiter^(a)
 1466

	Magnetosphere of Jupiter
Mass of neutrals	~70 kton
Mass of plasma	1.5 Mton
Plasma production	260-1400 kg/s
Neutral production	600-2600 kg/s
Fast neutral loss	320-1740 kg/s
Plasmoid loss ^(b)	~30 kg/s
Solar wind flux ^(c)	230 ton/s
Total Kinetic Energy ^(d)	7.5 x 10 ¹⁸ J
Power: Kinetic Energy ^(d)	1.4-7.8 TW
Total Thermal Energy ^(e)	1 x 10 ¹⁸ J
Power: Plasma Thermal Energy ^(e)	0.3-1.4 TW
Total Energetic Ion Energy ^(f)	1.4 x 10 ¹⁹ J
Power: Energetic Ion Energy ^(f)	2.7-15 TW
Net Heating of Plasma Disk	3-16 TW
Power: Atmosphere/ionosphere ^(g)	~200 - 300 TW
Power: Solar Wind ^(h)	~200 TW
Power: UV Torus Emission	1.2-2.5 TW
Power: Aurora	200-800 GW
Power: Magnetotail Flows	1 TW
Power: Satellite Interaction	1 TW
Power: Satellite Aurora	6 GW

1467 (a) From Bagenal & Delamere (2011)

1468 (b) Based on estimate of one plasmoid per day, from Bagenal (2007)

1469 (c) Flux of solar wind onto area of πR_T^2 where R_T is magnetopause distance at terminator
 1470 (~150 R_J)

1471 (d) Rotational kinetic energy of plasma. Power estimate assumes a range in time scales of
 1472 11-60 days.

1473 (e) Total thermal energy of the plasma in plasma disk. Power estimate assumes a range in
 1474 time scales of 11-60 days.

1475 (f) Total energy of the supra-thermal component of plasma in the plasma disk, from Mauk
 1476 et al. (2004). Power estimate assumes a range in time scales of 11-60 days.

1477 (g) Power transferred from the thermosphere/ionosphere to the magnetosphere for
 1478 models of Cowley et al. (2005) and of Yates et al. (2012).

1479 (h) About 1% of the kinetic energy flux of solar wind onto area of πR_T^2 where R_T is the
 1480 magnetopause distance at terminator (~150 R_J)

1481

References

- Alexeev, I. I., and E. S. Belenkaya, Modeling of the Jovian Magnetosphere, *Ann. Geophys.*, *23*, 809–826, 2005.
- Badman, S. V., and S. W. H. Cowley, Significance of Dungey-cycle flows in Jupiter's and Saturn's magnetospheres, and their identification on closed equatorial field lines, *Ann. Geophys.*, *25*, 941–951, 2007.
- Bagenal, F., Giant planet magnetospheres, *Ann. Rev. Earth Planet. Sci.*, *20*, 289–328, 1992.
- Bagenal, F., T. E. Dowling, and W. B. McKinnon (Eds.), *Jupiter: Planet, Satellites, Magnetosphere*, Cambridge University Press, 2004.
- Bagenal, F., The magnetosphere of Jupiter: Coupling the equator to the poles, *J. Atmos. Solar-Terr. Phys.*, *69*, 387–402, 2007.
- Bagenal, F., Comparative Planetary Environments, in *Heliophysics: Plasma Physics of the Local Cosmos*, C. J. Schrijver, G. L. Siscoe (eds), Cambridge University Press, 2009.
- Bagenal, F., and P. A. Delamere, Flow of mass and energy in the magnetospheres of Jupiter and Saturn, *J. Geophys. Res.*, *116*, 5209, 2011.
- Bahnsen, A.; Jespersen, M.; Ungstrup, E.; Pedersen, B. M.; Eliasson, L., Viking observations at the source region of auroral kilometric radiation, *J. Geophys. Res.*, *94*, 6643-6654, 1989
- Bame, S. J., B. L. Barraclough, W. C. Feldman, G. R. Gisler, J. T. Gosling, D. J. McComas, J. L. Phillips, M. F. Thomsen, B. E. Goldstein, and M. Neugebauer, Jupiter's Magnetosphere: Plasma Description from the Ulysses Flyby, *Science*, *257*, 1539–1543, 1992.
- Barbosa, D. D.; Scarf, F. L.; Kurth, W. S.; Gurnett, D. A., Broadband electrostatic noise and field-aligned currents in Jupiter's middle magnetosphere, *J. Geophys. Res.*, *86*, 8357-8369, 1981
- Belcher, J. W., The low-energy plasma in the Jovian magnetosphere, in *Physics of the Jovian Magnetosphere*, A. J. Dessler (ed.), Cambridge Univ. Press, Cambridge, U. K., 1983
- Belenkaya, E. S., The Jovian magnetospheric magnetic and electric fields: Effects of the interplanetary magnetic field, *Planet. Space Sci.*, *52*, 499–511, 2004.
- Belenkaya, E. S., S. Y. Bobrovnikov, I. I. Alexeev, V. V. Kalegaev, and S. W. H. Cowley, A model of Jupiter's magnetospheric magnetic field with variable magnetopause flaring, *Planet. Space Sci.*, *53*, 863–872, 2005.
- Belenkaya, E. S., P. A. Bespalov, S. S. Davydenko, and V. V. Kalegaev, Magnetic field influence on aurorae and the Jovian plasma disk radial structure, *Ann. Geophys.*, *24*, 973–988, 2006.
- Bigg, E. K., Influence of the Satellite Io on Jupiter's Decametric Emission, *Nature*, *203*, 1008–1010, 1964.
- Bolton, S., R. Thorne, S. Bourdarie, I. DePater, and B. Mauk, Jupiter's Inner Radiation Belts, in *Jupiter: Planet, Satellites, Magnetosphere*, F. Bagenal, T. E. Dowling, and W. B. McKinnon (Eds.), Cambridge University Press, 2004.
- Bonfond, B., D. Grodent, J.-C. Gérard, A. Radioti, J. Saur, and S. Jacobsen, UV Io footprint leading spot: A key feature for understanding the UV Io footprint multiplicity? *Geophys. Res. Lett.*, *35*, 5107, 2008.
- Bonfond, B., D. Grodent, J.-C. Gérard, A. Radioti, V. Dols, P. A. Delamere, and J. T. Clarke, The Io UV footprint: Location, inter-spot distances and tail vertical extent, *J. Geophys. Res.*, *114*, 7224, 2009.
- Bonfond, B.D., M. F. Vogt, J.-C. Gérard, D. Grodent, A. Radioti, V. Coumans, Quasiperiodic polar flares at Jupiter: A signature of pulsed dayside reconnections? *Geophys. Res. Lett.* *380*, L02104, 2011.
- Bonfond, B., D. Grodent, J.-C. Gerard, T. Stallard, J. T. Clarke, M. Yoneda, A. Radioti, and J. Gustin, Auroral evidence of Io's control over the magnetosphere of Jupiter, *Geophys. Res.*

- Lett.*, 39, 1105, 2012.
- Branduardi-Raymont, G., A. Bhardwaj, R. F. Elsner, G. R. Gladstone, G. Ramsay, P. Rodriguez, R. Soria, J. H. Waite, and T. E. Cravens, Latest results on Jovian disk X-rays from XMM-Newton, *Planet. Space Sci.*, 55, 1126–1134, 2007a.
- Branduardi-Raymont, G., A. Bhardwaj, R. F. Elsner, G. R. Gladstone, G. Ramsay, P. Rodriguez, R. Soria, J. H. Waite, Jr., and T. E. Cravens, A study of Jupiter’s aurorae with XMM-Newton, *A&A*, 463, 761–774, 2007b.
- Branduardi-Raymont, G., R. F. Elsner, M. Galand, D. Grodent, T. E. Cravens, P. Ford, G. R. Gladstone, and J. H. Waite, Spectral morphology of the X-ray emission from Jupiter’s aurorae, *J. Geophys. Res.*, 109, 2202, 2008.
- Branduardi-Raymont, G., A. Bhardwaj, R. F. Elsner, and P. Rodriguez, X-rays from Saturn: a study with XMM-Newton and Chandra over the years 2002-05, *A&A*, 510, A73, 2010.
- Bunce, E. J., S. W. H. Cowley, and T. K. Yeoman, Jovian cusp processes: Implications for the polar aurora, *J. Geophys. Res.*, 109, A09513, 2004.
- Burke, B. F., and K. L. Franklin, Observations of a Variable Radio Source Associated with the Planet Jupiter, *J. Geophys. Res.*, 60, 213–217, 1955.
- Carbary, J. F., and D. G. Mitchell, Periodicities in Saturn’s magnetosphere, *Rev. Geophys.*, 51, 78–90, 2013.
- Carlson, C. W., R. F. Pfaff, and J. G. Watzin, The Fast Auroral SnapshoT (FAST) Mission, *Geophys. Res. Lett.*, 25, 2013–2016, 1998.
- Carlson, C. W., J. P. McFadden, P. Turin, D. W. Curtis, and A. Magoncelli, The Electron and Ion Plasma Experiment for Fast, *Space Sci. Rev.*, 98, 33–66, 2001.
- Carr, T., M. Desch, and J. Alexander, Phenomenology of Magnetospheric Radio Emissions, in *Physics of the Jovian Magnetosphere*, A. J. Dessler (ed), Cambridge University Press, 1983.
- Caudal, G., A self-consistent model of Jupiter’s magnetodisc including the effects of centrifugal force and pressure, *J. Geophys. Res.*, 91, 4201–4221, 1986.
- Caudal, G., and J. E. P. Connerney, Plasma pressure in the environment of Jupiter, inferred from Voyager 1 magnetometer observations, *J. Geophys. Res.*, 94, 15,055–15,061, 1989.
- Chané, E., J. Saur, S. Poedts, Modeling Jupiter’s magnetosphere: Influence of the internal sources, *J. Geophys. Res.*, 118, 2157–2172, 2013.
- Chapman, S., and V. C. A. Ferraro, A New Theory of Magnetic Storms, *Nature*, 126, 129–130, 1930.
- Clarke, J., D. Grodent, S. Cowley, E. Bunce, P. Zarka, J. Connerney, and T. Satoh, Jupiter’s Aurora, in *Jupiter: Planet, Satellites, Magnetosphere*, F. Bagenal, T. E. Dowling, and W. B. McKinnon (Eds.), Cambridge University Press, 2004.
- Clarke, J. T., J. Nichols, J.-C. Gérard, D. Grodent, K. C. Hansen, W. Kurth, G. R. Gladstone, J. Duval, S. Wannawichian, E. Bunce, S. W. H. Cowley, F. Crary, M. Dougherty, L. Lamy, D. Mitchell, W. Pryor, K. Retherford, T. Stallard, B. Zieger, P. Zarka, and B. Cecconi, Response of Jupiter’s and Saturn’s auroral activity to the solar wind, *J. Geophys. Res.*, 114, 5210, 2009.
- Connerney, J. E. P., The magnetic field of Jupiter: A generalized inverse approach, *J. Geophys. Res.*, 86, 7679–7693, 1981.
- Connerney, J. E. P., Doing more with Jupiter’s magnetic field, in *Planetary Radio Emissions III*, H. O. Rucker, S. J. Bauer, and M. L. Kaiser (eds), 1992.
- Connerney, J. E. P.; Baron, R.; Satoh, T.; Owen, T., Images of Excited H₃⁺ at the Foot of the Io Flux Tube in Jupiter’s Atmosphere, *Science*, 262, 1035–1038, 1993.
- Connerney, J. E. P., M. H. Acuna, N. F. Ness, and T. Satoh, New models of Jupiter’s magnetic field constrained by the Io flux tube footprint, *J. Geophys. Res.*, 103, 11,929–11,940, 1998.

- Connerney, J. E. P., Planetary Magnetism, in *Treatise in Geophysics, Volume 10: Planets and Satellites*, G. Schubert, T. Spohn (eds), Elsevier, Oxford, UK, 2007.
- Cowley, S. W. H., and E. J. Bunce, Origin of the main auroral oval in Jupiter's coupled magnetosphere-ionosphere system, *Planet. Space Sci.*, *49*, 1067–1088, 2001.
- Cowley, S. W. H., and E. J. Bunce, Corotation-driven magnetosphere-ionosphere coupling currents in Saturn's magnetosphere and their relation to the auroras, *Ann. Geophys.*, *21*, 1691–1707, 2003.
- Cowley, S. W. H., E. J. Bunce, T. S. Stallard, and S. Miller, Jupiter's polar ionospheric flows: Theoretical interpretation, *Geophys. Res. Lett.*, *30*, 1220, 2003.
- Cowley, S. W. H., I. I. Alexeev, E. S. Belenkaya, E. J. Bunce, C. E. Cottis, V. V. Kalegaev, J. D. Nichols, R. Prange, and F. J. Wilson, A simple axisymmetric model of magnetosphere-ionosphere coupling currents in Jupiter's polar ionosphere, *J. Geophys. Res.*, *110*, 11,209, 2005.
- Cowley, S. W. H., Current-voltage and kinetic energy flux relations for relativistic field-aligned acceleration of auroral electrons, *Ann. Geophys.*, *24*, 325–338, 2006.
- Cowley, S. W. H., J. D. Nichols, and D. J. Andrews, Modulation of Jupiter's plasma flow, polar currents, and auroral precipitation by solar wind-induced compressions and expansions of the magnetosphere: a simple theoretical model, *Ann. Geophys.*, *25*, 1433–1463, 2007.
- Cowley, S. W. H., S. V. Badman, S. M. Imber, and S. E. Milan, Comment on “Jupiter: A fundamentally different magnetospheric interaction with the solar wind” by D. J. McComas and F. Bagenal, *Geophys. Res. Lett.*, *35*, 10,101, 2008a.
- Cowley, S. W. H., A. J. Deason, and E. J. Bunce, Axi-symmetric models of auroral current systems in Jupiter's magnetosphere with predictions for the Juno mission, *Ann. Geophys.*, *26*, 4051–4074, 2008b.
- Cravens, T. E., and N. Ozak, Auroral Ion Precipitation and Acceleration at the Outer Planets, in *Auroral Phenomenology and Magnetospheric Processes*, A. Keiling, E. Donovan, F. Bagenal, T. Karlsson (eds), AGU monograph series, Washington DC, 2012.
- Cravens, T. E., J. H. Waite, T. I. Gombosi, N. Lugaz, G. R. Gladstone, B. H. Mauk, and R. J. MacDowall, Implications of Jovian X-ray emission for magnetosphere-ionosphere coupling, *J. Geophys. Res.*, *108*, 1465, 2003.
- Delamere, P. A., and F. Bagenal, Modeling variability of plasma conditions in the Io torus, *J. Geophys. Res.*, *108*, 1276, 2003.
- Delamere, P. A., and F. Bagenal, Longitudinal plasma density variations at Saturn caused by hot electrons, *Geophys. Res. Lett.*, *35*, 3107, 2008.
- Delamere, P. A., and F. Bagenal, Solar wind interaction with Jupiter's magnetosphere, *J. Geophys. Res.*, *115*, 10,201, 2010.
- Delamere, P. A., A. Steffl, and F. Bagenal, Modeling temporal variability of plasma conditions in the Io torus during the Cassini era, *J. Geophys. Res.*, *109*, 10,216, 2004.
- Delamere, P. A., R. J. Wilson, and A. Masters, Kelvin-Helmholtz instability at Saturn's magnetopause: Hybrid simulations, *J. Geophys. Res.*, *116*, 10,222, 2011.
- Delamere, P. A., R. J. Wilson, S. Eriksson, and F. Bagenal, Magnetic signatures of Kelvin-Helmholtz vortices on Saturn's magnetopause: Global survey, *J. Geophys. Res.*, *118*, 393–404, 2013.
- Desroche, M., F. Bagenal, P. A. Delamere, and N. Erkaev, Conditions at the expanded Jovian magnetopause and implications for the solar wind interaction, *J. Geophys. Res.*, *117*, 7202, 2012.
- Desroche, M., F. Bagenal, P. A. Delamere, and N. Erkaev, Conditions at the magnetopause of Saturn and implications for the solar wind interaction, *J. Geophys. Res.*, *118*, 2013.

- Dessler, A. (Ed.), *Physics of the Jovian Magnetosphere*, Cambridge University Press, 1983.
- Dougherty, M. K., L. W. Esposito, and S. M. Krimigis (Eds.), *Saturn from Cassini-Huygens*, Springer, 2009.
- Drake, F. D., and S. Hvatum, Non-thermal microwave radiation from Jupiter, *Ap. J.*, *64*, 329–330, 1959.
- Dungey, J. W., Interplanetary Magnetic Field and the Auroral Zones, *Phys. Rev. Lett.*, *6*, 47–48, 1961.
- Ebert, R. W., D. J. McComas, F. Bagenal, and H. A. Elliott, Location, structure, and motion of Jupiter's dusk magnetospheric boundary from 1625 to 2550 RJ, *J. Geophys. Res.*, *115*, 12,223, 2010.
- Echer, E.; Zarka, P.; Gonzalez, W. D.; Morioka, A.; Denis, L., Solar wind effects on Jupiter non-Io DAM emissions during Ulysses distant encounter (2003-2004), *A. & A.*, *519*, A84, 2010
- Elsner, R. F., N. Lugaz, J. H. Waite, T. E. Cravens, G. R. Gladstone, P. Ford, D. Grodent, A. Bhardwaj, R. J. MacDowall, M. D. Desch, and T. Majeed, Simultaneous Chandra X ray, Hubble Space Telescope ultraviolet, and Ulysses radio observations of Jupiter's aurora, *J. Geophys. Res.*, *110*, 1207, 2005a.
- Elsner, R. F., B. D. Ramsey, J. H. Waite, P. Rehak, R. E. Johnson, J. F. Cooper, and D. A. Swartz, X-ray probes of magnetospheric interactions with Jupiter's auroral zones, the Galilean satellites, and the Io plasma torus, *Icarus*, *178*, 417–428, 2005b.
- Ergun, R. E., L. Ray, P. A. Delamere, F. Bagenal, V. Dols, and Y.-J. Su, Generation of parallel electric fields in the Jupiter-Io torus wake region, *J. Geophys. Res.*, *114*, 5201, 2009.
- Field, G. B., The Source of Radiation from Jupiter at Decimeter Wavelengths, *J. Geophys. Res.*, *64*, 1169–1177, 1959.
- Frank, L. A., and W. R. Paterson, Plasmas observed with the Galileo spacecraft during its flyby over Io's northern polar region, *J. Geophys. Res.*, *107*, 1220, 2002.
- Fukazawa, K., T. Ogino, and R. J. Walker, Dynamics of the Jovian magnetosphere for northward interplanetary magnetic field (IMF), *Geophys. Res. Lett.*, *32*, 3202, 2005.
- Fukazawa, K., T. Ogino, and R. J. Walker, Configuration and dynamics of the Jovian magnetosphere, *J. Geophys. Res.*, *111*, 10,207, 2006.
- Fukazawa, K., T. Ogino, and R. J. Walker, A simulation study of dynamics in the distant Jovian magnetotail, *J. Geophys. Res.*, *115*, 9219, 2010.
- Garrett, H. B., S. M. Levin, S. J. Bolton, R. W. Evans, and B. Bhattacharya, A revised model of Jupiter's inner electron belts: Updating the Divine radiation model, *Geophys. Res. Lett.*, *32*, 4104, 2005.
- Ge, Y. S., C. T. Russell, and K. K. Khurana, Reconnection sites in Jupiter's magnetotail and relation to Jovian auroras, *Planet. Space Sci.*, *58*, 1455–1469, 2010.
- Gladstone, G. Randall; Stern, S. Alan; Slater, David C.; Versteeg, Maarten; Davis, Michael W.; Retherford, Kurt D.; Young, Leslie A.; Steffl, Andrew J.; Throop, Henry; Parker, Joel Wm.; Weaver, Harold A.; Cheng, Andrew F.; Orton, Glenn S.; Clarke, John T.; Nichols, Jonathan D., Jupiter's Nightside Airglow and Aurora, *Science*, *318*, 229, 2007.
- Goertz, C. K., Detached plasma in Saturn's front side magnetosphere, *Geophys. Res. Lett.*, *10*, 455–458, 1983.
- Gombosi, Tamas I.; Armstrong, Thomas P.; Arridge, Christopher S.; Khurana, Krishan K.; Krimigis, Stamatios M.; Krupp, Norbert; Persoon, Ann M.; Thomsen, Michelle F., Saturn's Magnetospheric Configuration, in *Saturn from Cassini-Huygens*, Dougherty, M. K.; Esposito, L. W.; Krimigis, S. M., Springer, 2009.
- Grocott, A., S. V. Badman, S. W. H. Cowley, S. E. Milan, J. D. Nichols, and T. K. Yeoman, Magnetosonic Mach number dependence of the efficiency of reconnection between planetary

- and interplanetary magnetic fields, *J. Geophys. Res.*, *114*, 7219, 2009.
- Grodent, D., J. T. Clarke, J. Kim, J. H. Waite Jr., and S. W. H. Cowley, Jupiter's main auroral oval observed with HST-STIS, *J. Geophys. Res.*, *108*, 1389, 2003a.
- Grodent, D., J. T. Clarke, J. H. Waite, S. W. H. Cowley, J.-C. Gerard, and J. Kim, Jupiter's polar auroral emissions, *J. Geophys. Res.*, *108*, 1366, 2003b.
- Grodent, D., J.-C. Gerard, J. T. Clarke, G. R. Gladstone, and J. H. Waite, A possible auroral signature of a magnetotail reconnection process on Jupiter, *J. Geophys. Res.*, *109*, 5201, 2004.
- Grodent, D., B. Bonfond, J.-C. Gerard, A. Radioti, J. Gustin, J. T. Clarke, J. Nichols, and J. E. P. Connerney, Auroral evidence of a localized magnetic anomaly in Jupiter's northern hemisphere, *J. Geophys. Res.*, *113*, 9201, 2008.
- Gustin, J.; Cowley, S. W. H.; Gérard, J.-C.; Gladstone, G. R.; Grodent, D.; Clarke, J. T., Characteristics of Jovian morning bright FUV aurora from Hubble Space Telescope/Space Telescope Imaging Spectrograph imaging and spectral observations, *J. Geophys. Res.*, *111*, A09220, 2006.
- Gustin, J., J.-C. Gerard, D. Grodent, G. Gladstone, J. Clarke, W. Pryor, V. Dols, B. Bonfond, A. Radioti, L. Lamy, and J. Ajello, Effects of methane on giant planets UV emissions and implications for the auroral characteristics, *J. Mol. Spectro.*, 2013.
- Hess, S., F. Mottez, P. Zarka, and T. Chust, Generation of the jovian radio decametric arcs from the Io Flux Tube, *J. Geophys. Res.*, *113*, A03209, 2008a.
- Hess, S. B. Cecconi, and P. Zarka, ng of Io-Jupiter decameter arcs, emission beaming and energy source, *Geophys. Res. Lett.*, *35*, L13107, 2008b.
- Hess, S. L. G., P. Delamere, V. Dols, B. Bonfond, and D. Swift, Power transmission and particle acceleration along the Io flux tube, *J. Geophys. Res.*, *115*, 6205, 2010a.
- Hess, S. L. G., A. Petin, P. Zarka, B. Bonfond, and B. Cecconi, Lead angles and emitting electron energies of Io-controlled decameter radio arcs, *Planet. Space Sci.*, *58*, 1188–1198, 2010b.
- Hess, S. L. G., B. Bonfond, P. Zarka, and D. Grodent, Model of the Jovian magnetic field topology constrained by the Io auroral emissions, *J. Geophys. Res.*, *116*, 5217, 2011.
- Hess, S. L. G.; Echer, E.; Zarka, P., Solar wind pressure effects on Jupiter decametric radio emissions independent of Io, *Planet. Space Sci.*, *70*, 114-125, 2012.
- Higgins, C. A., T. D. Carr, and F. Reyes, A new determination of Jupiter's radio rotation period, *Geophys. Res. Lett.*, *23*, 2653–2656, 1996.
- Higgins, C. A., T. D. Carr, F. Reyes, W. B. Greenman, and G. R. Lebo, A redefinition of Jupiter's rotation period, *J. Geophys. Res.*, *102*, 22,033–22,042, 1997.
- Hill, M. E., D. K. Haggerty, R. L. McNutt, and C. P. Paranicas, Energetic particle evidence for magnetic filaments in Jupiter's magnetotail, *J. Geophys. Res.*, *114*, 11,201, 2009.
- Hill, T. W., Inertial limit on corotation, *J. Geophys. Res.*, *84*, 6554–6558, 1979.
- Hill, T. W., The Jovian auroral oval, *J. Geophys. Res.*, *106*, 8101–8108, 2001.
- Hill, T. W., and V. M. Vasylunas, Jovian auroral signature of Io's corotational wake, *J. Geophys. Res.*, *107*, 1464, 2002.
- Hospodarsky, G. B.; Kurth, W. S.; Cecconi, B.; Gurnett, D. A.; Kaiser, M. L.; Desch, M. D.; Zarka, P., Simultaneous observations of Jovian quasi-periodic radio emissions by the Galileo and Cassini spacecraft, *J. Geophys. Res.*, *109*, A09S07, 2004.
- Huang, T. S., and T. W. Hill, Corotation lag of the Jovian atmosphere, ionosphere, and magnetosphere, *J. Geophys. Res.*, *94*, 3761–3765, 1989.
- Huddleston, D. E., C. T. Russell, M. G. Kivelson, K. K. Khurana, and L. Bennett, Location and shape of the Jovian magnetopause and bow shock, *J. Geophys. Res.*, *103*, 20,075–20,082, 1998.

- Hui, Y., D. R. Schultz, V. A. Kharchenko, A. Bhardwaj, G. Branduardi-Raymont, P. C. Stancil, T. E. Cravens, C. M. Lisse, and A. Dalgarno, Comparative analysis and variability of the Jovian X-ray spectra detected by the Chandra and XMM-Newton observatories, *J. Geophys. Res.*, *115*, 7102, 2010.
- Jackman C.M., N. Achilleos, E.J. Bunce, S.W.H. Cowley, M.K. Dougherty, G.H. Jones, and S.E. Milan, interplanetary magnetic field conditions at ~ 9 A.U. during the declining phase of the solar cycle and its implications for Saturn's magnetospheric dynamics, *J. Geophys. Res.*, *109*, 2004.
- Jia, X., M. G. Kivelson, K. K. Khurana, and R. Walker, Magnetic fields of the satellites of Jupiter and Saturn, *Space Sci. Rev.*, *152*, 271–305, 2009.
- Jones, S. T. and Y.-J. Su, Role of dispersive Alfvén waves in generating parallel electric fields along the Io-Jupiter fluxtube, *J. Geophys. Res.*, *113*, A12205, 2008
- Joy, S. P., M. G. Kivelson, R. J. Walker, K. K. Khurana, C. T. Russell, and T. Ogino, Probabilistic models of the Jovian magnetopause and bow shock locations, *J. Geophys. Res.*, *107*, 1309, 2002.
- Kanani, S. J., C. S. Arridge, G. H. Jones, A. N. Fazakerley, H. J. McAndrews, N. Sergis, S. M. Krimigis, M. K. Dougherty, A. J. Coates, D. T. Young, K. C. Hansen, and N. Krupp, A new form of Saturn's magnetopause using a dynamic pressure balance model, based on in situ, multi-instrument Cassini measurements, *J. Geophys. Res.*, *115*, 6207, 2010.
- Kasahara, S., E. A. Kronberg, T. Kimura, C. Tao, S. V. Badman, A. Masters, A. Retino, N. Krupp, and M. Fujimoto, Asymmetric distribution of reconnection jet fronts in the Jovian nightside magnetosphere, *J. Geophys. Res.*, *118*, 375–384, 2013.
- Keiling, A., E. Donovan, F. Bagenal, and T. Karlsson (Eds.), *Auroral Phenomenology and Magnetospheric Processes*, AGU, Washington, DC, 2012.
- Khurana, K., M. G. Kivelson, V. Vasyliunas, N. Krupp, J. Woch, A. Lagg, B. Mauk, and W. Kurth, The configuration of Jupiter's magnetosphere, in *Jupiter: Planet, Satellites, Magnetosphere*, Bagenal, Dowling, McKinnon (eds), Cambridge University Press, 2004.
- Khurana, K. K., Euler potential models of Jupiter's magnetospheric field, *J. Geophys. Res.*, *102*, 11,295–11,306, 1997.
- Khurana, K. K., Influence of solar wind on Jupiter's magnetosphere deduced from currents in the equatorial plane, *J. Geophys. Res.*, *106*, 25,999–26,016, 2001.
- Khurana, K. K., and M. G. Kivelson, On Jovian plasma sheet structure, *J. Geophys. Res.*, *94*, 11,791–11,803, 1989.
- Khurana, K. K., and H. K. Schwarzl, Global structure of Jupiter's magnetospheric current sheet, *J. Geophys. Res.*, *110*, 7227, 2005.
- Kimura, Tomoki; Tsuchiya, Fuminori; Misawa, Hiroaki; Morioka, Akira; Nozawa, Hiromasa, Occurrence statistics and ray tracing study of Jovian quasiperiodic radio bursts observed from low latitudes, *J. Geophys. Res.*, *115*, A05217, 2010.
- Kivelson, M. G., K. K. Khurana, and R. J. Walker, Sheared magnetic field structure in Jupiter's dusk magnetosphere: Implications for return currents, *J. Geophys. Res.*, *107*, 1116, 2002.
- Kivelson, M. G., F. Bagenal, W. S. Kurth, F. M. Neubauer, C. Paranicas, and J. Saur, Magnetospheric interactions with satellites, in *Jupiter: Planet, Satellites, Magnetosphere*, F. Bagenal, T. E. Dowling, and W. B. McKinnon (Eds.), Cambridge University Press, 2004.
- Kivelson, M. G., and D. J. Southwood, Dynamical consequences of two modes of centrifugal instability in Jupiter's outer magnetosphere, *J. Geophys. Res.*, *110*, 12,209, 2005.
- Kivelson, M., and F. Bagenal, Planetary Magnetospheres, in *Encyclopedia of the Solar System*, McFadden, Weissman, Johnson (eds), 2007.
- Kivelson, M. G., Planetary Magnetospheres, in *Handbook of the Solar-Terrestrial Environment*, Y.

- Kamide and A. C.-L. Chian (Eds.), 2007.
- Kronberg, E. A., J. Woch, N. Krupp, A. Lagg, K. K. Khurana, and K.-H. Glassmeier, Mass release at Jupiter: Substorm-like processes in the Jovian magnetotail, *J. Geophys. Res.*, *110*, 3211, 2005.
- Kronberg, E. A., K.-H. Glassmeier, J. Woch, N. Krupp, A. Lagg, and M. K. Dougherty, A possible intrinsic mechanism for the quasi-periodic dynamics of the Jovian magnetosphere, *J. Geophys. Res.*, *112*, 5203, 2007.
- Kronberg, E. A., J. Woch, N. Krupp, A. Lagg, P. W. Daly, and A. Korth, Comparison of periodic substorms at Jupiter and Earth, *J. Geophys. Res.*, *113*, 4212, 2008.
- Krupp, N., V. Vasyliunas, J. Woch, A. Lagg, K. Khurana, M. Kivelson, B. Mauk, E. Roelof, D. Williams, S. Krimigis, W. Kurth, L. Frank, and W. Paterson, Dynamics of the jovian magnetosphere, in *Jupiter: Planet, Satellites, Magnetosphere*, F. Bagenal, T. E. Dowling, and W. B. McKinnon (Eds.), Cambridge University Press.
- Kurth, W. S., Comparative observations of plasma waves at the outer planets, *Adv. Space Res.*, *12*, 83–90, 1992.
- Kurth, W. S.; Bunce, E. J.; Clarke, J. T.; Crary, F. J.; Grodent, D. C.; Ingersoll, A. P.; Dyudina, U. A.; Lamy, L.; Mitchell, D. G.; Persoon, A. M.; Pryor, W. R.; Saur, J.; Stallard, T., Auroral Processes, in *Saturn from Cassini-Huygens*, Dougherty, M. K.; Esposito, L. W.; Krimigis, S. M., Springer, 2009.
- Ladreiter, H. P., P. Zarka, and A. Lacacheux, Direction finding study of Jovian hectometric and broadband kilometric radio emissions: Evidence for their auroral origin, *Planet. Space Sci.*, *42*, 919–931, 1994.
- Lamy, L.; Schippers, P.; Zarka, P.; Cecconi, B.; Arridge, C. S.; Dougherty, M. K.; Louarn, P.; André, N.; Kurth, W. S.; Mutel, R. L.; Gurnett, D. A.; Coates, A. J., Properties of Saturn kilometric radiation measured within its source region, *Geophys. Res. Lett.*, *39*, L12104, 2010.
- Lindal, G. F., G. E. Wood, G. S. Levy, J. D. Anderson, D. N. Sweetnam, H. B. Hotz, B. J. Buckles, D. P. Holmes, P. E. Doms, V. R. Eshleman, G. L. Tyler, and T. A. Croft, The atmosphere of Jupiter: An analysis of the Voyager radio occultation measurements, *J. Geophys. Res.*, *86*, 8721–8727, 1981.
- Masters, A., N. Achilleos, C. Bertucci, M. K. Dougherty, S. J. Kanani, C. S. Arridge, H. J. McAndrews, and A. J. Coates, Surface waves on Saturn’s dawn flank magnetopause driven by the Kelvin-Helmholtz instability, *Planet. Space Sci.*, *57*, 1769–1778, 2009.
- Masters, A., N. Achilleos, M. G. Kivelson, N. Sergis, M. K. Dougherty, M. F. Thomsen, C. S. Arridge, S. M. Krimigis, H. J. McAndrews, S. J. Kanani, N. Krupp, and A. J. Coates, Cassini observations of a Kelvin-Helmholtz vortex in Saturn’s outer magnetosphere, *J. Geophys. Res.*, *115*, 7225, 2010.
- Masters, A., D. G. Mitchell, A. J. Coates, and M. K. Dougherty, Saturn’s low-latitude boundary layer: 1. Properties and variability, *J. Geophys. Res.*, *116*, 6210, 2011a.
- Masters, A., A. P. Walsh, A. N. Fazakerley, A. J. Coates, and M. K. Dougherty, Saturn’s low-latitude boundary layer: 2. Electron structure, *J. Geophys. Res.*, *116*, 6211, 2011b.
- Masters, A., J. P. Eastwood, M. Swisdak, M. F. Thomsen, C. T. Russell, N. Sergis, F. J. Crary, M. K. Dougherty, A. J. Coates, and S. M. Krimigis, The importance of plasma β conditions for magnetic reconnection at Saturn’s magnetopause, *Geophys. Res. Lett.*, *39*, 8103, 2012.
- Mauk, B. H., D. G. Mitchell, R. W. McEntire, C. P. Paranicas, E. C. Roelof, D. J. Williams, S. M. Krimigis, and A. Lagg, Energetic ion characteristics and neutral gas interactions in Jupiter’s magnetosphere, *J. Geophys. Res.*, *109*, 9, 2004.
- Mauk, B. H., and J. Saur, Equatorial electron beams and auroral structuring at Jupiter, *J. Geophys.*

- Res.*, 112, 10,221, 2007.
- Mauk, B. H.; Hamilton, D. C.; Hill, T. W.; Hospodarsky, G. B.; Johnson, R. E.; Paranicas, C.; Roussos, E.; Russell, C. T.; Shemansky, D. E.; Sittler, E. C.; Thorne, R. M., Fundamental Plasma Processes in Saturn's Magnetosphere, in *Saturn from Cassini-Huygens*, Dougherty, M. K.; Esposito, L. W.; Krimigis, S. M., Springer, 2009.
- Mauk, B., and F. Bagenal, Auroral Phenomenology and Magnetospheric Processes: Earth and Other Planets, in *Auroral Phenomenology and Magnetospheric Processes*, Keiling, Donovan, Bagenal, Karlsson (eds), AGU monograph series, Washington DC, 2012.
- McComas, D. J., and F. Bagenal, Jupiter: A fundamentally different magnetospheric interaction with the solar wind, *Geophys. Res. Lett.*, 34, 20,106, 2007.
- McComas, D. J., and F. Bagenal, Reply to comment by S. W. H. Cowley et al. on “Jupiter: A fundamentally different magnetospheric interaction with the solar wind”, *Geophys. Res. Lett.*, 35, 10,103, 2008.
- McComas, D. J., F. Allegrini, F. Bagenal, F. Cray, R. W. Ebert, H. Elliott, A. Stern, and P. Valek, Diverse Plasma Populations and Structures in Jupiter’s Magnetotail, *Science*, 318, 217, 2007.
- McFadden, J. P., C. W. Carlson, and R. E. Ergun, Microstructure of the auroral acceleration region as observed by FAST, *J. Geophys. Res.*, 104, 14,453–14,480, 1999.
- McNutt, R. L., D. K. Haggerty, M. E. Hill, S. M. Krimigis, S. Livi, G. C. Ho, R. S. Gurnee, B. H. Mauk, D. G. Mitchell, E. C. Roelof, D. J. McComas, F. Bagenal, H. A. Elliott, L. E. Brown, M. Kusterer, J. Vandegriff, S. A. Stern, H. A. Weaver, J. R. Spencer, and J. M. Moore, Energetic Particles in the Jovian Magnetotail, *Science*, 318, 220, 2007.
- McNutt, R. L., Jr., J. W. Belcher, J. D. Sullivan, F. Bagenal, and H. S. Bridge, Departure from rigid co-rotation of plasma in Jupiter’s dayside magnetosphere, *Nature*, 280, 803, 1979.
- Mitchell, D. G.; Carbary, J. F.; Cowley, S. W. H.; Hill, T. W.; Zarka, P., The Dynamics of Saturn's Magnetosphere, in *Saturn from Cassini-Huygens*, Dougherty, M. K.; Esposito, L. W.; Krimigis, S. M., Springer, 2009.
- Morris, D., and G. L. Berge, Measurements of the polarization and angular extent of the decametric radiation of Jupiter, *Ap. J.*, 136, 276–282, 1962.
- Mutel, R. L.; Menietti, J. D.; Gurnett, D. A.; Kurth, W.; Schippers, P.; Lynch, C.; Lamy, L.; Arridge, C.; Cecconi, B., CMI growth rates for Saturnian kilometric radiation, *Geophys. Res. Lett.*, 37, L19105, 2010
- Nichols, J., and S. Cowley, Magnetosphere-ionosphere coupling currents in Jupiter’s middle magnetosphere: effect of precipitation-induced enhancement of the ionospheric Pedersen conductivity, *Ann. Geophys.*, 22, 1799–1827, 2004.
- Nichols, J. D., Magnetosphere-ionosphere coupling in Jupiter’s middle magnetosphere: Computations including a self-consistent current sheet magnetic field model, *J. Geophys. Res.*, 116, 10,232, 2011.
- Nichols, J. D., S. W. H. Cowley, and D. J. McComas, Magnetopause reconnection rate estimates for Jupiter’s magnetosphere based on interplanetary measurements at ~5AU, *Ann. Geophys.*, 24, 393–406, 2006.
- Nichols, J. D., E. J. Bunce, J. T. Clarke, S. W. H. Cowley, J.-C. Ge’rard, D. Grodent, and W. R. Pryor, Response of Jupiter’s UV auroras to interplanetary conditions as observed by the Hubble Space Telescope during the Cassini flyby campaign, *J. Geophys. Res.*, 112, A02203, 2007
- Nichols, J. D., J. T. Clarke, J. C. Gerard, and D. Grodent, Observations of Jovian polar auroral filaments, *Geophys. Res. Lett.*, 36, 8101, 2009a.
- Nichols, J. D., J. T. Clarke, J. C. Gerard, D. Grodent, and K. C. Hansen, Variation of different

- components of Jupiter's auroral emission, *J. Geophys. Res.*, *114*, 6210, 2009b.
- Northrop, T. G. and T. J. Birmingham, Adiabatic Charged Particle Motion in Rapidly Rotating Magnetospheres, *J. Geophys. Res.*, *87*, 661-669, 1982.
- Ozak, N., D. R. Schultz, T. E. Cravens, V. Kharchenko, and Y.-W. Hui, Auroral X-ray emission at Jupiter: Depth effects, *J. Geophys. Res.*, *115*, 11,306, 2010.
- Pallier, L., and R. Prange, More about the structure of the high latitude Jovian aurorae, *Planet. Space Sci.*, *49*, 1159–1173, 2001.
- Pallier, L., and R. Prange, Detection of the southern counterpart of the Jovian northern polar cusp: Shared properties, *Geophys. Res. Lett.*, *31*, L06701, 2004.
- Paschmann, G., S. Haaland, and R. Treumann (eds), Auroral Plasma Physics, *Space Sci. Rev.*, *103*, 2002.
- Pontius, D. H., Jr., and T. W. Hill, Departure from corotation of the Io plasma torus: Local plasma production, *Geophys. Res. Lett.*, *9*, 1321–1324, 1982.
- Prange, R., P. Zarka, G. E. Ballester, T. A. Livengood, L. Denis, T. D. Carr, F. Reyes, S. J. Bame, and H. W. Moos, Correlated variations of UV and Radio emissions during an outstanding Jovian auroral event, *J. Geophys. Res.*, *98*, 18,779–18,791, 1993
- Queinnee, J., and P. Zarka, Io-controlled decameter arcs and Io-Jupiter interaction, *J. Geophys. Res.*, *103*, 26,649–26,666, 1998.
- Radioti, A., D. Grodent, J.-C. Gerard, B. Bonfond, and J. T. Clarke, Auroral polar dawn spots: Signatures of internally driven reconnection processes at Jupiter's magnetotail, *Geophys. Res. Lett.*, *35*, 3104, 2008.
- Radioti, A., D. Grodent, J.-C. Gerard, and B. Bonfond, Auroral signatures of flow bursts released during magnetotail reconnection at Jupiter, *J. Geophys. Res.*, *115*, 7214, 2010.
- Radioti, A., D. Grodent, J.-C. Gerard, M. F. Vogt, M. Lystrup, and B. Bonfond, Nightside reconnection at Jupiter: Auroral and magnetic field observations from 26 July 1998, *J. Geophys. Res.*, *116*, 3221, 2011.
- Ray, L. C., R. E. Ergun, P. A. Delamere, and F. Bagenal, Magnetosphere-ionosphere coupling at Jupiter: Effect of field-aligned potentials on angular momentum transport, *J. Geophys. Res.*, *115*, 9211, 2010.
- Ray, L.C., N. Achilleos, Y.N. Yates, Including field-aligned potentials in the coupling between Jupiter's thermosphere, ionosphere, and magnetosphere, *Planet. Space Sci.*, *62*, submitted, 2013
- Reiner, M. J.; Fainberg, J.; Stone, R. G.; Kaiser, M. L.; Desch, M. D.; Manning, R.; Zarka, P.; Pedersen, B.-M., Source characteristics of Jovian narrow-band kilometric radio emissions, *J. Geophys. Res.*, *98*, 13,163-13,176, 1993.
- Roussos, E., N. Krupp, C. P. Paranicas, P. Kollmann, D. G. Mitchell, S. M. Krimigis, T. P. Armstrong, D. R. Went, M. K. Dougherty, and G. H. Jones, Long- and short-term variability of Saturn's ionic radiation belts, *J. Geophys. Res.*, *116*, 2217, 2011.
- Roux, A.; Hilgers, A.; de Feraudy, H.; Le Queau, D.; Louarn, P.; Perraut, S.; Bahnsen, A.; Jespersen, M.; Ungstrup, E.; Andre, M., Auroral kilometric radiation sources - In situ and remote observations from Viking, *J. Geophys. Res.*, *98*, 11,657-11,670, 1993.
- Ryabov, V. B.; Ryabov, B. P.; Vavriv, D. M.; Zarka, P.; Kozhin, R.; Vinogradov, V. V.; Shevchenko, V. A., Jupiter S-bursts: Narrow-band origin of microsecond subpulses, *J. Geophys. Res.*, *112*, A09206, 2007.
- Russell, C. T., Outer planet magnetospheres: a tutorial, *Advances in Space Research*, *33*, 2004–2020, 2004.
- Russell, C. T., New horizons in planetary magnetospheres, *Adv. Space Res.*, *37*, 1467–1481, 2006.
- Russell, C. T., K. K. Khurana, M. G. Kivelson, and D. E. Huddleston, Substorms at Jupiter:

- Galileo Observations of Transient Reconnection in the Near Tail, *Adv. Space Res.*, 26, 1499–1504, 2000.
- Russell, C. T., Z. J. Yu, and M. G. Kivelson, The rotation period of Jupiter, *Geophys. Res. Lett.*, 28, 1911–1912, 2001.
- Santos-Costa, D., and S. J. Bolton, Discussing the processes constraining the Jovian synchrotron radio emission's features, *Planet. Space Sci.*, 56, 326–345, 2008.
- Santos-Costa, D., S. J. Bolton, R. M. Thorne, Y. Miyoshi, and S. M. Levin, Investigating the origins of the Jovian decimetric emission's variability, *J. Geophys. Res.*, 113, 1204, 2008.
- Saur, J., A. Pouquet, and W. H. Matthaeus, An acceleration mechanism for the generation of the main auroral oval on Jupiter, *Geophys. Res. Lett.*, 30, 1260, 2003.
- Saur, J., F. M. Neubauer, J. E. P. Connerney, P. Zarka, and M. G. Kivelson, Plasma interaction of Io with its plasma torus, in *Jupiter: Planet, Satellites, Magnetosphere*, F. Bagenal, T. E. Dowling, and W. B. McKinnon (Eds.), Cambridge University Press, 2004.
- Schardt, A. W., and C. K. Goertz, High-energy particles, in *Physics of the Jovian Magnetosphere*, A. J. Dessler (ed), Cambridge University Press, 1983.
- Schippers, P.; Arridge, C. S.; Menietti, J. D.; Gurnett, D. A.; Lamy, L.; Cecconi, B.; Mitchell, D. G.; André, N.; Kurth, W. S.; Grimald, S.; Dougherty, M. K.; Coates, A. J.; Krupp, N.; Young, D. T., Auroral electron distributions within and close to the Saturn kilometric radiation source region, *J. Geophys. Res.*, 116, A05203, 2011
- Sergis, N., S. M. Krimigis, E. C. Roelof, C. S. Arridge, A. M. Rymer, D. G. Mitchell, D. C. Hamilton, N. Krupp, M. F. Thomsen, M. K. Dougherty, A. J. Coates, and D. T. Young, Particle pressure, inertial force, and ring current density profiles in the magnetosphere of Saturn, based on Cassini measurements, *Geophys. Res. Lett.*, 37, 2102, 2010.
- Siscoe, G. L., Towards a comparative theory of magnetospheres, in *Solar System Plasma Physics Vol. 2*, Parker, Kennel, Lanzerotti (eds), North-Holland Publishing, 1979.
- Slavin, J. A., E. J. Smith, J. R. Spreiter, and S. S. Stahara, Solar wind flow about the outer planets: Gas dynamic modeling of the Jupiter and Saturn bow shocks, *J. Geophys. Res.*, 90, 6275–6286, 1985.
- Smith, C. G. A.; Aylward, A. D., Coupled rotational dynamics of Jupiter's thermosphere and magnetosphere, *Ann. Geophys.*, 23, 199-230, 2009.
- Southwood, D., and M. Kivelson, A new perspective concerning the influence of the solar wind on Jupiter, *J. Geophys. Res.*, 106, 6123– 6130, 2001.
- Stallard, T., S. Miller, G. Millward, and R. D. Joseph, On the Dynamics of the Jovian Ionosphere and Thermosphere. I: The Measurement of Ion Winds, *Icarus*, 154, 475–491, 2001.
- Stallard, T. S., S. Miller, S. W. H. Cowley, and E. J. Bunce, Jupiter's polar ionospheric flows: Measured intensity and velocity variations poleward of the main auroral oval, *Geophys. Res. Lett.*, 30, 1221, 2003.
- Steffl, A. J., A. I. F. Stewart, and F. Bagenal, Cassini UVIS observations of the Io plasma torus. I: Initial results, *Icarus*, 172, 78–90, 2004a.
- Steffl, A. J., F. Bagenal, and A. I. F. Stewart, Cassini UVIS observations of the Io plasma torus. II: Radial variations, *Icarus*, 172, 91–103, 2004b.
- Steffl, A. J., P. A. Delamere, and F. Bagenal, Cassini UVIS observations of the Io plasma torus. III: Observations of temporal and azimuthal variability, *Icarus*, 180, 124–140, 2006.
- Steffl, A. J., P. A. Delamere, and F. Bagenal, Cassini UVIS observations of the Io plasma torus. IV: Modeling temporal and azimuthal variability, *Icarus*, 194, 153–165, 2008.
- Su, Yi-Jiun, Robert E. Ergun, Fran Bagenal, and Peter A. Delamere, Io-related Jovian auroral arcs: Modeling parallel electric fields, *J. Geophys. Res.*, 108, 1094, 2003.
- Tao, C., S. V. Badman, and M. Fujimoto, UV and IR auroral emission model for the outer planets:

- Jupiter and Saturn comparison, *Icarus*, 213, 581–592, 2011.
- Tao, C., S. V. Badman, T. Uno, and M. Fujimoto, On the feasibility of characterizing jovian auroral electrons via H_3^+ infrared line-emission analysis, *Icarus*, 221, 236–247, 2012.
- Thomas, N., F. Bagenal, T. Hill, and J. Wilson, The Io Neutral Clouds and Plasma Torus, in *Jupiter: Planet, Satellites, Magnetosphere*, F. Bagenal, T. E. Dowling, and W. B. McKinnon (Eds.), Cambridge University Press, 2004.
- Trainor, J. H., F. B. McDonald, D. E. Stillwell, B. J. Teegarden, and W. R. Webber, Jovian protons and electrons: Pioneer 11, *Science*, 188, 462–465, 1975.
- Van Allen, J. A., and F. Bagenal, Planetary Magnetospheres and the Interplanetary Medium, Beatty, in *The New Solar System*, Collins-Petersen, Chaikin, (eds), Cambridge University Press, 1999.
- Vasavada, A. R., A. H. Bouchez, A. P. Ingersoll, B. Little, C. D. Anger, and Galileo SSI Team, Jupiter’s visible aurora and Io footprint, *J. Geophys. Res.*, 104, 27,133–27,142, 1999.
- Vasyliunas, V. M., Comparative magnetospheres: lessons for Earth, *Adv. Space Res.*, 33, 2113–2120, 2004.
- Vasyliunas, V., Plasma distribution and flow , in *Physics of the Jovian Magnetosphere*, A. J. Dessler (ed), Cambridge University Press, 1983.
- Vasyliunas, V., Fundamentals of Planetary Magnetospheres, in *Heliophysics: Plasma Physics of the Local Cosmos*, C. J. Schrijver, G. L. Siscoe (eds), Cambridge University Press, 2009.
- Vogt, M. F., M. G. Kivelson, K. K. Khurana, S. P. Joy, and R. J. Walker, Reconnection and flows in the Jovian magnetotail as inferred from magnetometer observations, *J. Geophys. Res.*, 115, 6219, 2010.
- Vogt, M. F., M. G. Kivelson, K. K. Khurana, R. J. Walker, B. Bonfond, D. Grodent, and A. Radioti, Improved mapping of Jupiter’s auroral features to magnetospheric sources, *J. Geophys. Res.*, 116 , 3220, 2011.
- Waite, J. H., G. R. Gladstone, W. S. Lewis, R. Goldstein, D. J. McComas, P. Riley, R. J. Walker, P. Robertson, S. Desai, J. T. Clarke, and D. T. Young, An auroral flare at Jupiter, *Nature*, 410, 787–789, 2001.
- Walker, R., and C. Russell, Solar wind interactions with magnetized planets, in *Introduction to Space Physics*, Kivelson, Russell (eds), Cambridge University Press, 1995.
- Walker, R. J., and T. Ogino, A simulation study of currents in the Jovian magnetosphere, *Planet. Space Sci.*, 51, 295–307, 2003.
- Walker, R. J., and C. T. Russell, Flux transfer events at the Jovian magnetopause, *J. Geophys. Res.*, 90, 7397–7404, 1985.
- Woch, J., N. Krupp, and A. Lagg, Particle bursts in the Jovian magnetosphere: Evidence for a near-Jupiter neutral line, *Geophys. Res. Lett.*, 29, 1138, 2002.
- Yates, J. N.; Achilleos, N.; Guio, P., Influence of upstream solar wind on thermospheric flows at Jupiter, *Planet. Space Sci.*, 61, 15-31, 2012.
- Yu, Z. J., and C. T. Russell, Rotation period of Jupiter from the observation of its magnetic field, *Geophys. Res. Lett.*, 36, 20,202, 2009.
- Zarka, P., Auroral radio emissions at the outer planets: Observations and theories, *J. Geophys. Res.*, 103 , 20,159–20,194, 1998.
- Zarka, P., Radio Emissions from the Planets and their Moons, in *Radio Astronomy at Long Wavelengths*, Stone, Weiler, Goldstein, Bougeret, (eds), AGU, Washington DC, 2000.
- Zarka, P., Radio and plasma waves at the outer planets, *Adv. Space Res.*, 33, 2045-2060, 2004.
- Zarka, P., J. Queinnec, and F. J. Crary, Low-frequency limit of Jovian radio emissions and implications on source locations and Io plasma wake, *Planet. Space Sci.*, 49, 1137-1149, 2001.

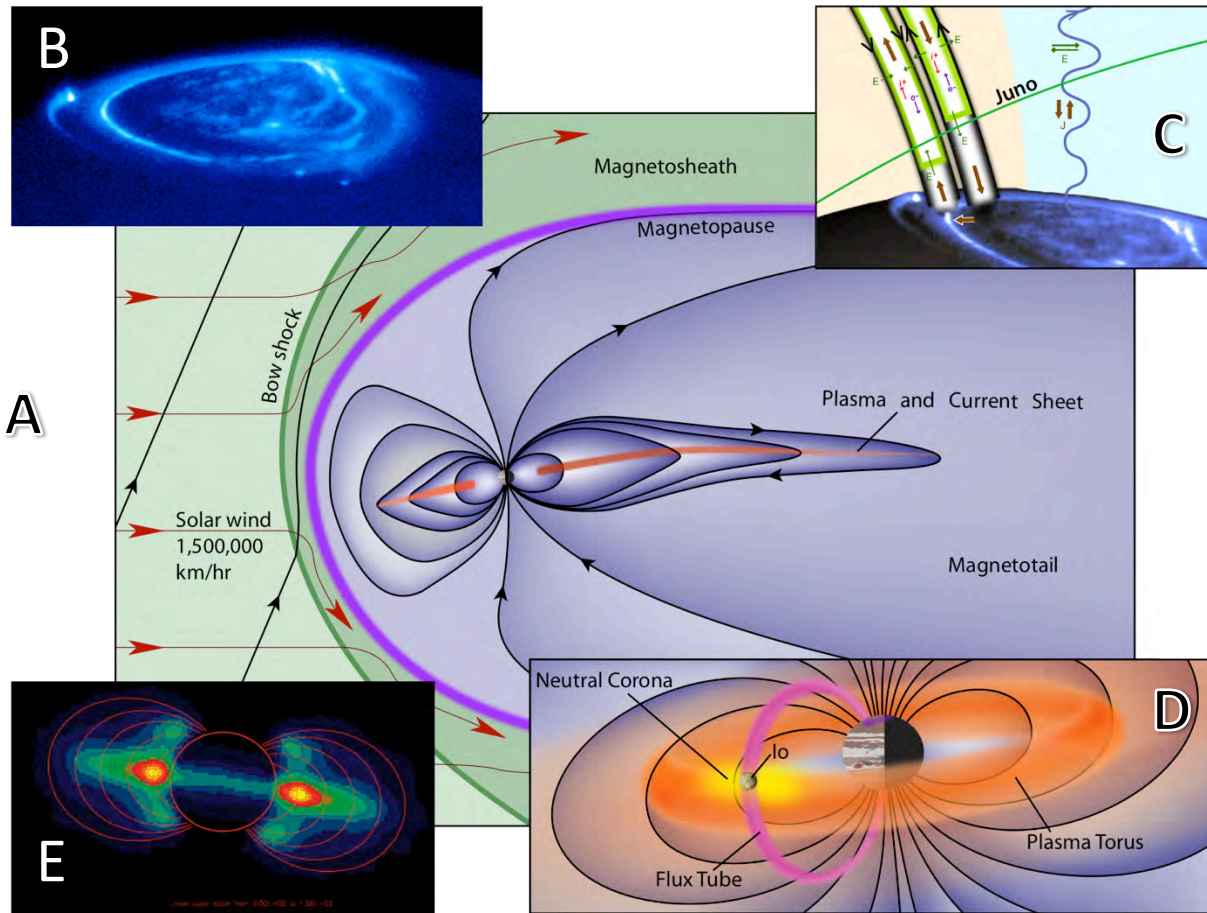


Figure 1: A – The magnetosphere of Jupiter extends an average of 75 jovian radii in the direction towards the Sun, with a tail that stretches beyond the orbit of Saturn >4 AU, and occupies a volume over a thousand times that of the Sun. B - Intense auroral emissions are signatures of the coupling between the planet and the magnetospheric plasmas. C - The *Juno* spacecraft will fly through the regions where the aurora-generating particles are excited. D - The magnetosphere is dominated by a ~ 1 ton/s source of plasma from Io's volcanic gases that forms a toroidal cloud around Jupiter. E - Close to the planet are strong radiation belts comprising energetic (MeV) electrons that emit synchrotron emission.

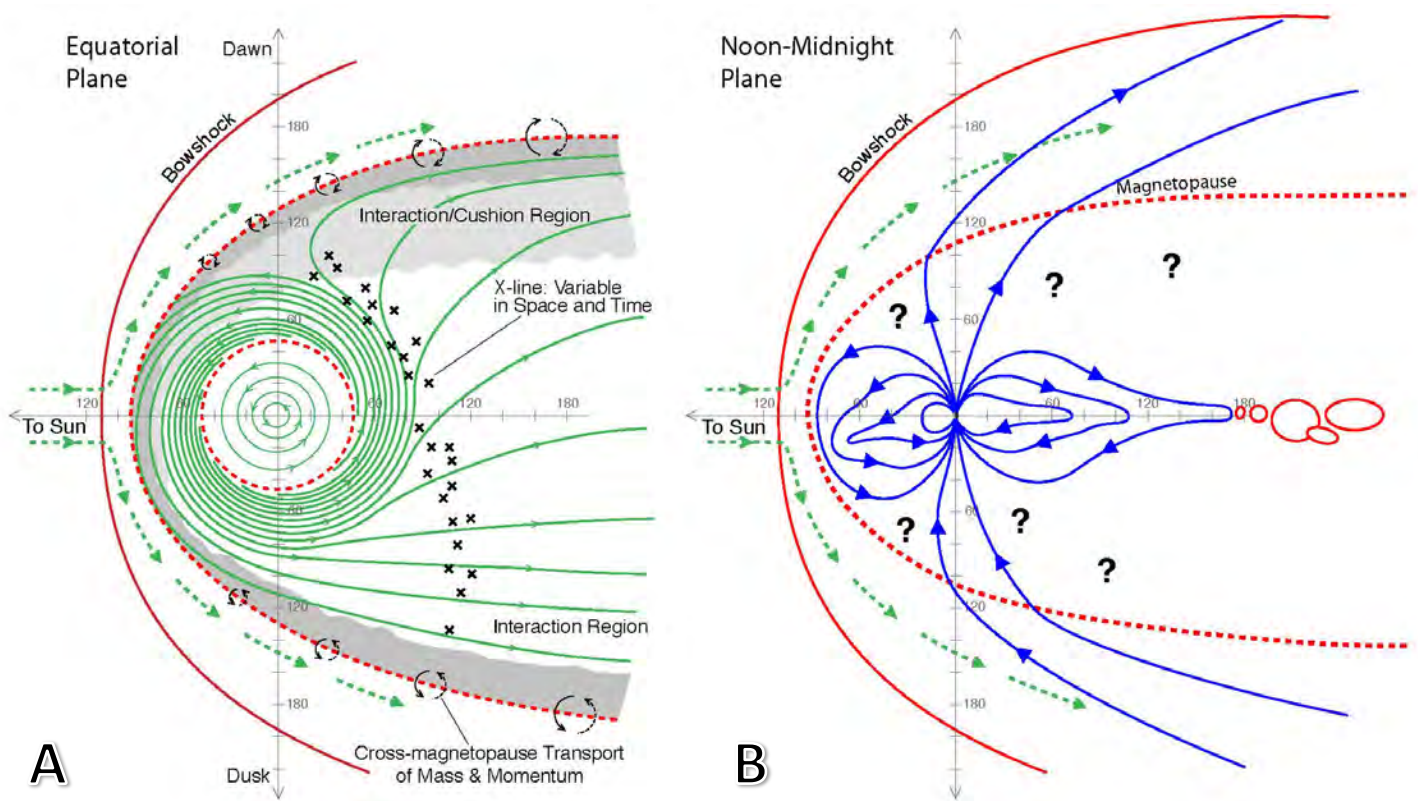


Figure 2: Magnetospheric structure and dynamics. A – While the equatorial plane has been traversed multiple times and is well mapped, the polar region (see noon-midnight plane on right, B) has barely been explored and major questions remain. Blue lines show magnetic field, green lines show flows and red lines show boundaries between plasma regimes. (Based on Vasyliunas 1983; Delamere & Bagenal 2010)

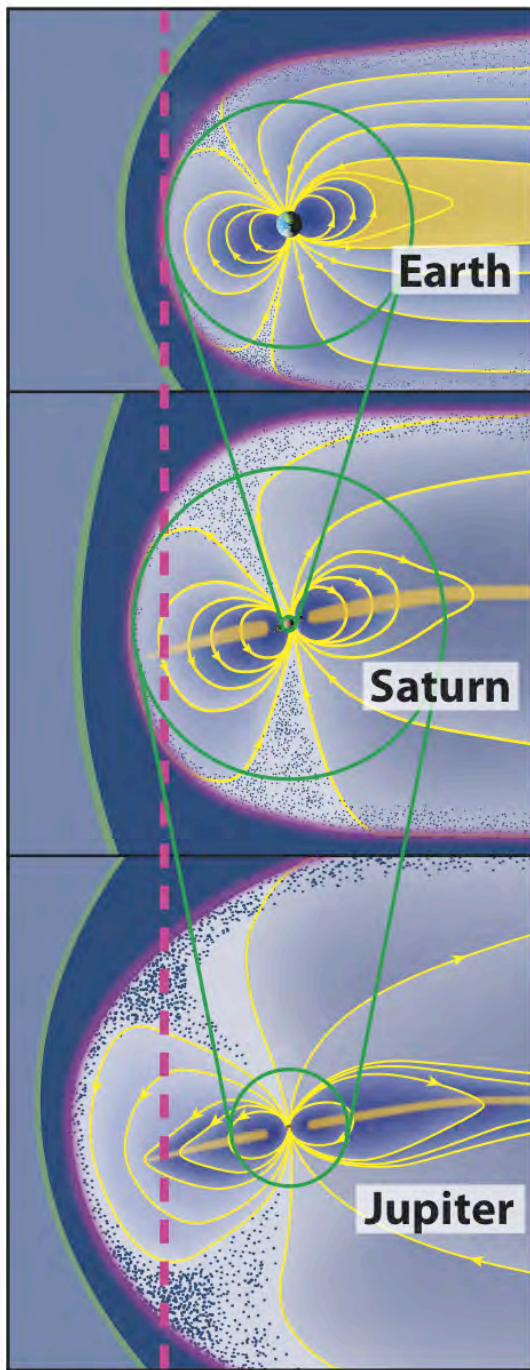


Figure 3: Comparison of the magnetospheres of Earth, Saturn and Jupiter. The green circles show how the magnetosphere of Earth scales to the planet Saturn and how the magnetosphere of Saturn scales to the inner 20% of Jupiter's magnetosphere. The dashed vertical line shows the scale of each magnetosphere for a pure dipole magnetic field with no internal plasma.

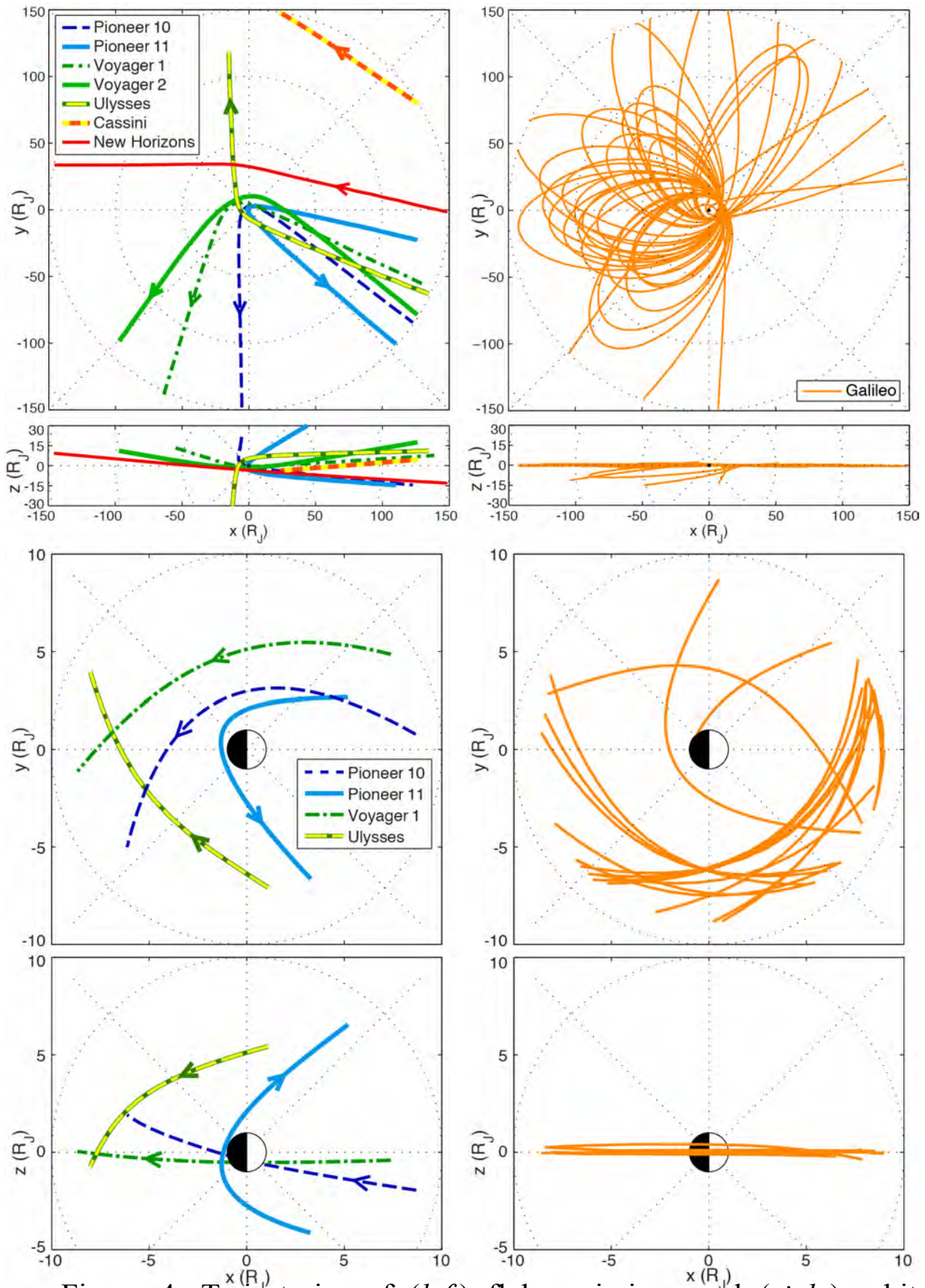


Figure 4: Trajectories of (left) flyby missions and (right) orbiter Galileo. The top 4 plots show positions within 150 R_J of Jupiter. The bottom 4 are limited to within 9 R_J . Note that the Sun is to the right.

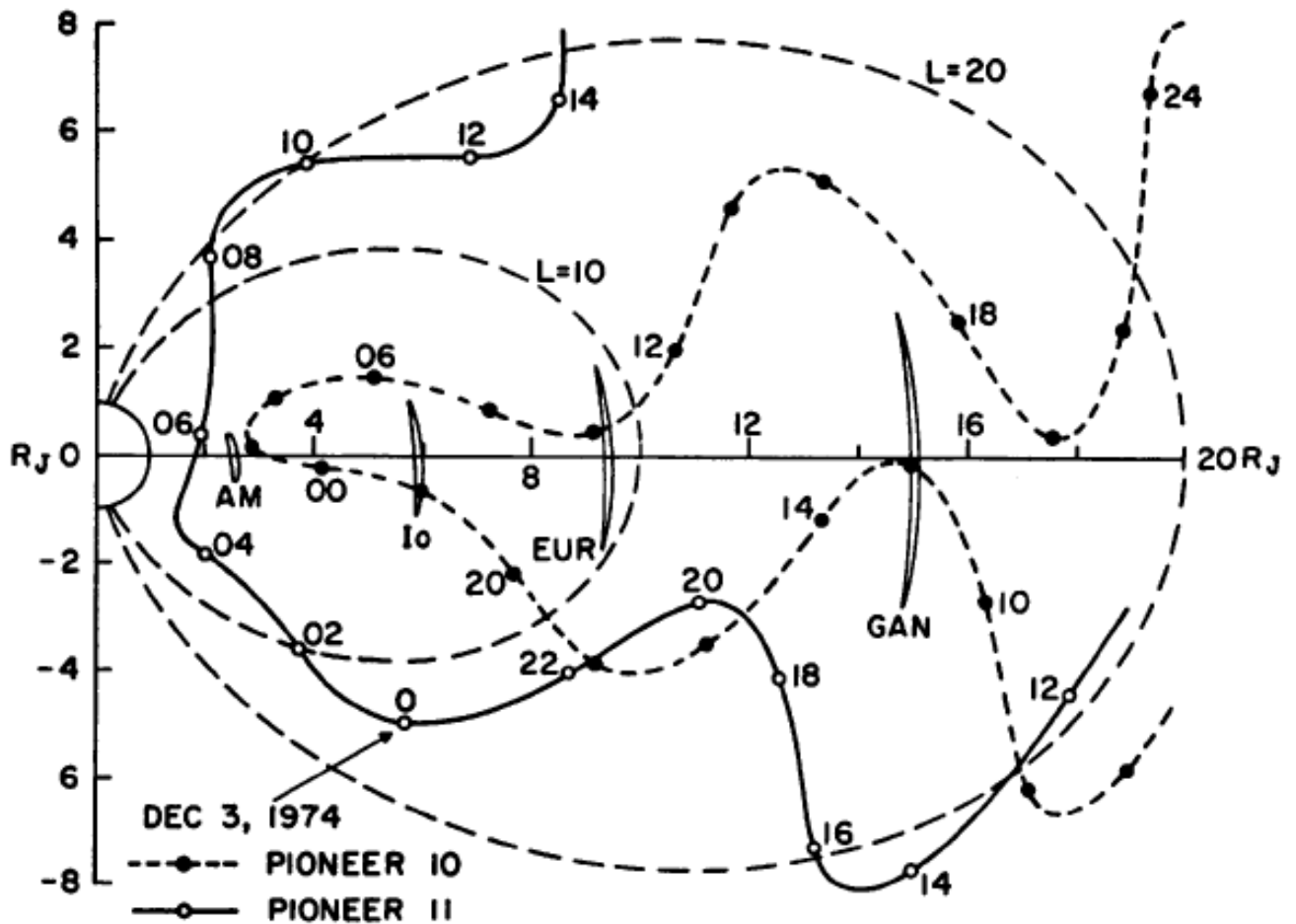


Figure 5: Projection of the trajectories of Pioneer 10 and Pioneer 11 on a magnetic meridian plane of Jupiter based on the (dipolar) D2 magnetic field model. The region sampled by Pioneer 10 was within 20° of the magnetic equator, whereas the Pioneer 11 trajectory was at much higher latitudes, usually above 40° but less than 80° (from Trainor et al. 1975). The dashed lines show the magnetic field lines that map from 10 and 20 R_J at the magnetic equator to the planet. Since the main aurora are generated around the $L=20$ flux shell and beyond, the Pioneer 11 barely entered these auroral field lines for a couple hours at distances of 4 to 6 R_J from the planet, probably above the acceleration region.

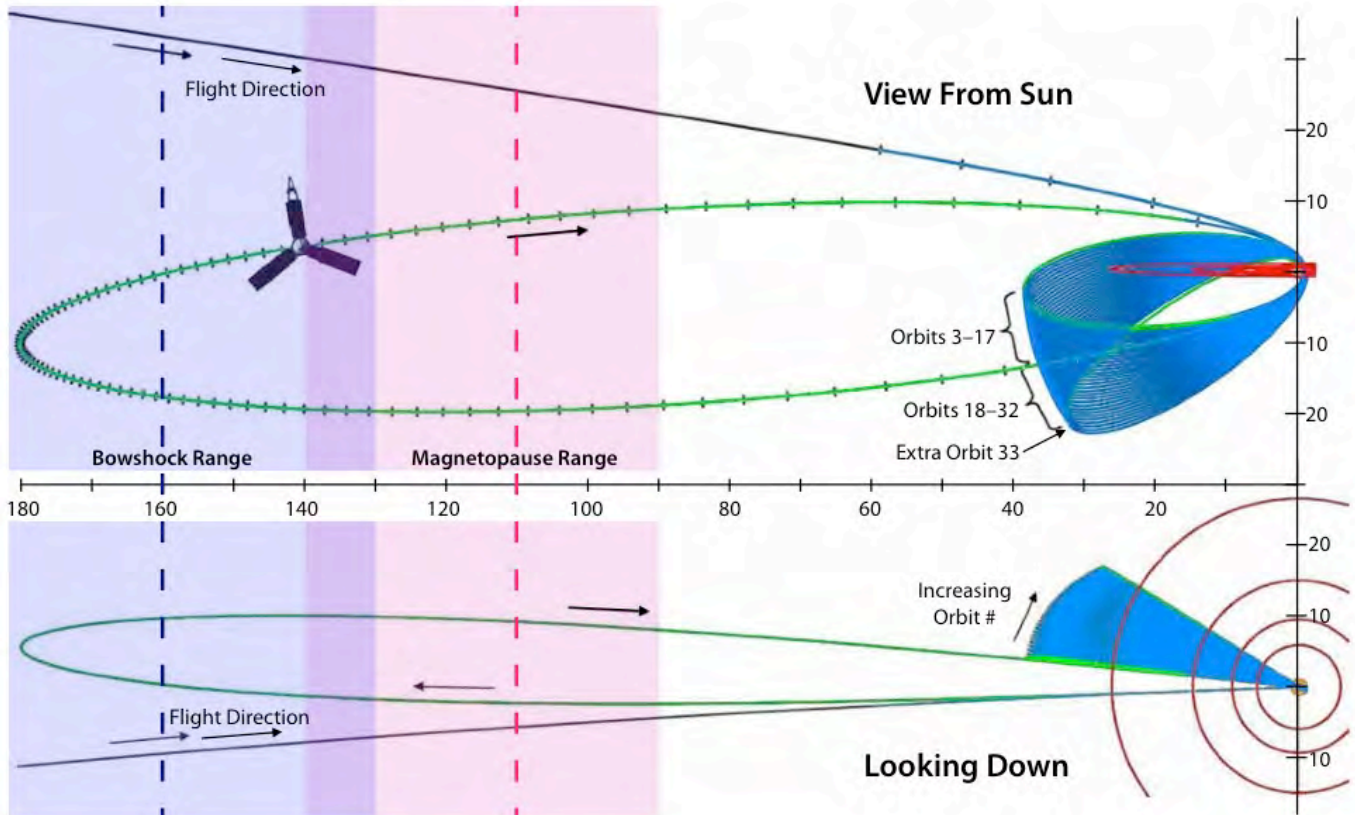


Figure 6: Geometry of *Juno*'s orbits viewed with the dawn flank on the left, (*top*) from the Sun with north up, and (*bottom*) looking down on the system, the Sun below. The pink (purple) shaded regions show the statistical ranges of the magnetopause (bow shock) from Joy et al. (2002). The smaller science orbits (3-33, in blue) precess both in local time and latitude at about 1° per orbit. Orbits of Galilean moons Io, Europa, Ganymede and Callisto are shown in red. The *Juno* spacecraft (not to scale) spins in an anti-clockwise direction as viewed in the top panel at 2 rpm.

Add nominal MP and BS on dawn flank.

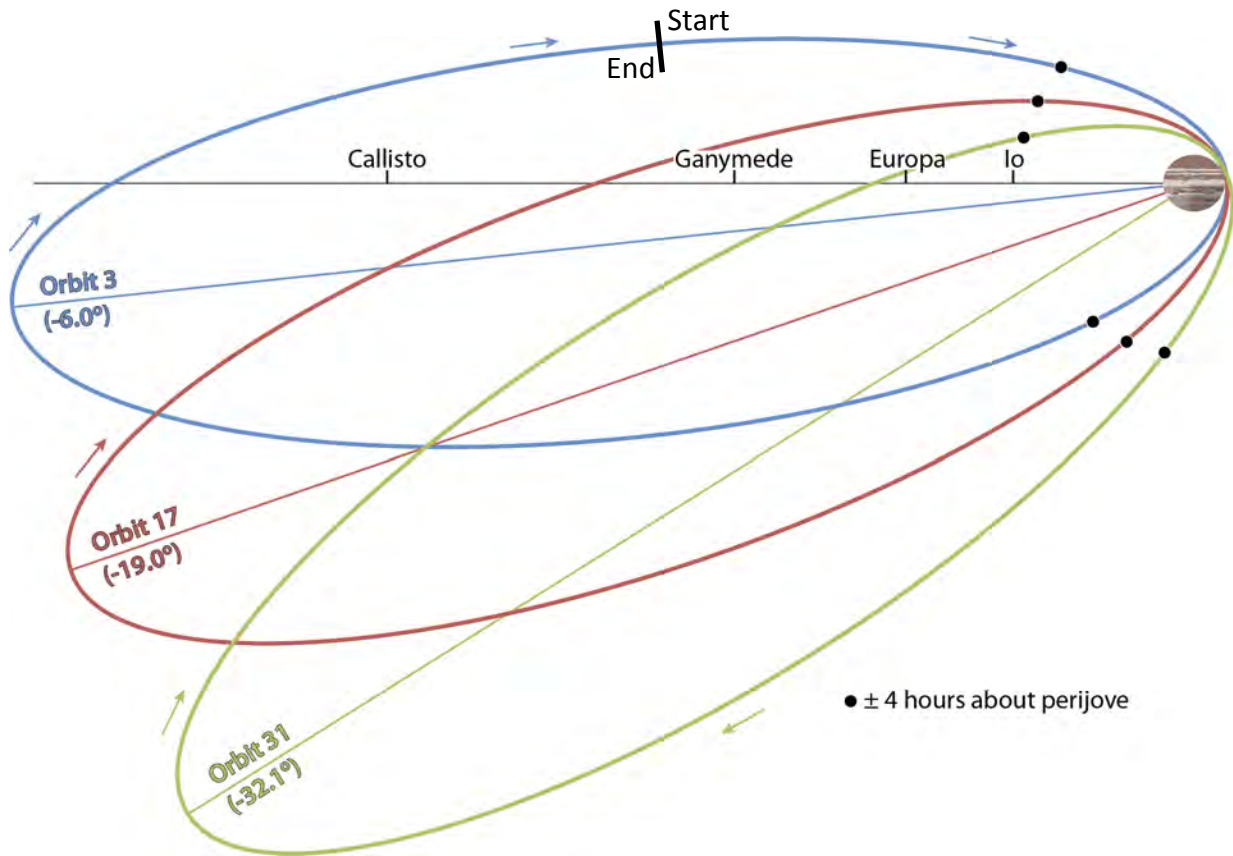


Figure 7: Three selected Juno orbits: early, (PJ3 2016 Nov. 10 16:46), middle (PJ17 2017 Apr. 13 07:27), end (PJ31 2017 Sep. 13 21:49) showing precession of line of apsides relative to Jupiter's geographic equator. The orbits are numbered according to the sequence of perijoves (PJ), where PJ0 is the initial orbit insertion, with the start/end of a numbered orbit about a day before perijove. The full orbit period is about 11 days. The ± 4 -hour periods of high-cadence observations around perijove are indicated by dots.

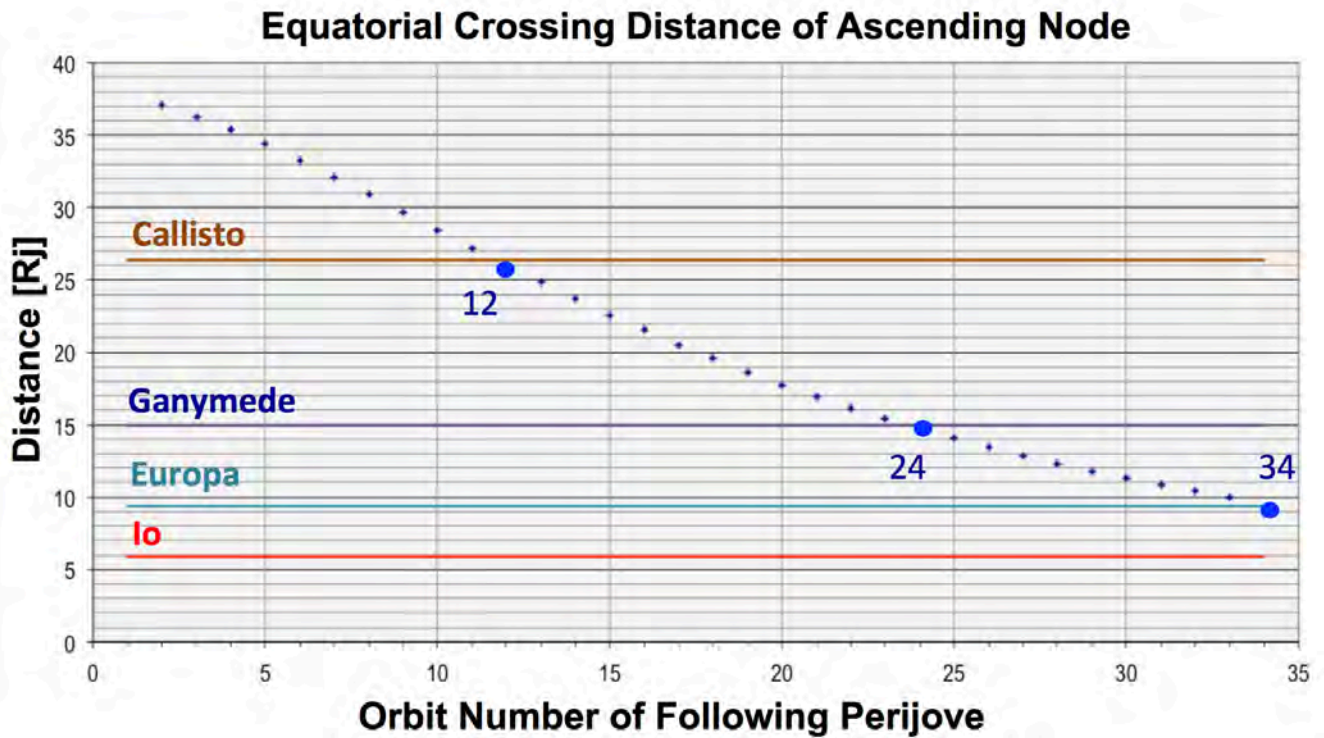


Figure 8: Distance that the Juno orbits cross the equatorial plane with the orbits of Callisto (26.33 R_j), Ganymede (14.97 R_j), Europa (9.38 R_j) being crossed on the orbits before perijoves 12, 24 and 34. The planned prime mission for Juno has the spacecraft entering Jupiter on PJ34 with the result that Juno does not come close to the orbit of Io (5.89 R_j).

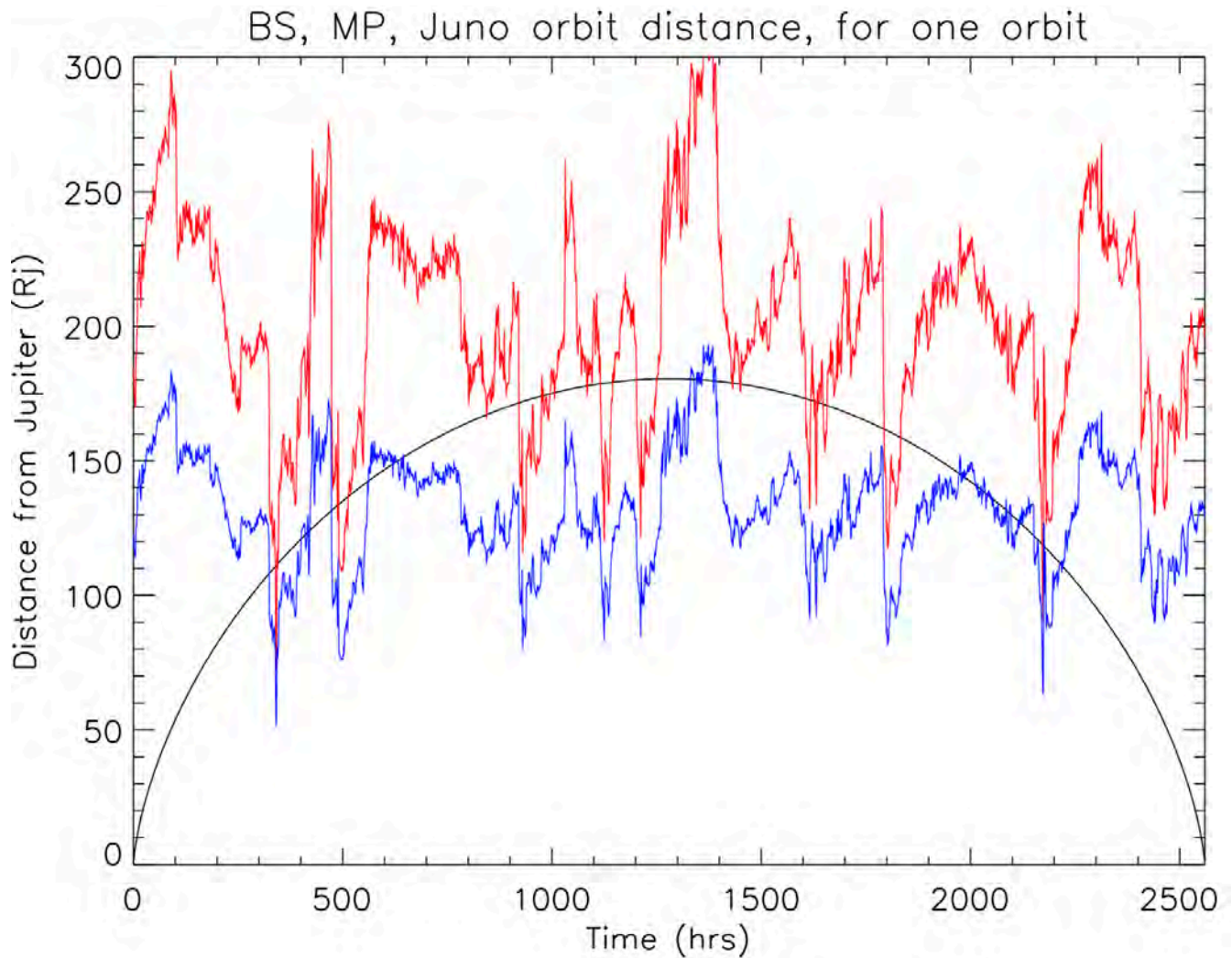


Figure 9: – Illustration of predicted variations in magnetopause (blue line) and bow shock (red line) distances on the dawn flank of the magnetosphere based on empirical dependence on solar wind pressure (Joy et al. 2002) and measurements from the *Ulysses* SWOOPS instrument at ~ 5 AU (Ebert et al. 2010). A sample *Juno* trajectory (black line) shows the frequent crossings Juno is expected to make of these boundaries on its capture orbit.

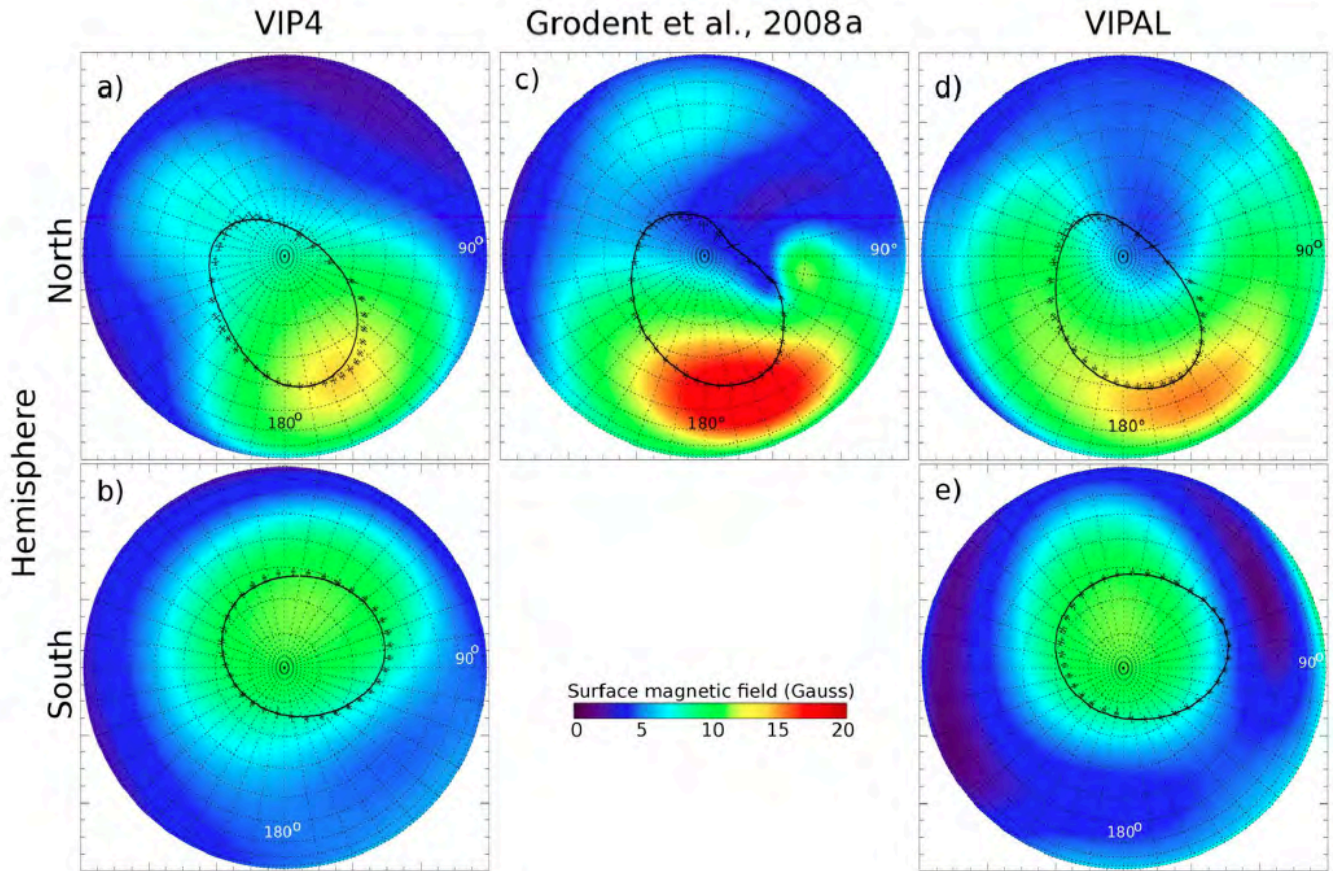


Figure 10: Surface magnetic field strength, observed Io's UV auroral footprint (crosses), and modeled footpaths (continuous line) of field lines that connect Io to Jupiter. All models include the $1/15.4$ oblateness of the planet to define the planetary "surface" (~ 1 bar level). *Left*: The VIP4 model of Connerney et al. (1998) for (a) the northern hemisphere and (b) the southern hemisphere; *Center*: The empirical model of Grodent et al., (2008a) for the (c) the northern hemisphere; *Right*: The VIPAL model of Hess et al. (2011) for (d) the northern hemisphere and (e) the southern hemisphere. From Hess et al. (2011).

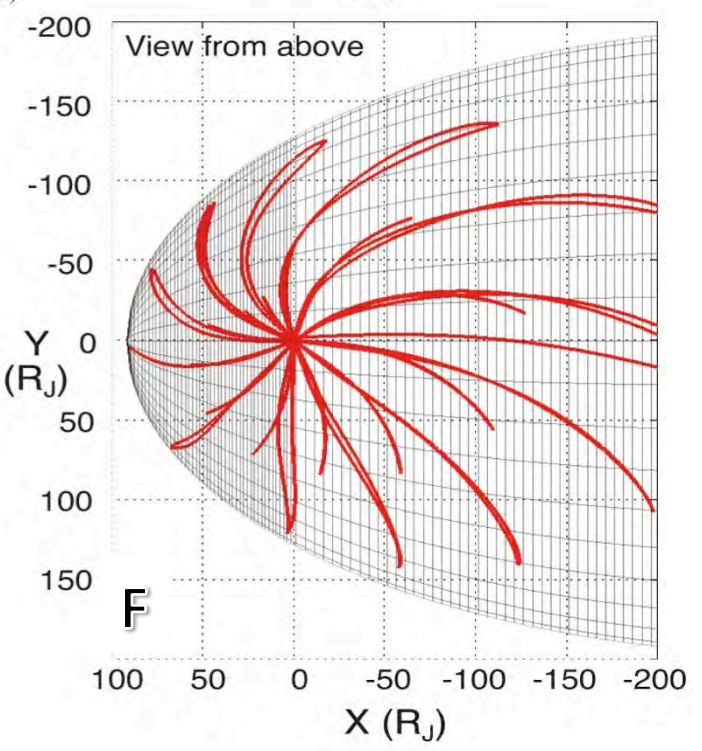
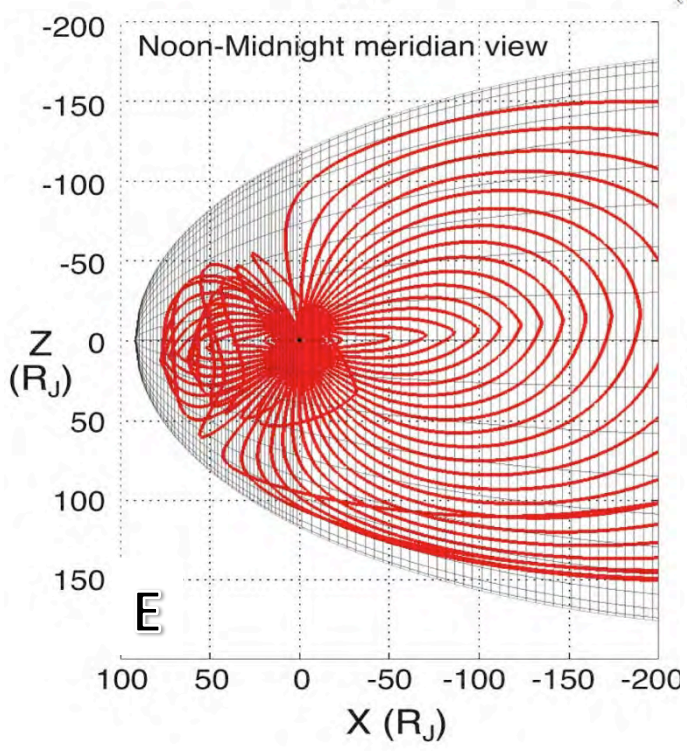
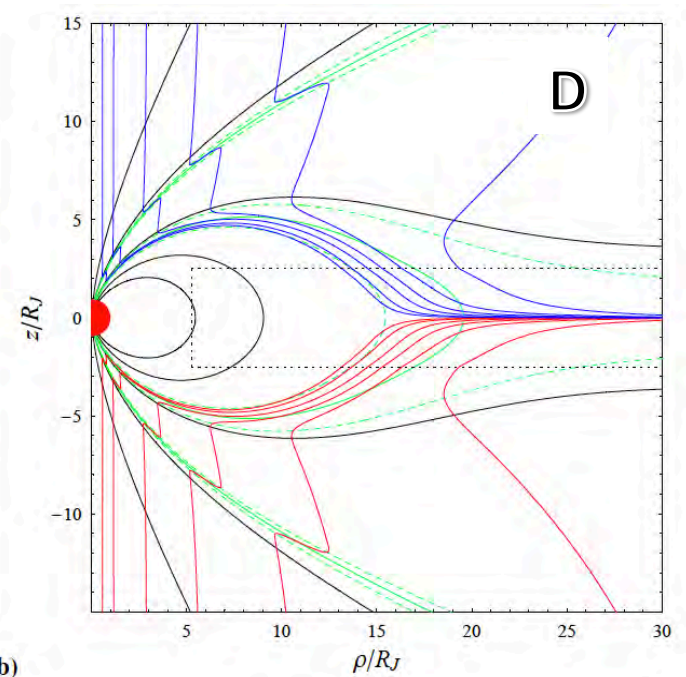
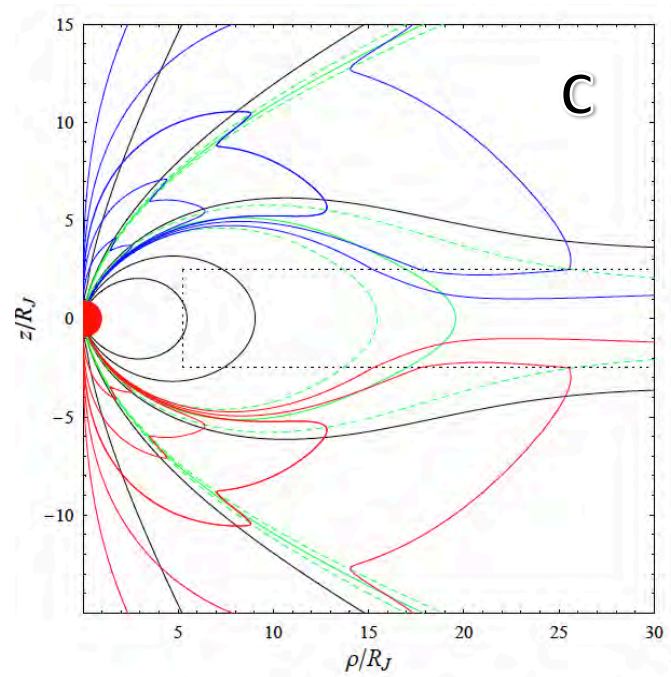
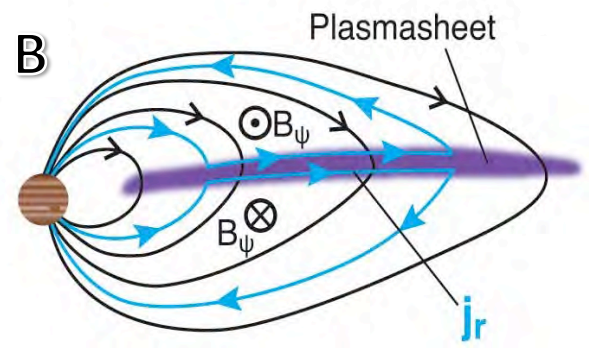
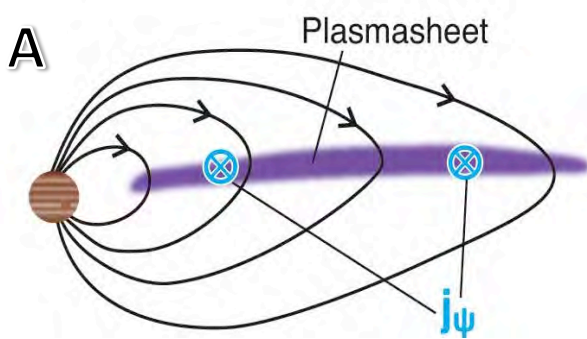


Figure 11: *Top:* Main plasmadisk currents. *Middle:* Axisymmetric magnetic field model of Cowley et al. (2008). *Bottom:* Three-dimensional magnetic field model of Khurana & Schwartzl (2005) that includes the VIP4 model for the interior field plus external magnetospheric currents. In C, D black solid lines show field lines mapping to the ionosphere at magnetic co-latitudes of $5\text{--}25^\circ$ in steps of 5° . The equatorial current sheet is restricted to the black dotted rectangle. The green lines show the regions of upward-directed field-aligned currents. Red and blue lines (C) show contours ($\pm 2, \pm 5, \pm 10, \pm 20, \pm 50$ nT), of the azimuthal field, and (D) show the tilt angle of the field out of magnetic meridian plane (from left to right the contours are for tilt angle magnitudes of $0.1^\circ, 0.2^\circ, 0.5^\circ, 1^\circ, 2^\circ, \text{ and } 5^\circ$).

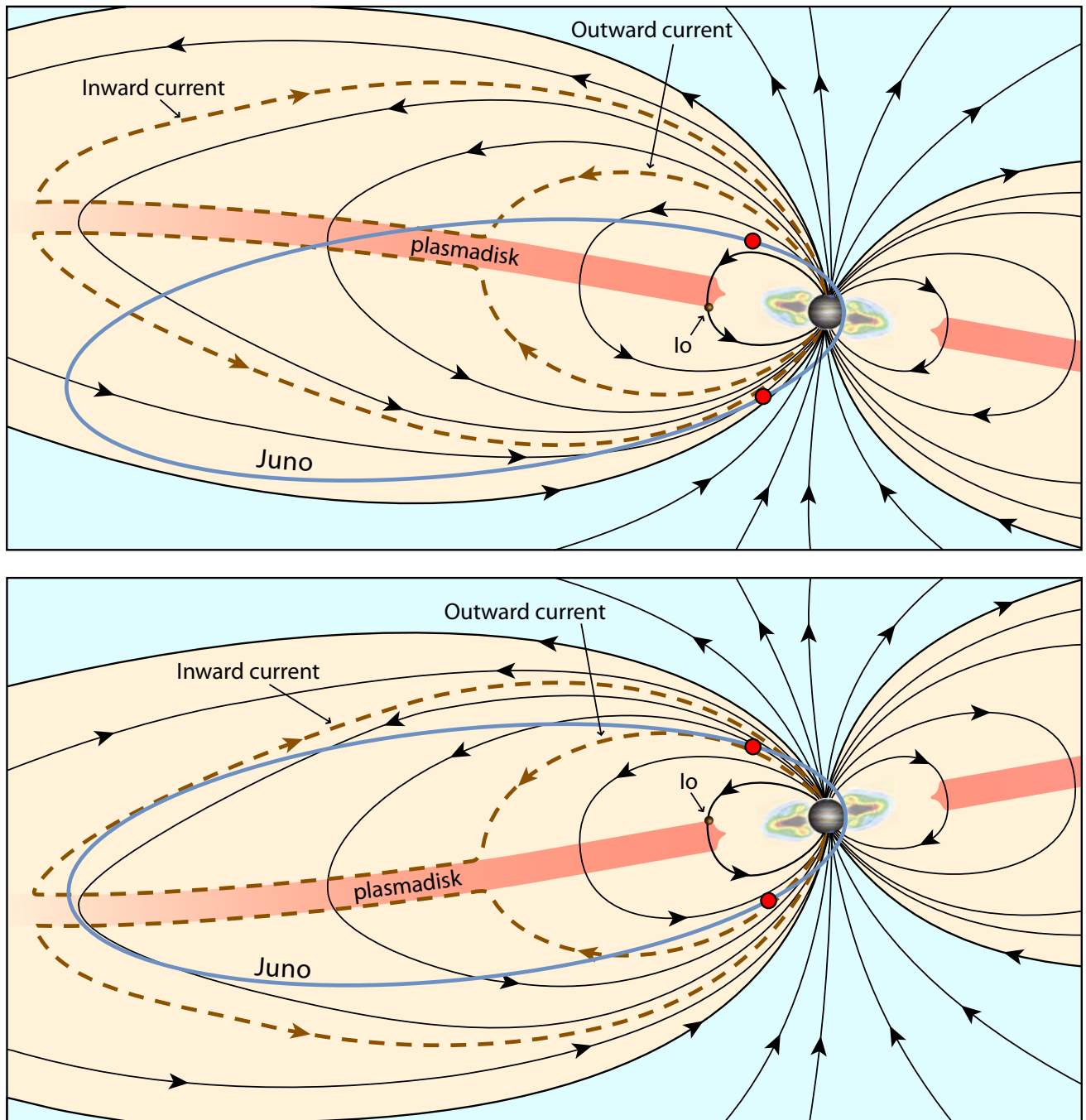


Figure 12: Due to the $\sim 9.5^\circ$ tilt of Jupiter's magnetic field from the planet's rotation axis, Juno will pass many times through the plasmadisk, particularly during apojoive of the early orbits. The blue line shows orbit of PJ3 (as shown in Fig 7). The top and bottom graphics illustrate the orientation of the field and plasmashet ~ 5 hours apart. The red dots are located on Juno's trajectory approximately ± 4 hours around perijove.

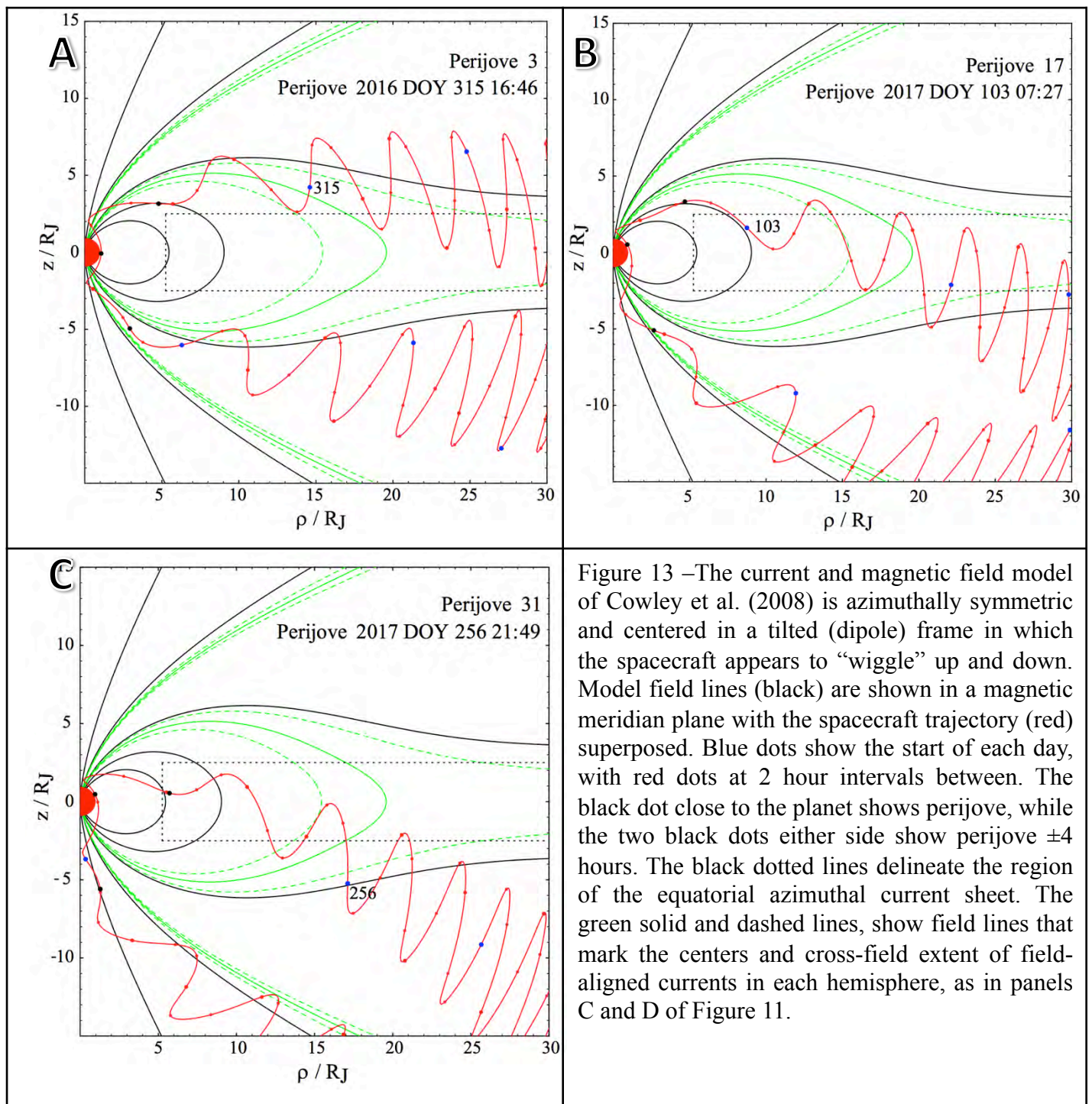


Figure 13 –The current and magnetic field model of Cowley et al. (2008) is azimuthally symmetric and centered in a tilted (dipole) frame in which the spacecraft appears to “wobble” up and down. Model field lines (black) are shown in a magnetic meridian plane with the spacecraft trajectory (red) superposed. Blue dots show the start of each day, with red dots at 2 hour intervals between. The black dot close to the planet shows perijove, while the two black dots either side show perijove ± 4 hours. The black dotted lines delineate the region of the equatorial azimuthal current sheet. The green solid and dashed lines, show field lines that mark the centers and cross-field extent of field-aligned currents in each hemisphere, as in panels C and D of Figure 11.

Make lines darker, dots bigger
 Put parts of caption onto figs?

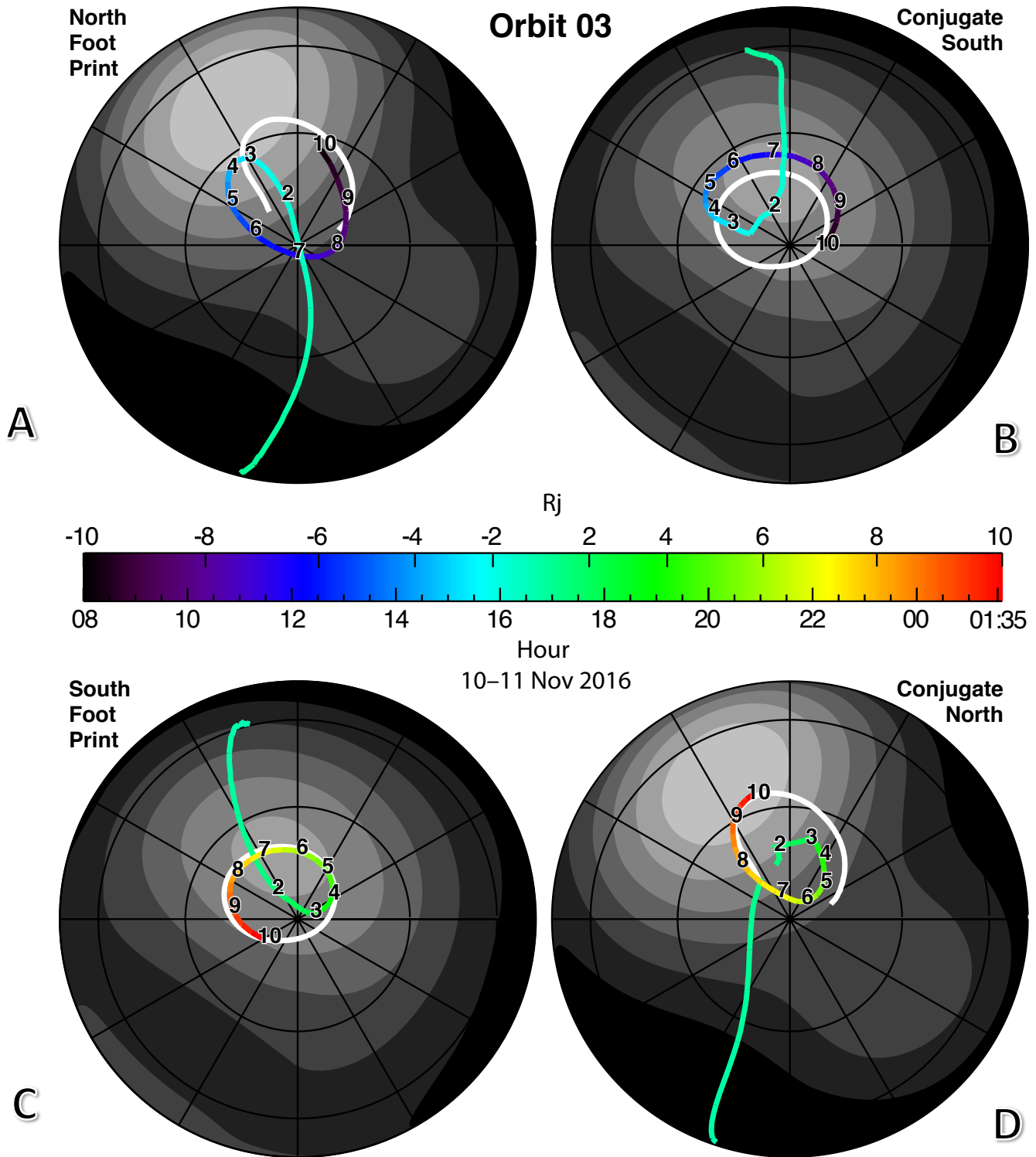


Figure 14a: Perijove 3. Locations of the footprints at each ends of the magnetic field passing through the spacecraft, mapped onto the “surface” of Jupiter using the VIP4+Khurana magnetic field. The north and south polar regions are shown fixed in System III longitude (0° towards the bottom of the page for the north, and towards the top for south). The curled path is due to the planet spinning under the spacecraft. The gray contours show the surface magnetic field strength. The white lines show the average location of the main aurora. The timescale corresponds to the time when $R < 10 R_j$ and the trajectory lines are colored corresponding to the timeline. The numbers on the trajectories correspond to the radial distance of the spacecraft at the time of the mapping. Top: The inbound trajectory mapping to the closest, north polar region (A) and conjugate, south (B) region. Bottom: The outbound trajectory mapping to the closest, south polar region (C) and conjugate, north (D) region.

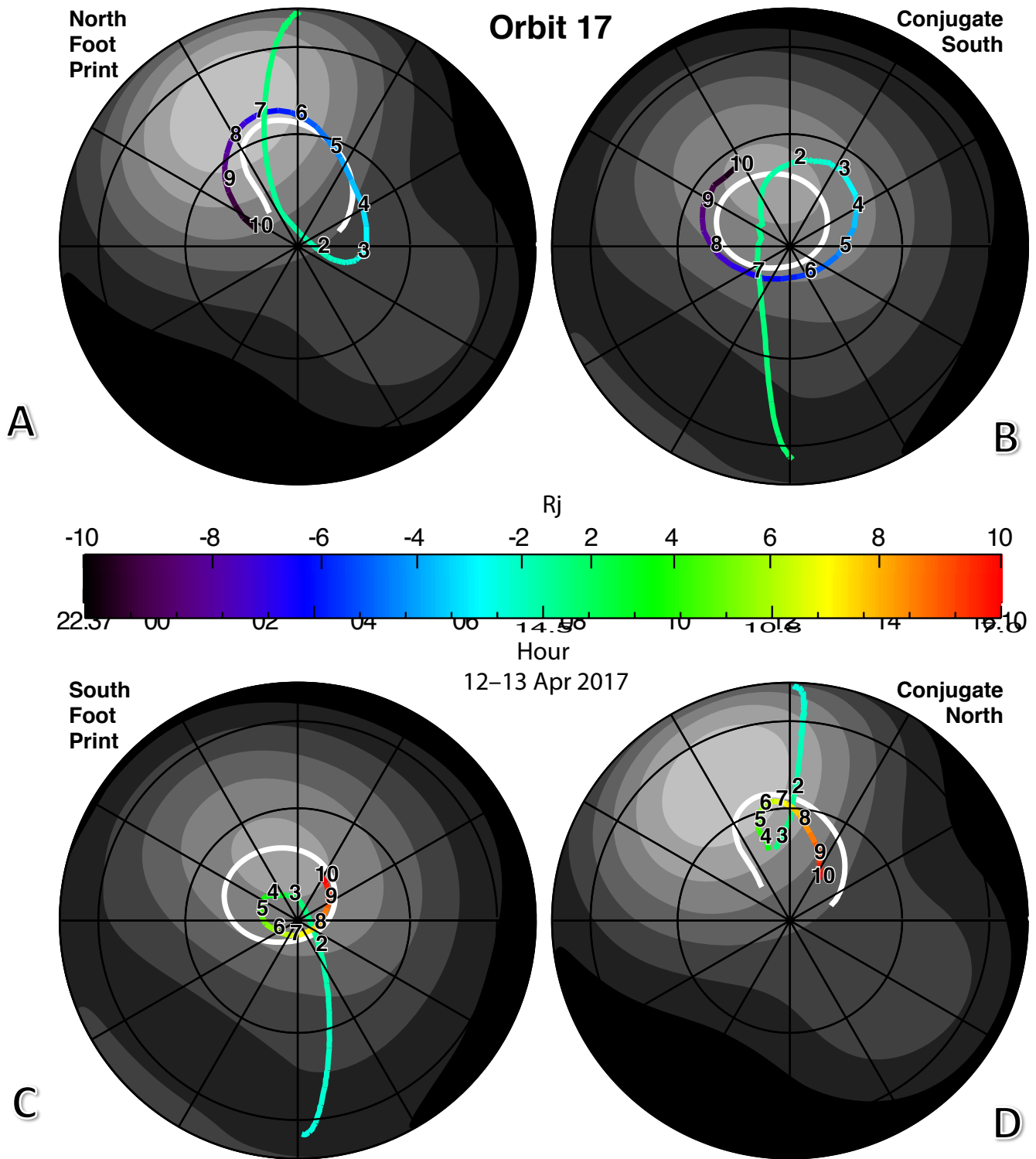


Figure 14b: Perijove 17.

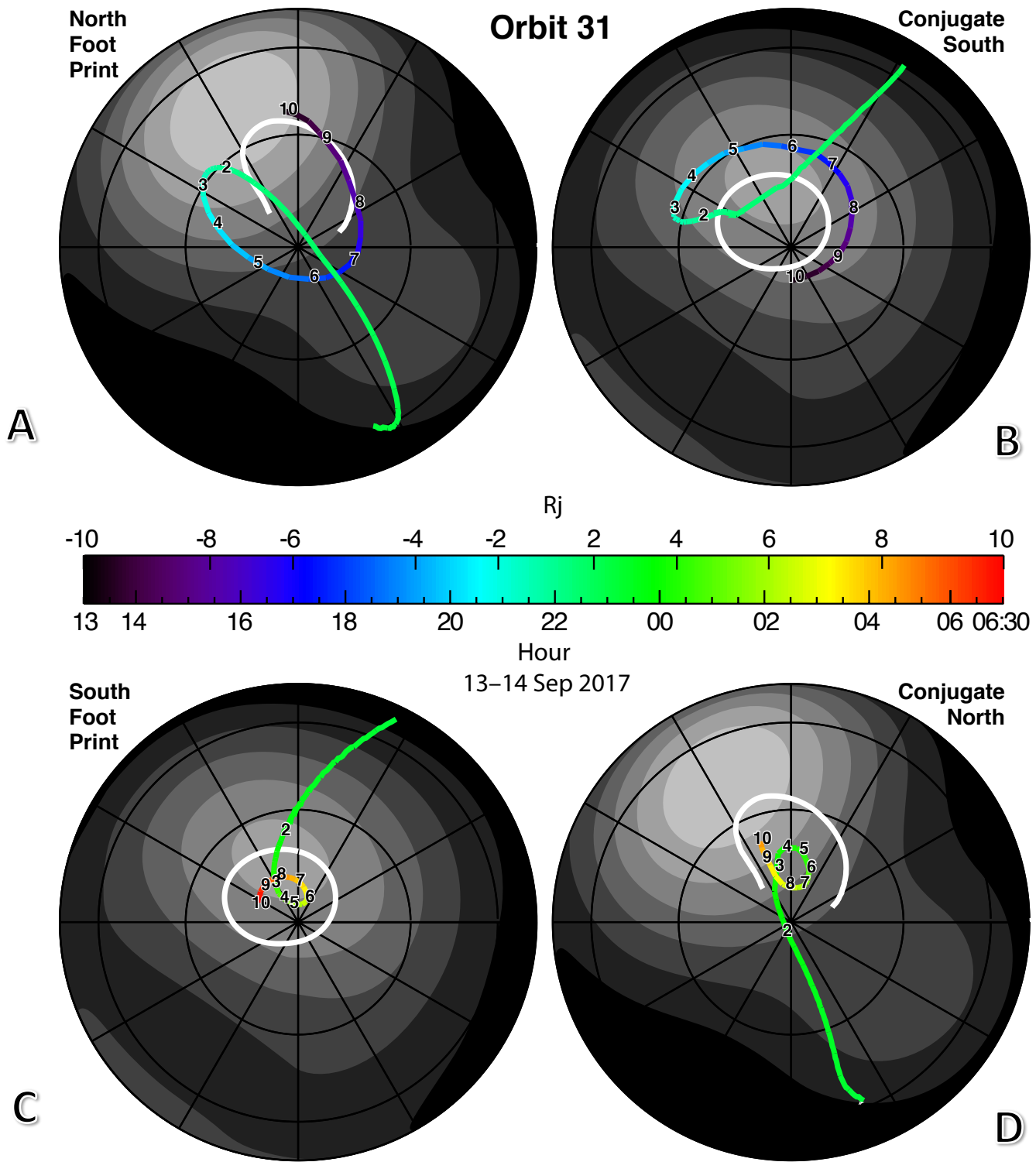


Figure 14c: Perijove 31.

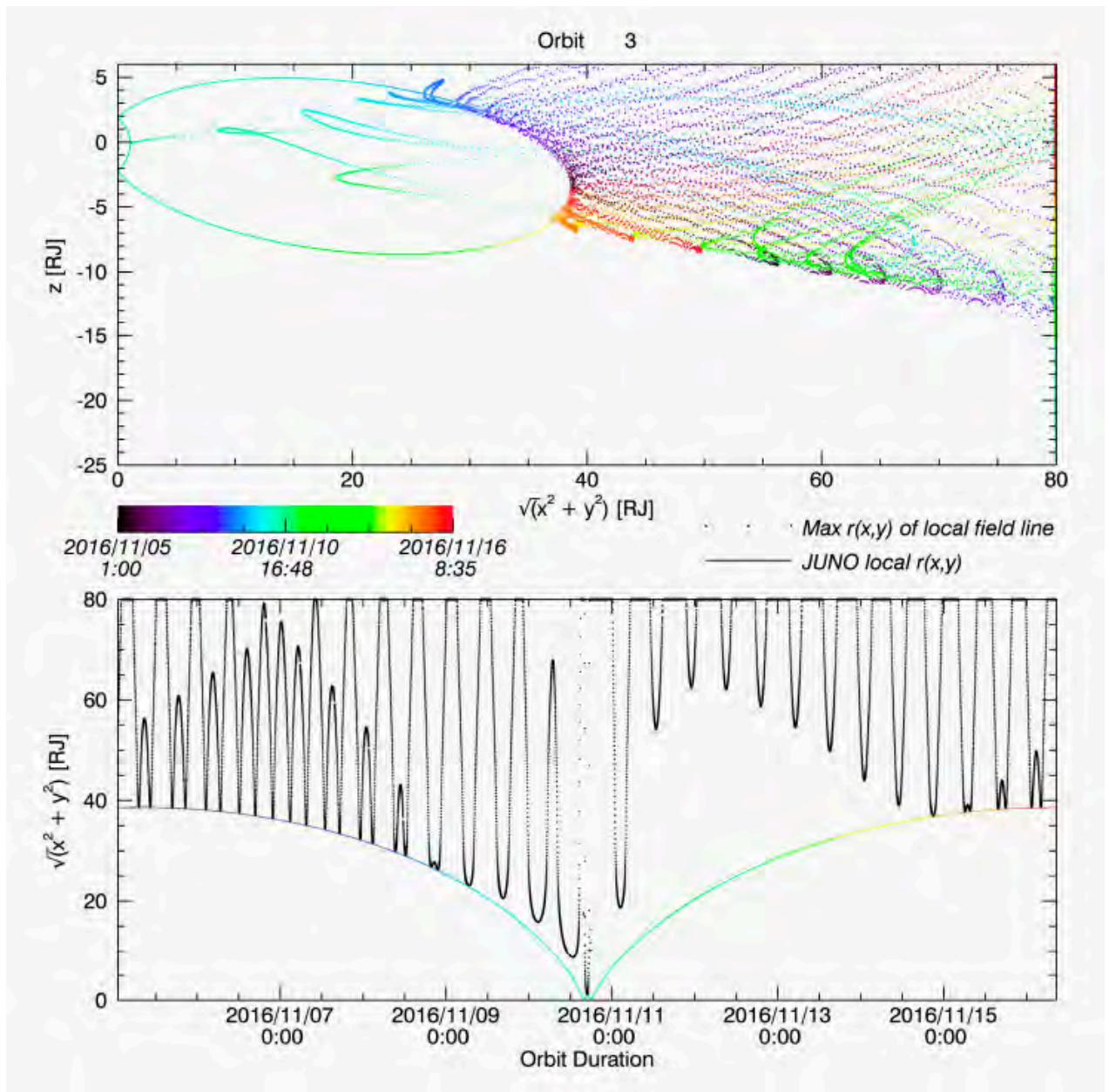


Figure 15a: Perijove 3. Mapping from the spacecraft along the Khurana magnetic field model to the farthest point from Jupiter for the orbit around perijove 3. *Top*: The spacecraft trajectory is shown in the (vertical) meridian plane with dots showing the location of the point farthest from the planet along the flux tube that instantaneously intersects Juno's trajectory. *Below*: the distance of the trajectory (color) and farthest crossing points (black curve) vs. time.

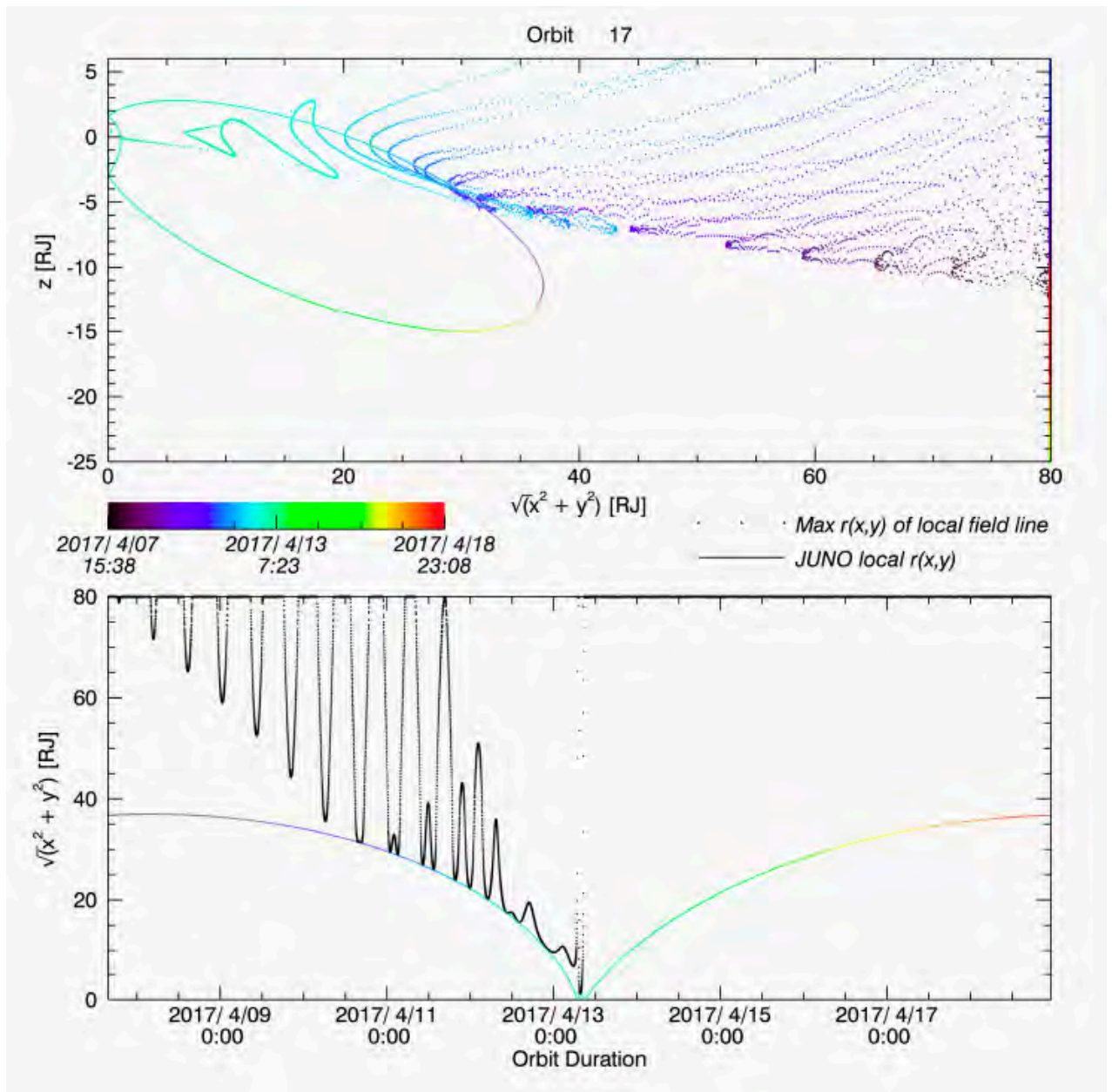


Figure 15b: Perijove 17.

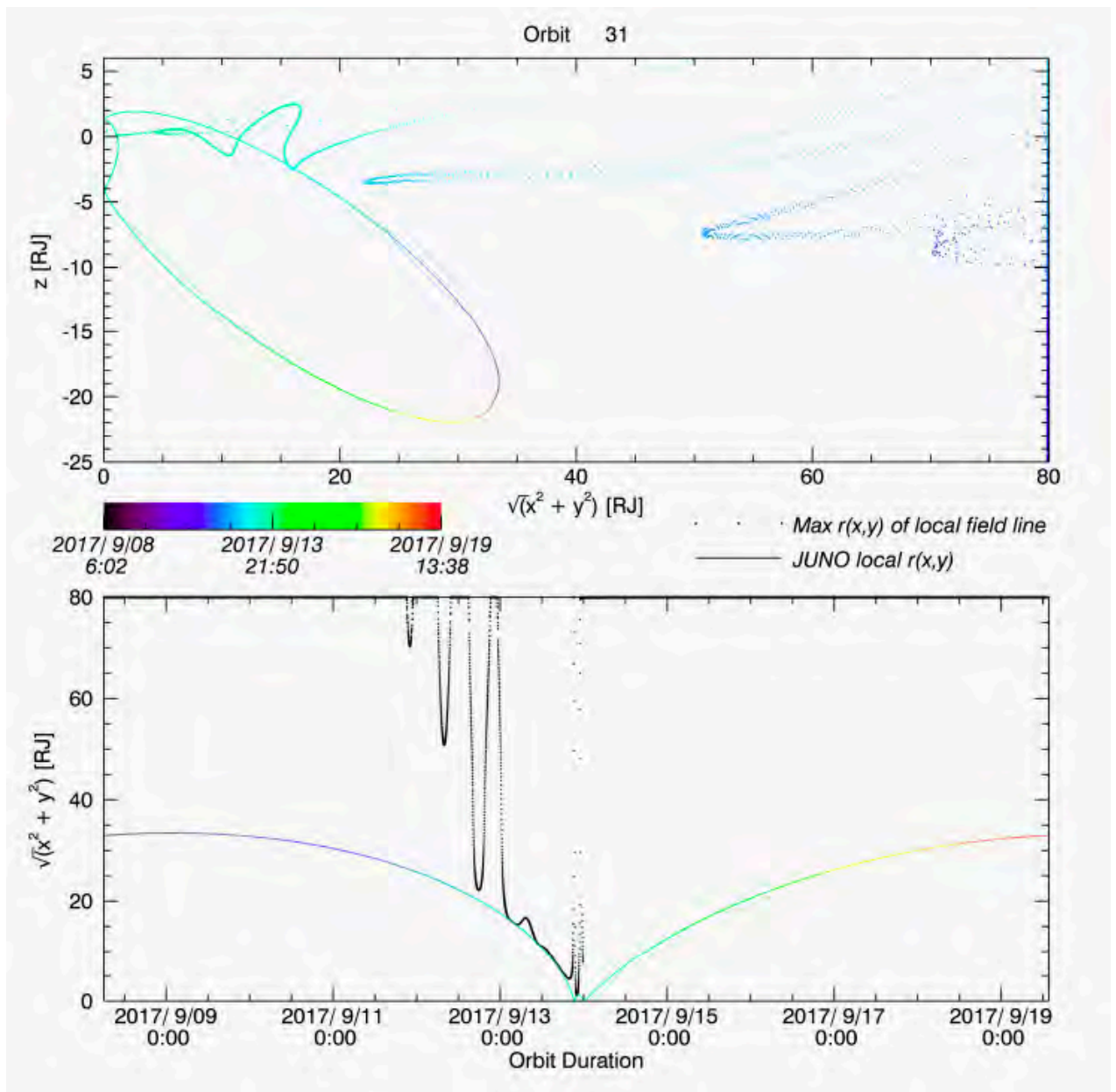


Figure 15c: Perijove 31.

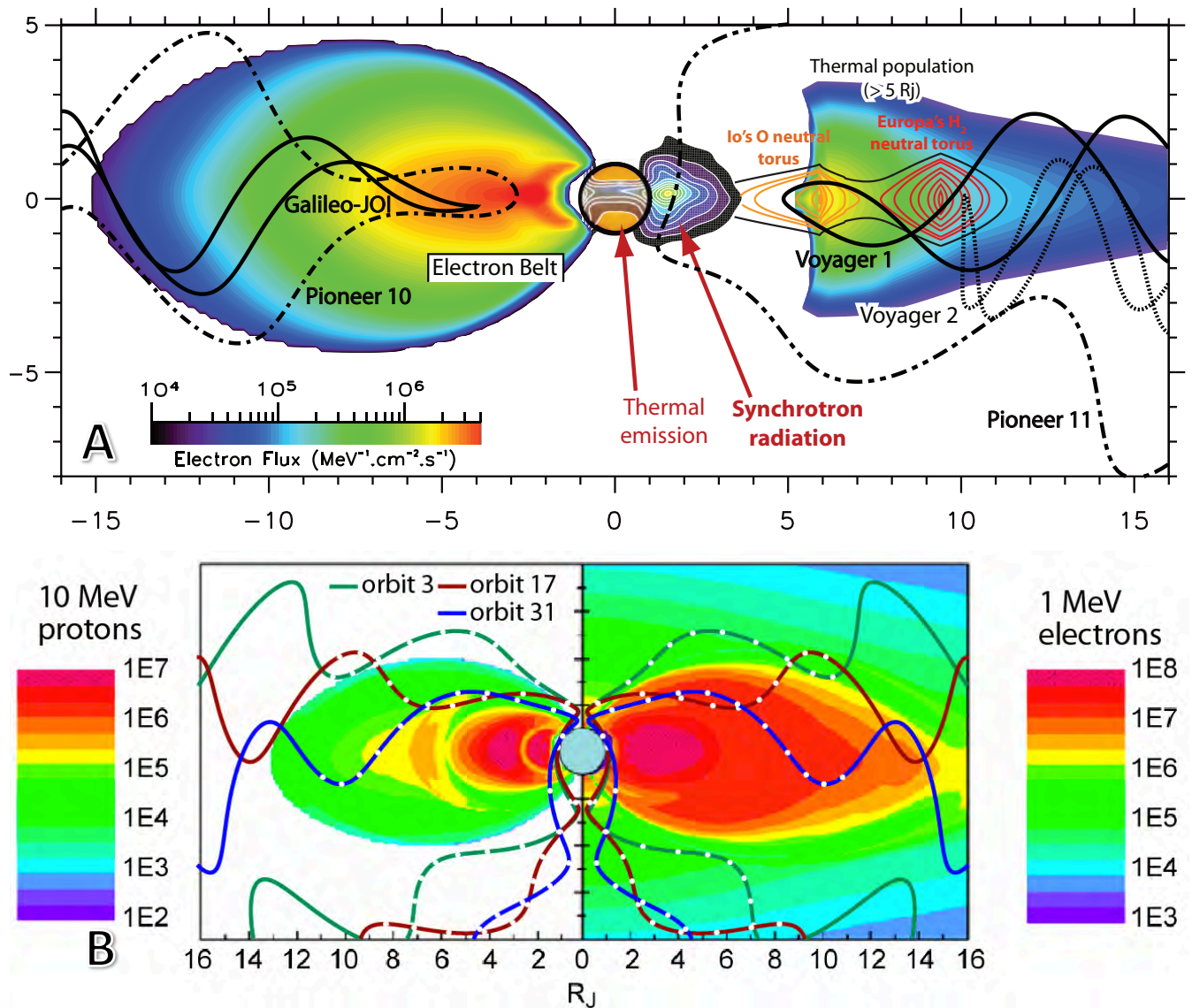
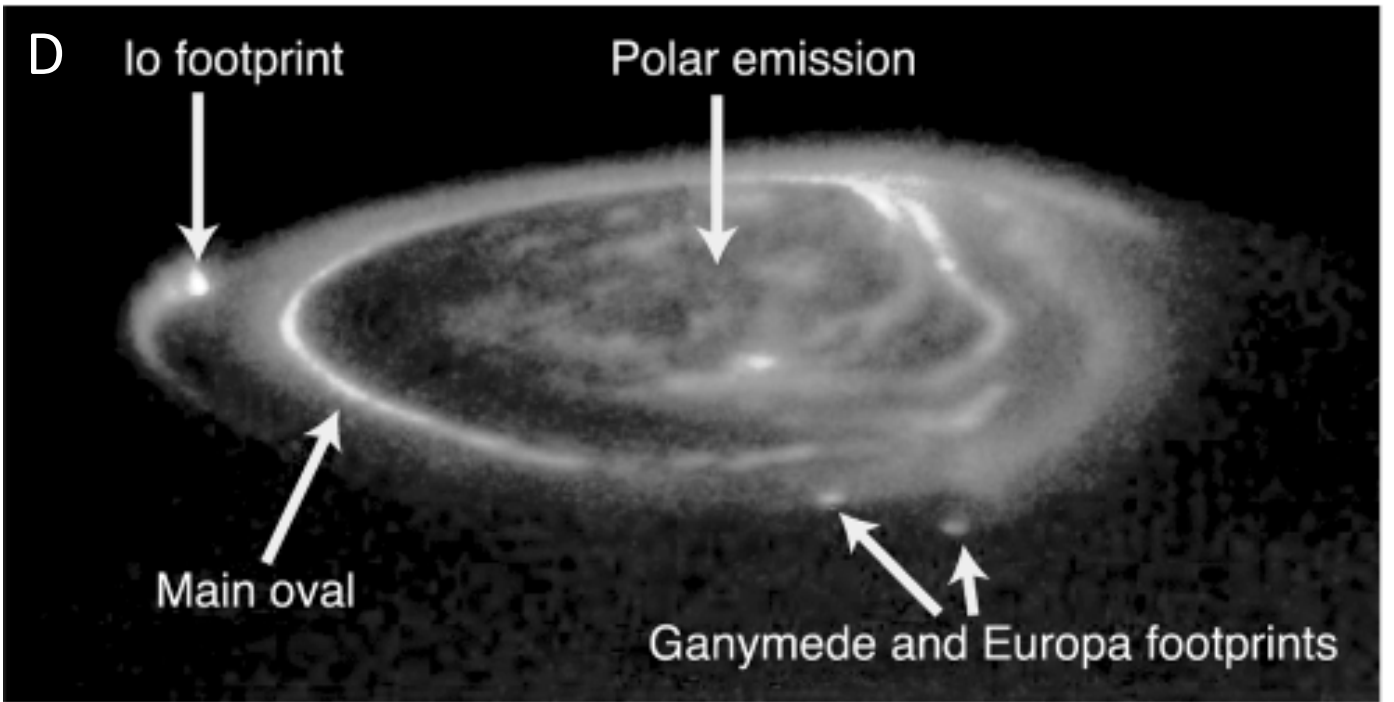
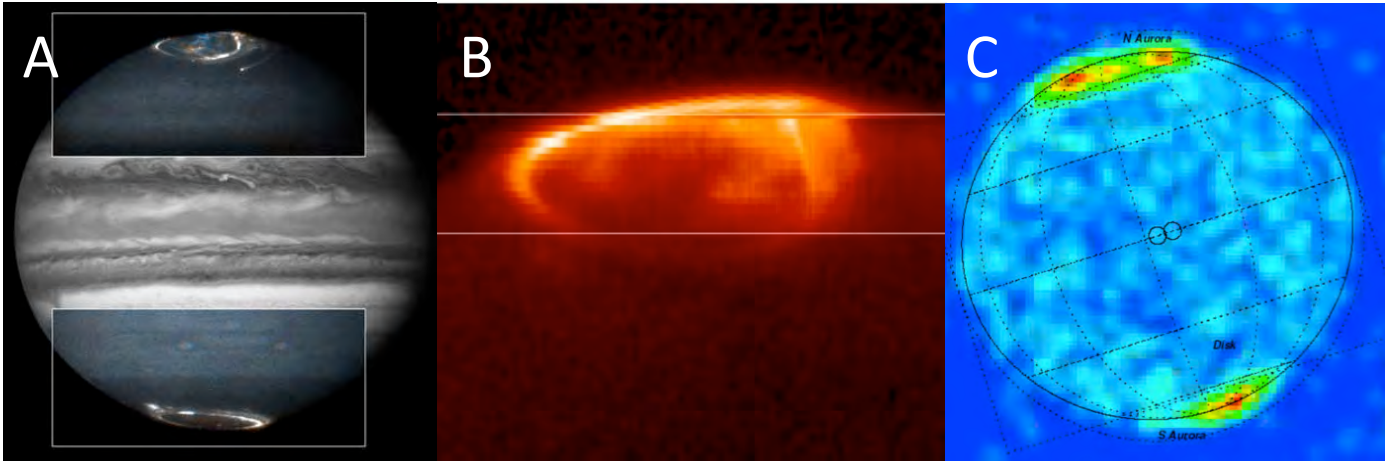
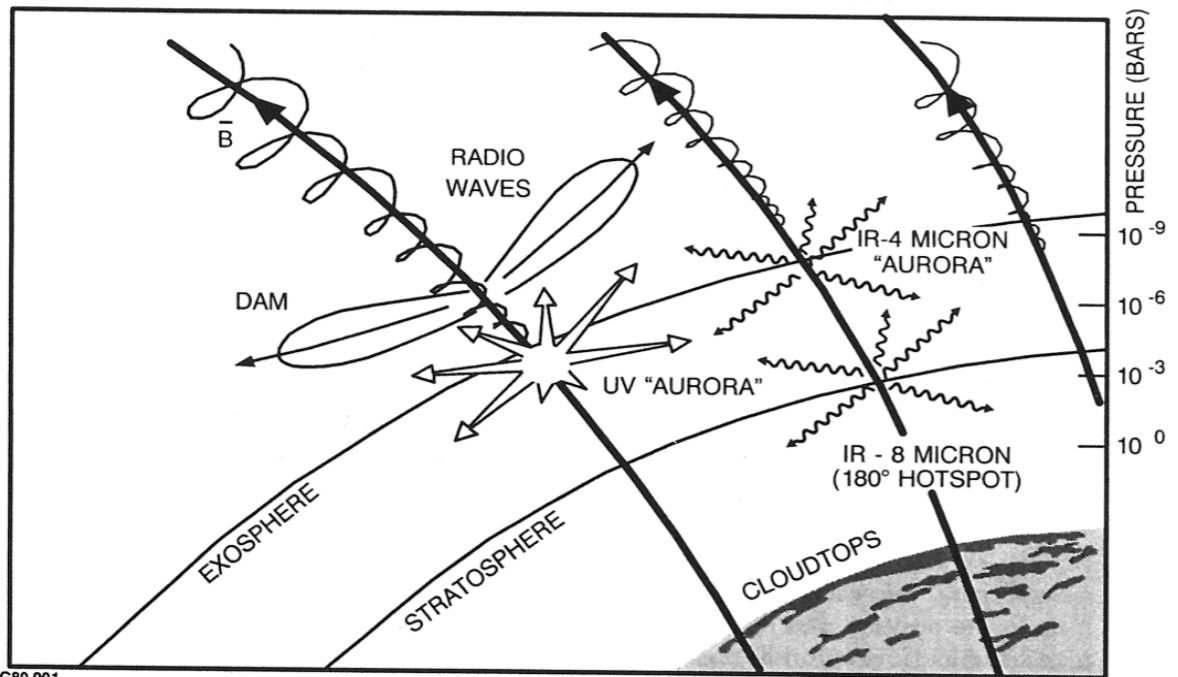


Figure 16: *Top:* Coverage of the inner magnetosphere by missions previous to Juno. *Bottom:* Coverage of the proton (left) and electron (right) inner radiation belts by Juno on orbits of perijoves 3, 17 and 31. The (integral) particle fluxes are calculated from the GIRE model and are in units of $(\text{cm s})^{-1}$. The white dots on the trajectories are shown with 1-hour tick marks for ± 10 hours around perijove. Note that the spacecraft appear to move in “wiggle” orbits in this coordinate system that is based on the magnetic dipole.



E



G80.001

Figure 17: Auroral emissions at different wavelengths: (A) UV from the HST (NASA / John Clarke, BU); (B) IR (ESO / Tom Stallard, U. Leicester); and (C) X-ray wavelengths from the Chandra Space Telescope (Elsner et al. 2005). (D) Morphology of the three main types of jovian aurora (Clarke et al. 2004). (E) Schematic illustration of charged particles spiralling along the magnetic field and the various emissions they generate as they approach the atmosphere in the north polar region (from Connerney 1992).

Orbit 4

21 Nov 2016

14:56

Dusk

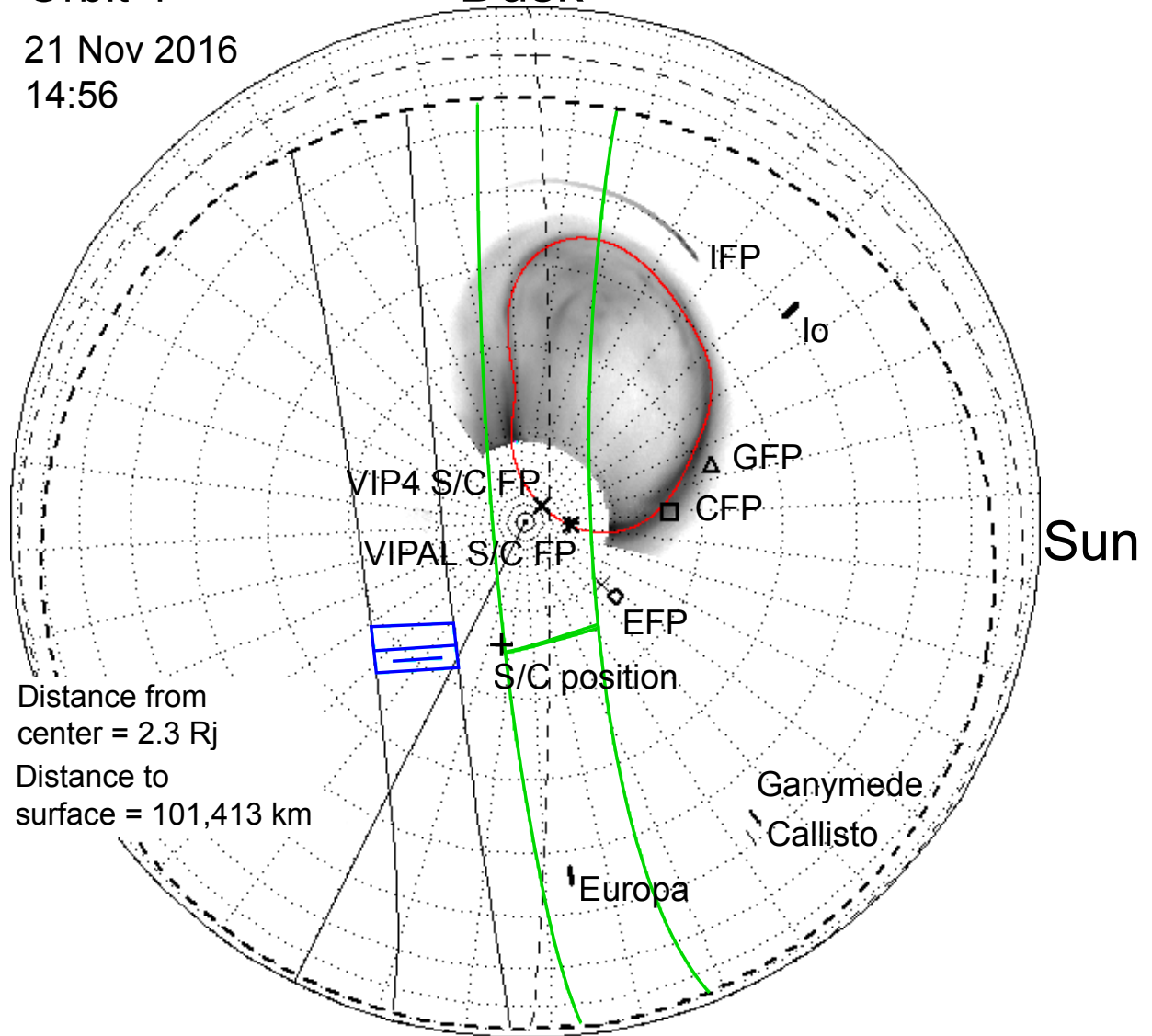


Figure 18: Polar projection of the predicted northern aurora on Jupiter for orbit 4 on 21 November 2016 at 14:56:00 UT. The 0° meridian is shown as a solid black line. The dashed circles are the *Juno* horizon at the 1 bar level (thick dashed line) and 1000 km above the surface (thin dashed line). The grey shape is the averaged UV aurora for February 2007 from HST. The red contour highlights the statistical auroral oval for this month. The swath and the slit of the *Juno*-UVS instrument are drawn in green, assuming a pointing mirror angle of +10°. The field of view of the JIRAM instrument is shown in blue along with its swath (thin black line). The predicted latitude and longitude of the spacecraft is represented by a cross (+). The tick marks indicate the longitude of the four Galilean satellites, with predicted location of footprints (IFP, EFP, GFP, CFP). The foot of the field line passing through *Juno* has been computed with two magnetic field models: VIP4 (thick X) and VIPAL (*).

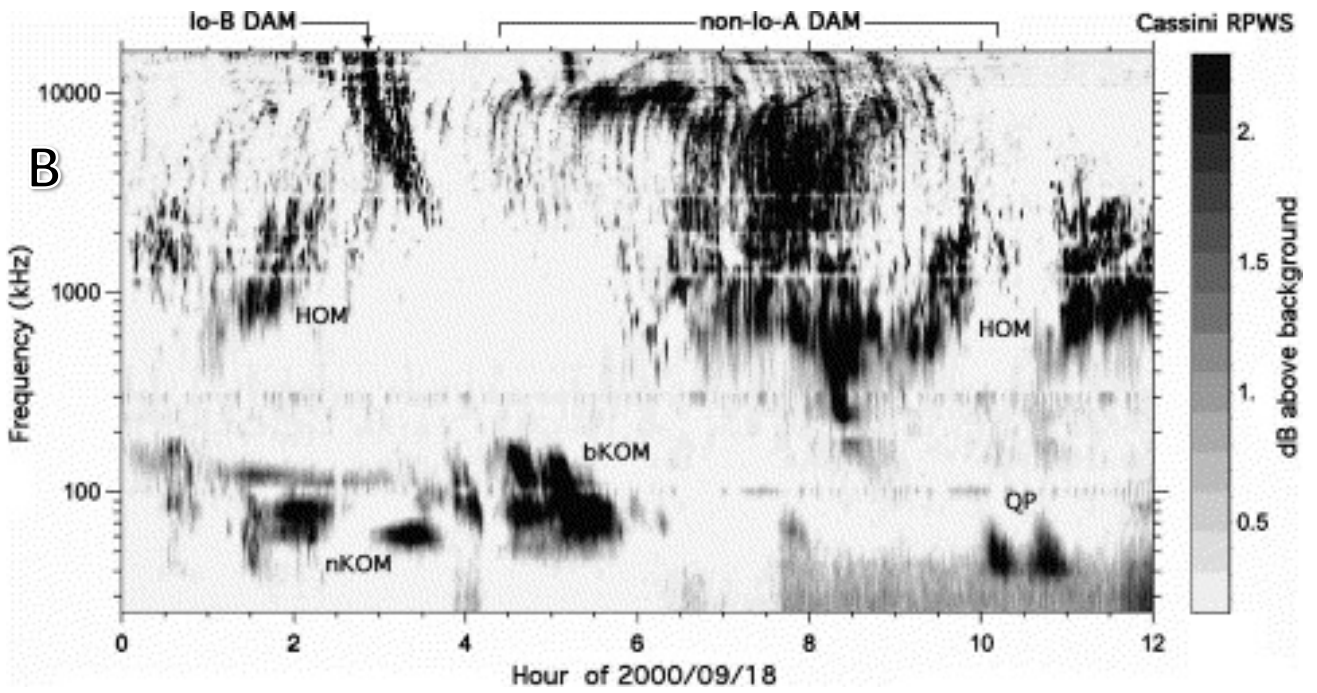
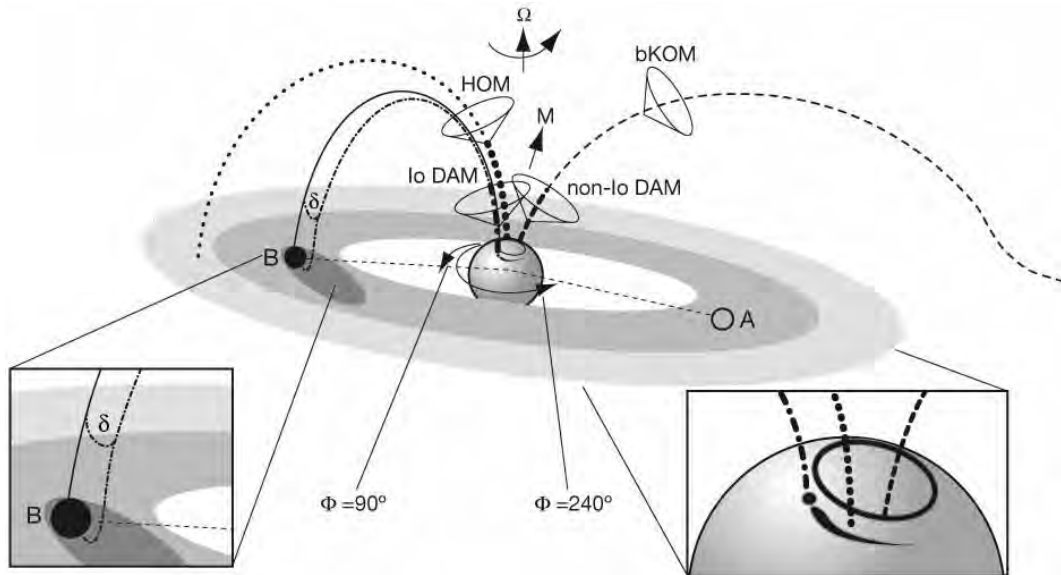
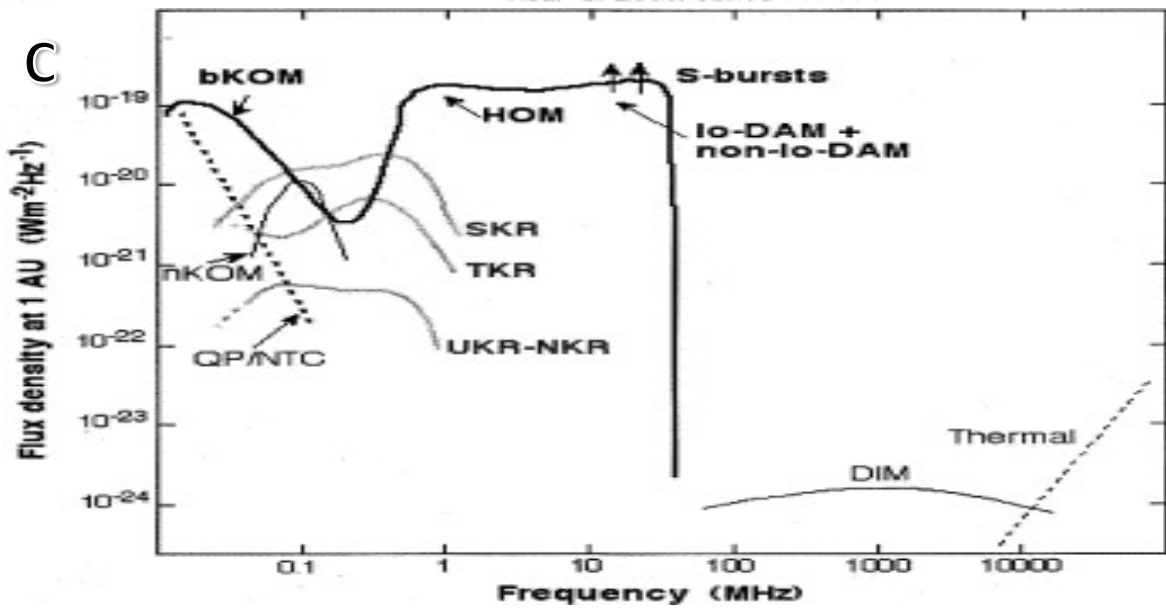
A**C**

Figure 19: (A) Morphology of the types of jovian radio emissions from Zarka (2000). (B) Frequency-time spectrogram of radio emissions obtained by Cassini when it flew past Jupiter in 2000 (from Zarka et al. 2001). (C) Power of emissions (as received at Earth) for jovian radio emissions versus frequency. Kilometric radiation from Saturn, Earth, Uranus and Neptune are indicated as S-, T-, U-, and NKR. Note that the decimetric synchrotron emission (DIM) is over four orders of magnitude weaker than the high latitude radio bursts. From Zarka (2004)

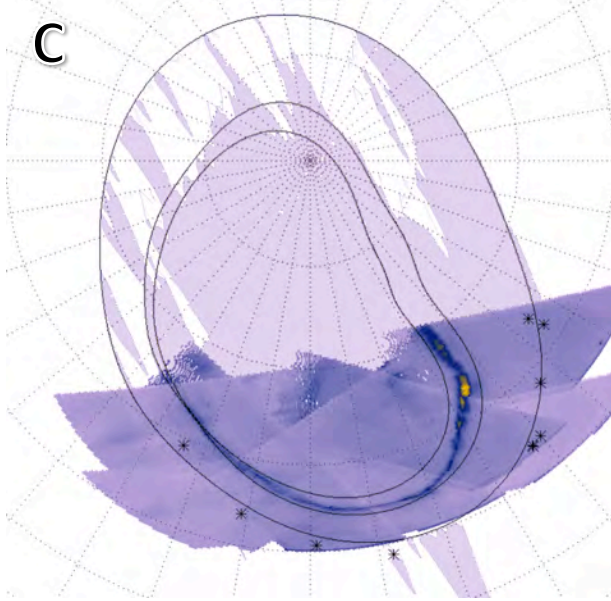
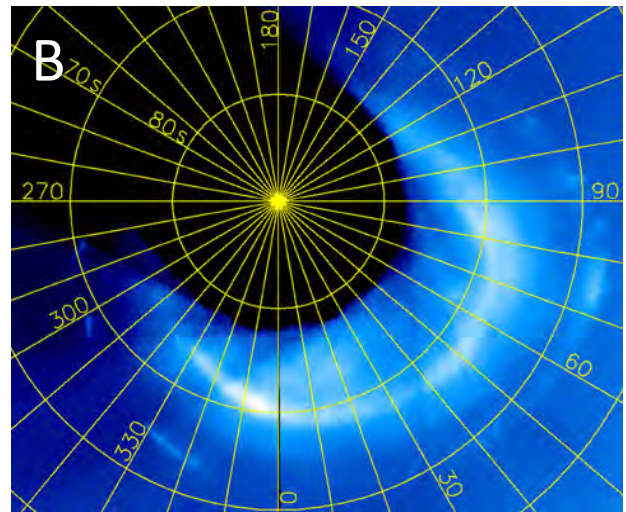
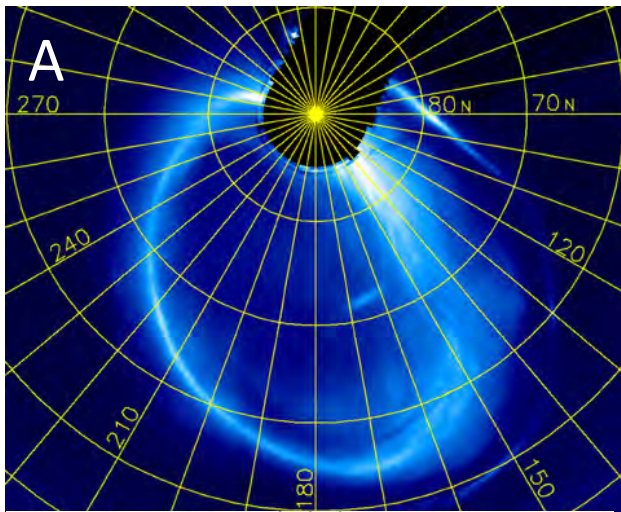
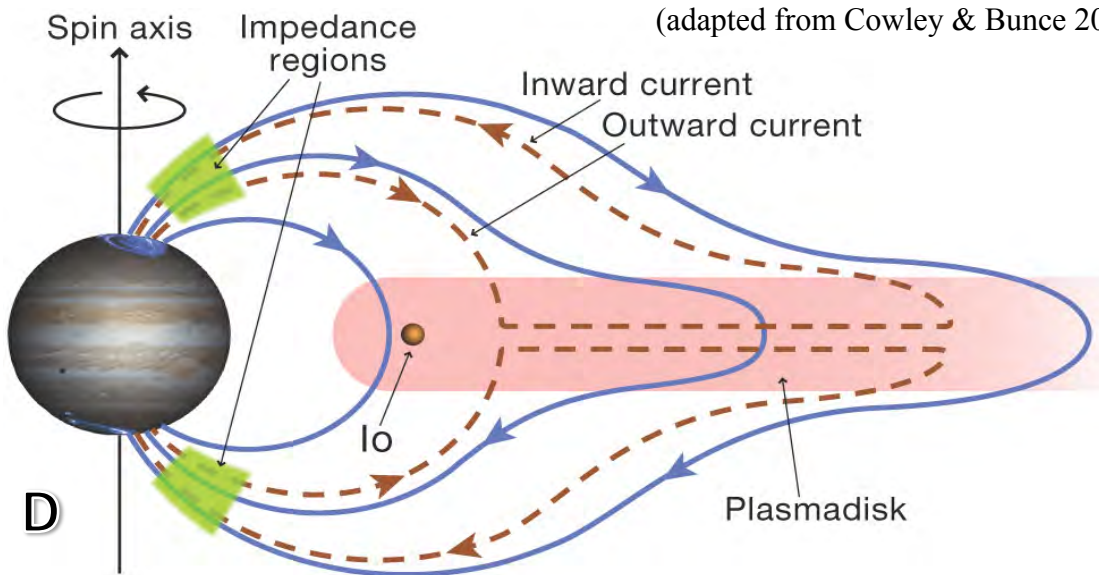


Figure 20: *Top*: Jupiter's main auroral emission in the (A) north and (B) south hemispheres (Grodent et al. (2003)). Grid lines indicate System III longitude and planetocentric latitude. The arcs at the lowest latitudes are from Io footprint emissions on different days. *Left*: optical emissions observed by Galileo (Vasavada et al. 1999) projected onto the same grid as A, with lines illustrating locations of the main emissions and the Io footprint. *Bottom*: The Iogenic magnetospheric plasma is coupled to the rotating planet via electrical currents (brown dashed lines) that flow along magnetic field lines (blue solid lines) to the auroral regions of Jupiter's atmosphere. (adapted from Cowley & Bunce 2001).



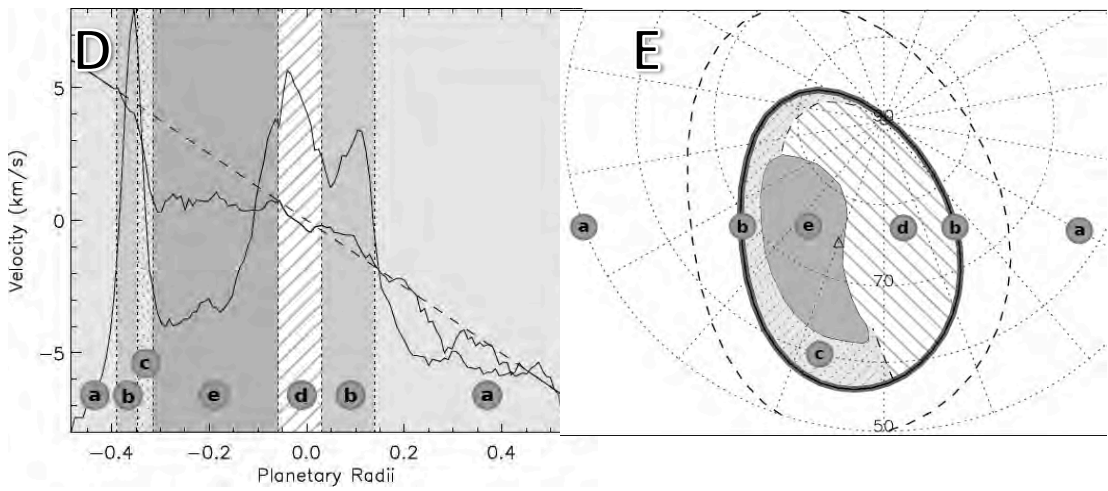
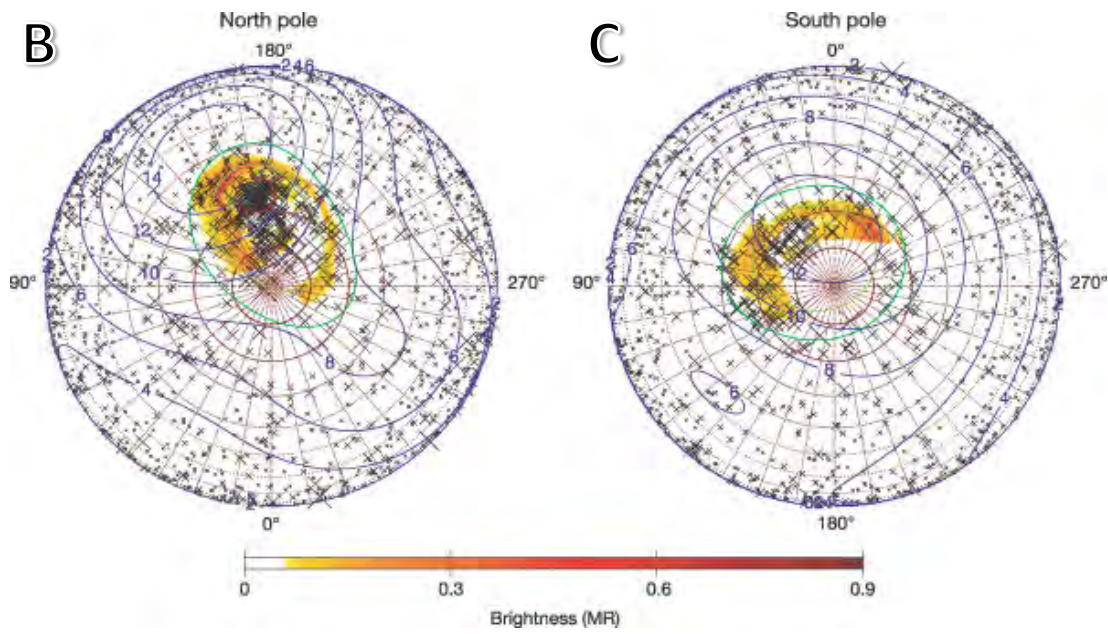
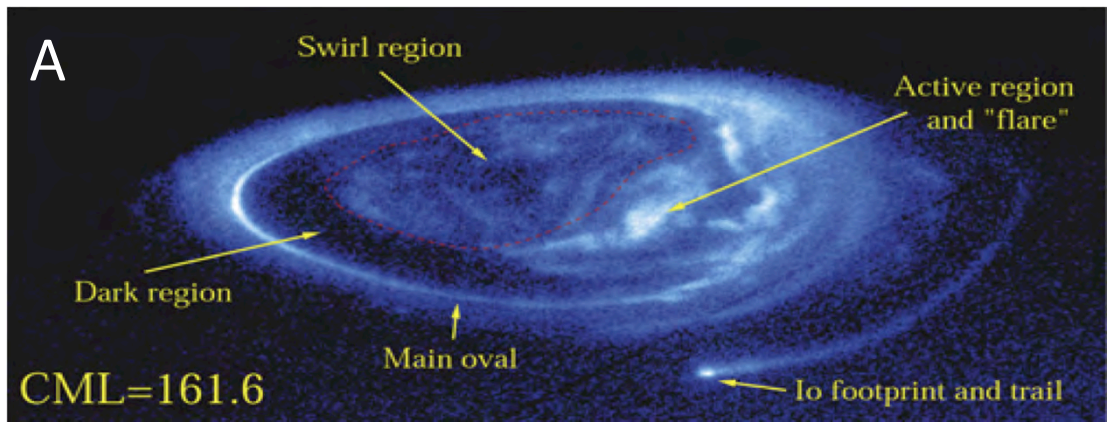


Figure 21: *Top:* A - HST image (14 Dec. 2000) illustrates the auroral features poleward of the main oval – the polar aurora. Arrows point to the dark region and the active region where “flares” and “arcs” are often observed. From Grodent et al. (2003). *Middle:* Polar projections of X-rays seen by Chandra and simultaneous HST UV images. The mapped locations of individual X-ray photons (crosses) are overlaid on averages of several northern (B) and southern (C) auroral images made with HST-STIS during 10 ± 20 UT on 18 December 2000. Contours show the surface VIP4 model magnetic field strength, the Io footprint path (green) and L=30 (yellow). From Gladstone et al. (2002). *Bottom:* D Spectroscopic IR diagnostics of Jupiter’s polar region. The typical H_3^+ line-of-sight velocity (bold line) and normalized intensity (thin line) plotted against the rotational rate (dashed line). The velocity profile is divided into regions with patterned backgrounds and letters, directly relating to the lettered sections in the (E) map of ion flow in the northern auroral regions of Jupiter (at a CML of 160°): *a* is low latitude emission; *b* is the main auroral region; *c* is the dark region; *d* is the active, variable region; *e* is the stagnant/low speed region. From Stallard et al. (2012).

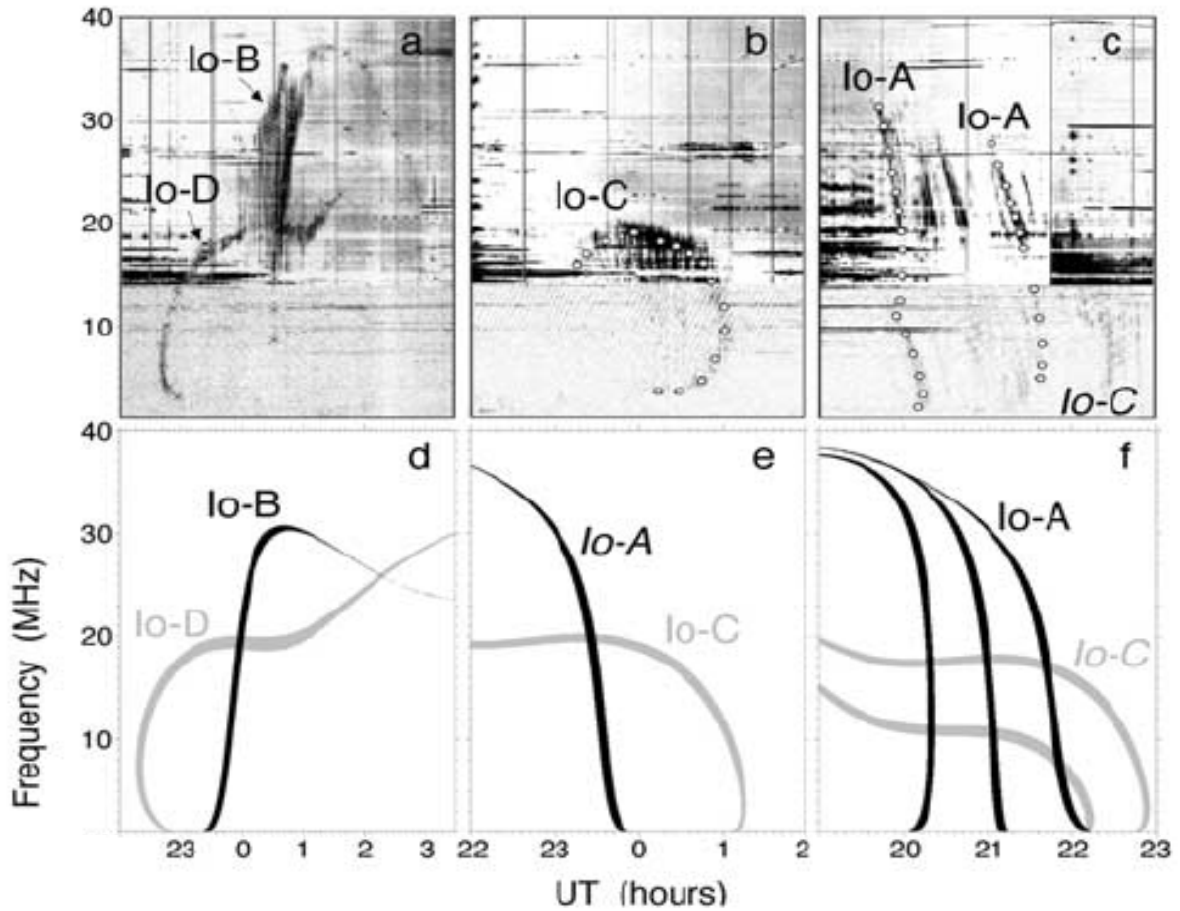


Figure 22: *Top* (a,b,c) Dynamic spectra of typical Io-Jupiter arcs observed by Wind/Waves and the Nancay decameter array (adapted from Quinnee & Zarka 1998). The various symbols superimposed along the arcs were used to identify their line of maximum intensity in the frequency-time plane. *Bottom* (d, e, f) Dynamic spectra of Io-Jupiter emission for the same time intervals as above simulated using loss-cone cyclotron maser instability where the black arcs are generated in the northern hemisphere and grey arcs are in the south. From Hess et al. (2008).

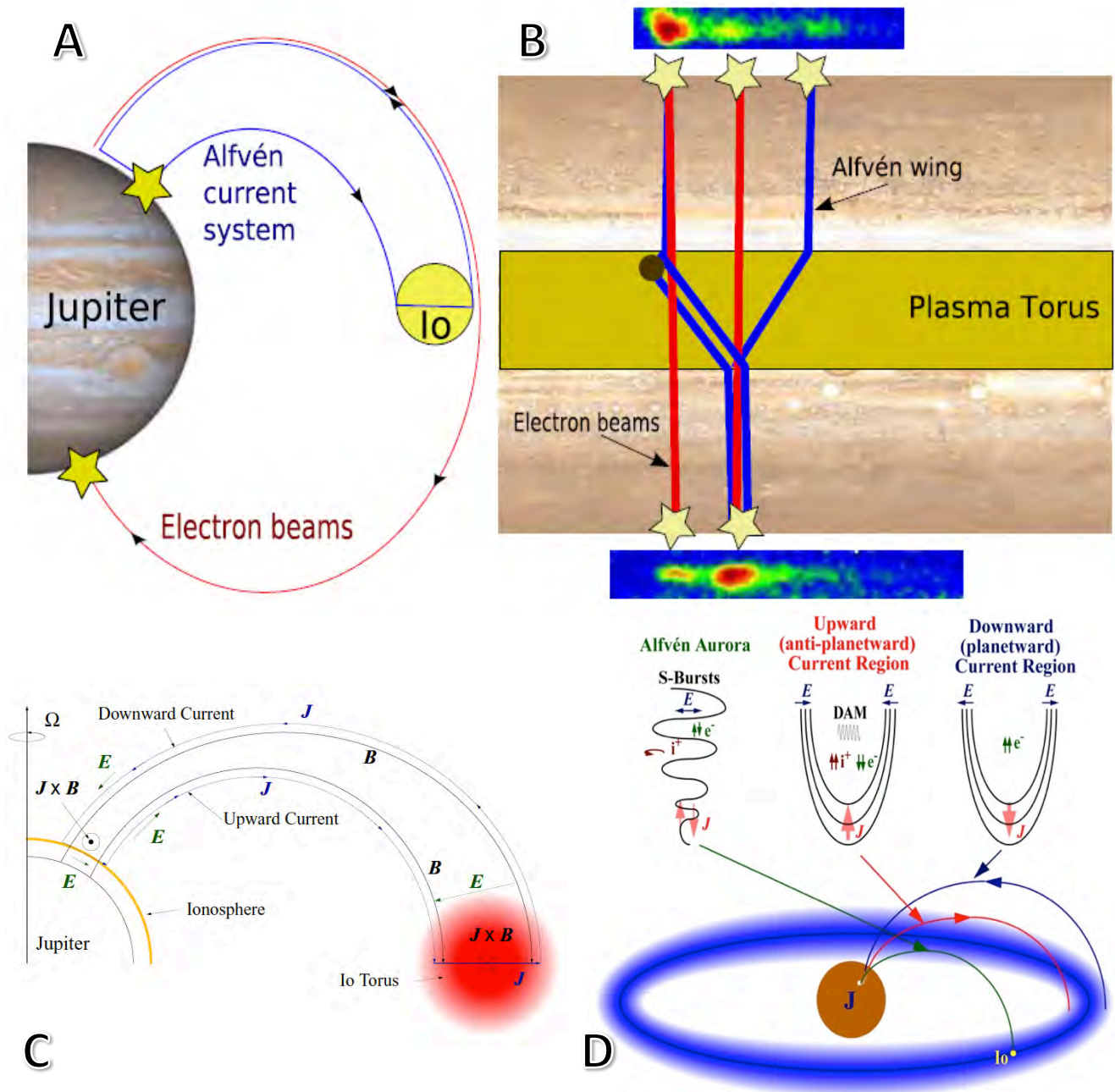


Figure 23: Satellite aurora, shown here for Io, but similar processes are expected to be responsible for auroral spots produced by Europa and Ganymede. *Top:* The Alfvén waves generated by the Io-plasma interaction accelerate electrons. Some of these electrons bombard the atmosphere of Jupiter and excite aurora. But some of the electrons are reflected between the hemispheres. Bonfond et al. (2008) used combinations of electron beams and Alfvén waves to explain the spacing of Iogenic auroral spots. *Bottom:* The disturbance at Io is coupled to the planet via Alfvén waves that propagate along the magnetic field. It takes some time for the additional material added to the torus to be brought up to corotation with the surrounding plasma resulting in a quasi-steady upward and downward current system in the “wake” downstream of Io. From Ergun et al. (2009)

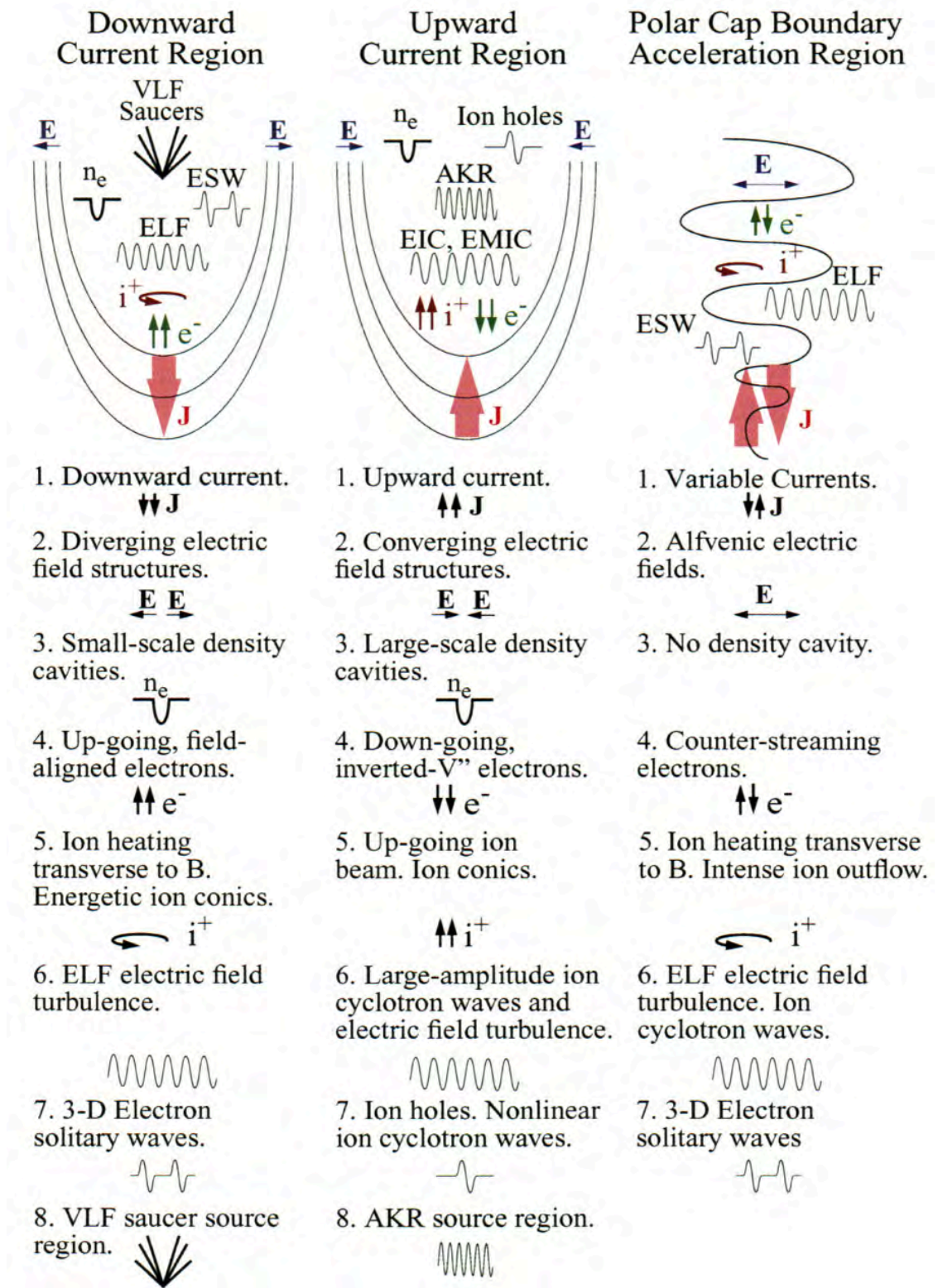


Figure 24: The three types of auroral zones based on experience from Earth: upward currents, downward currents and Alfvénic regions. Adapted from Carlson et al. (1998).

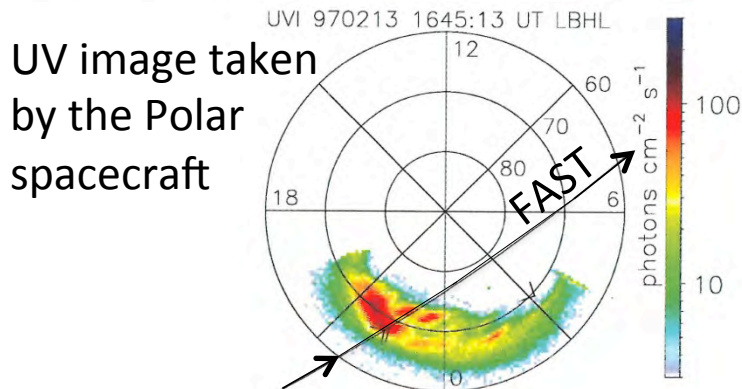
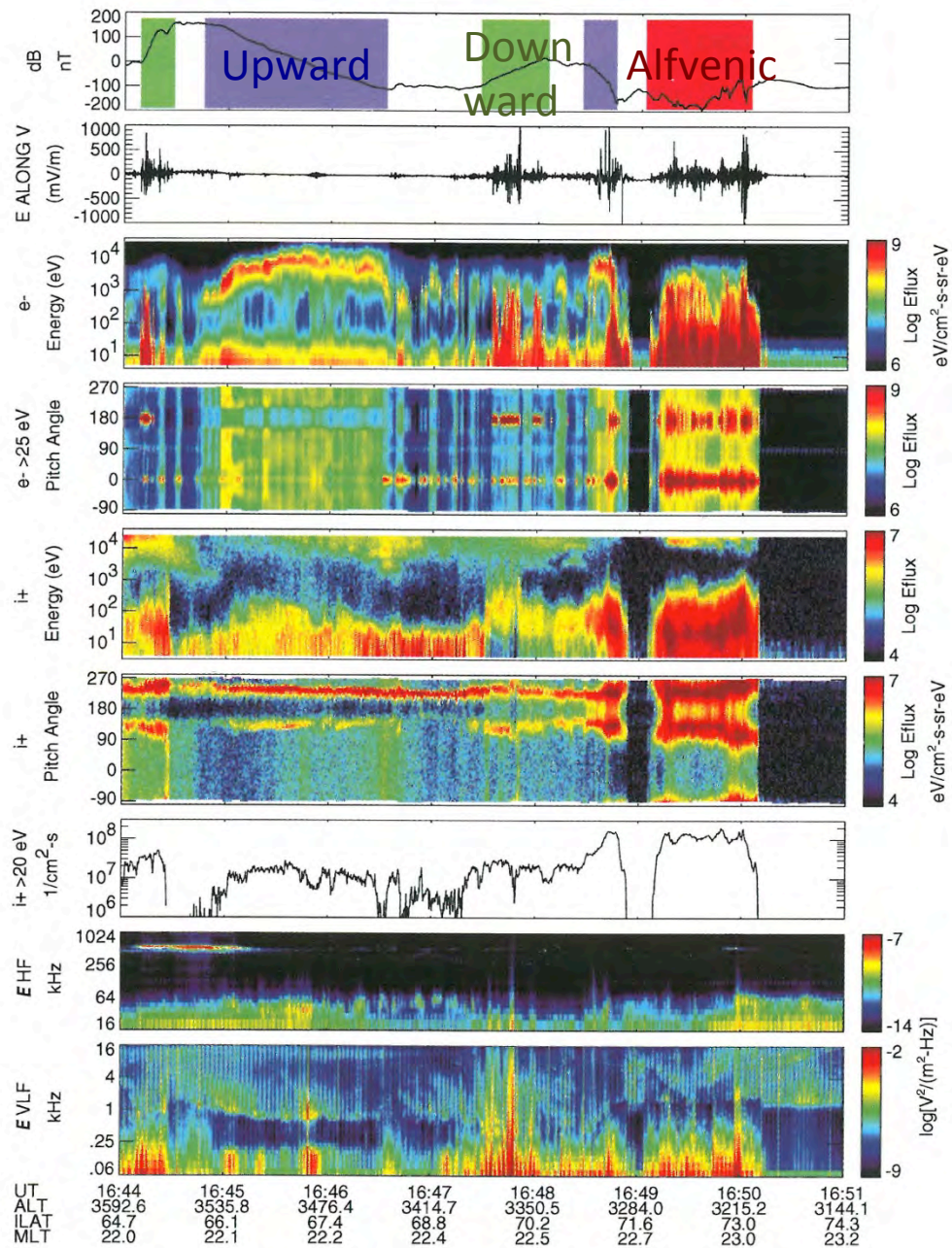


Figure 25: FAST data obtained as the spacecraft passed through the 3 types of coupling regions illustrated in Figure 22. *Below*: UV image of the aurora taken by the Polar satellite. The projection of the FAST trajectory shows the spacecraft crossing the night side auroral region. From Paschmann et al. (2002)

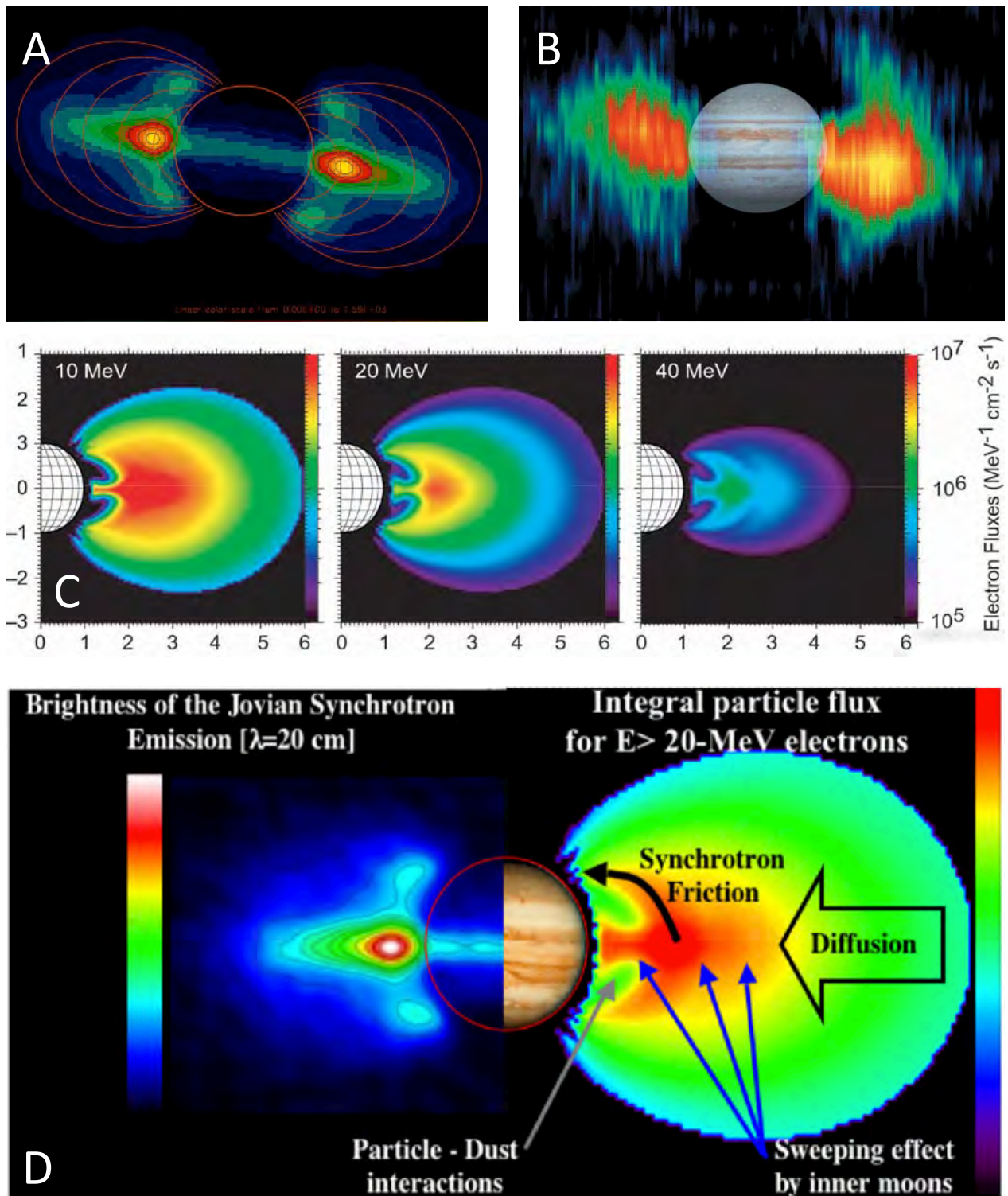


Figure 26: Jupiter's synchrotron/radiation belts. Images of radio emission at (A) 1400 MHz obtained by the VLA; (B) 13.8 GHz obtained by the *Cassini* spacecraft (From Bolton et al. 2004). *Middle:* Models of omni-directional differential electron fluxes in a meridian plane for three energies (from Santos-Costa 2001). *Bottom:* Schematic of electron transport, energization, and loss processes at Jupiter that contribute to the spatial and spectral characteristics of the synchrotron emissions from Jupiter's inner magnetosphere. From Santos-Costa & Bolton (2008).

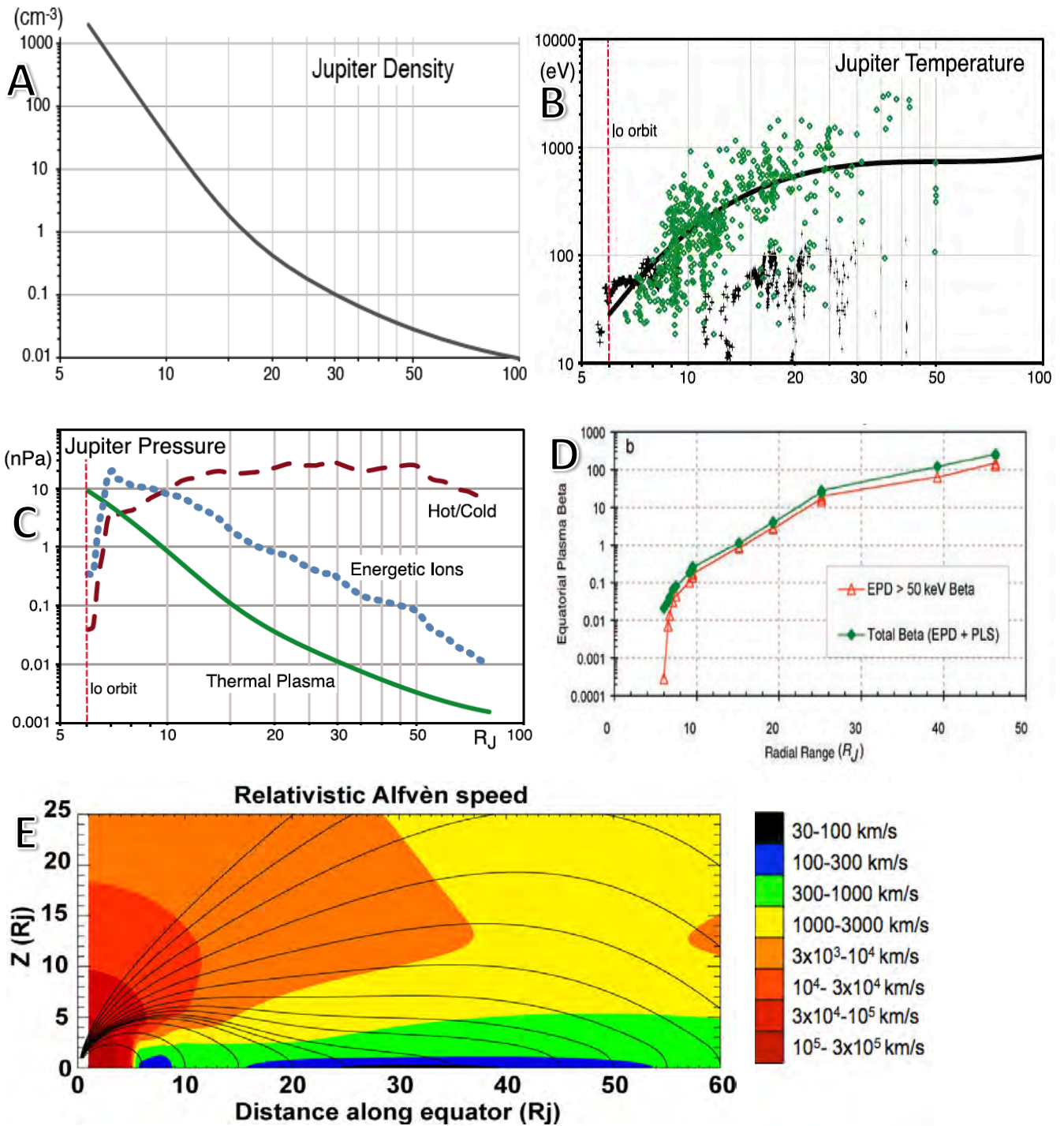


Figure 27: Electron density (A), ion temperature (B), and particle pressure (C), based on *Galileo* and *Voyager* data (Bagenal & Delamere 2011). D shows the ratio of particle pressure to magnetic field pressure (plasma beta) from Mauk et al.(2004). E: By combining mass density and the Connerney (1992) O4+current sheet magnetic field model, a local Alfvén speed can be estimated.

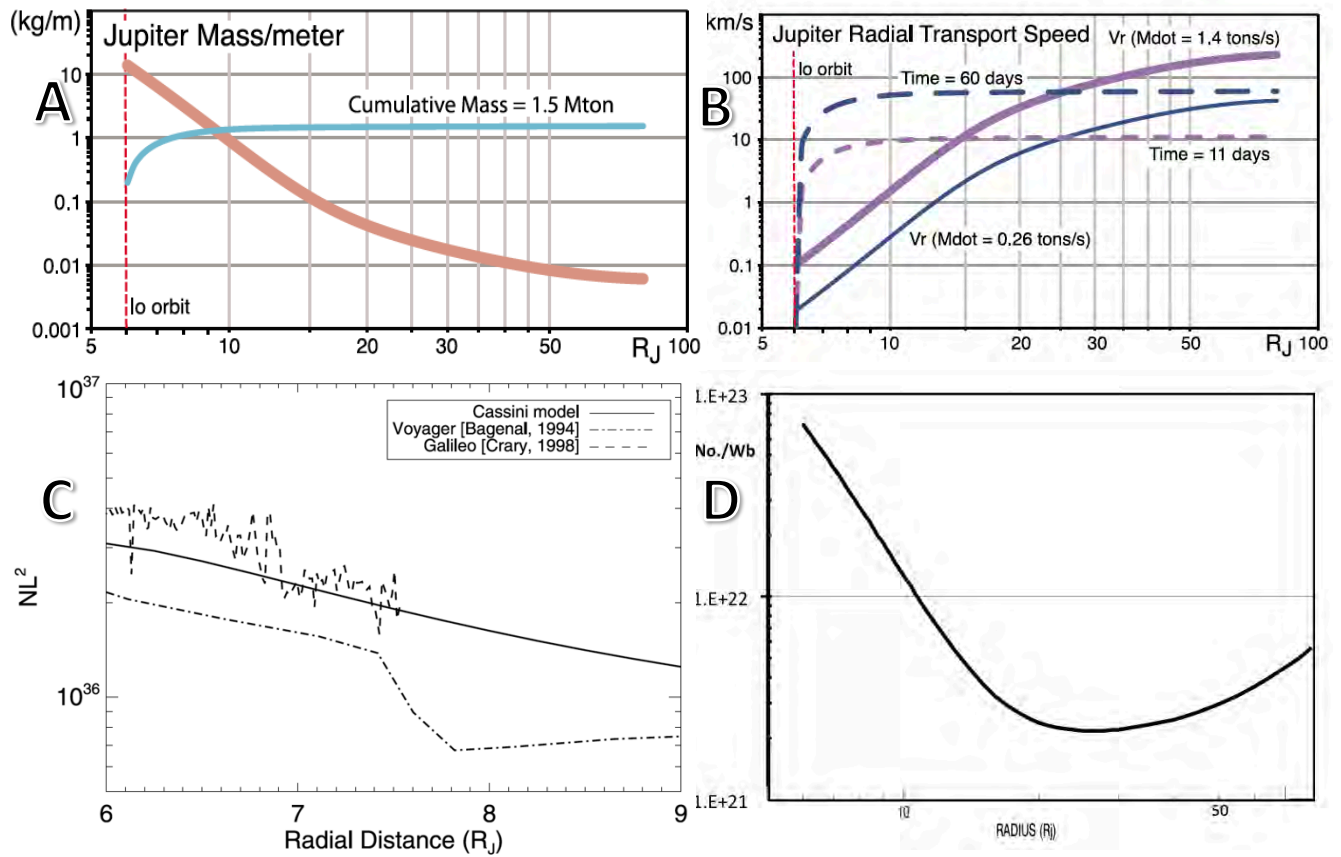


Figure 28: A: Mass per unit radial distance and cumulative mass of the jovian plasma disk (based on the density and temperature profiles in Figure 25 A & B); B: Radial transport speed and cumulative time for radial transport assuming a high (1.4 tons/s) and low (0.26 tons/s) mass transport rate. (Both from Bagenal & Delamere 2011). C: Total flux tube content vs. radial distance based on *Voyager* measurements (Bagenal 1994), *Galileo* data (Crary et al. 1998) and *Cassini* UV emissions (from Delamere et al. 2005). D: Number of electrons per magnetic flux shell vs. distance based on the plot in A.

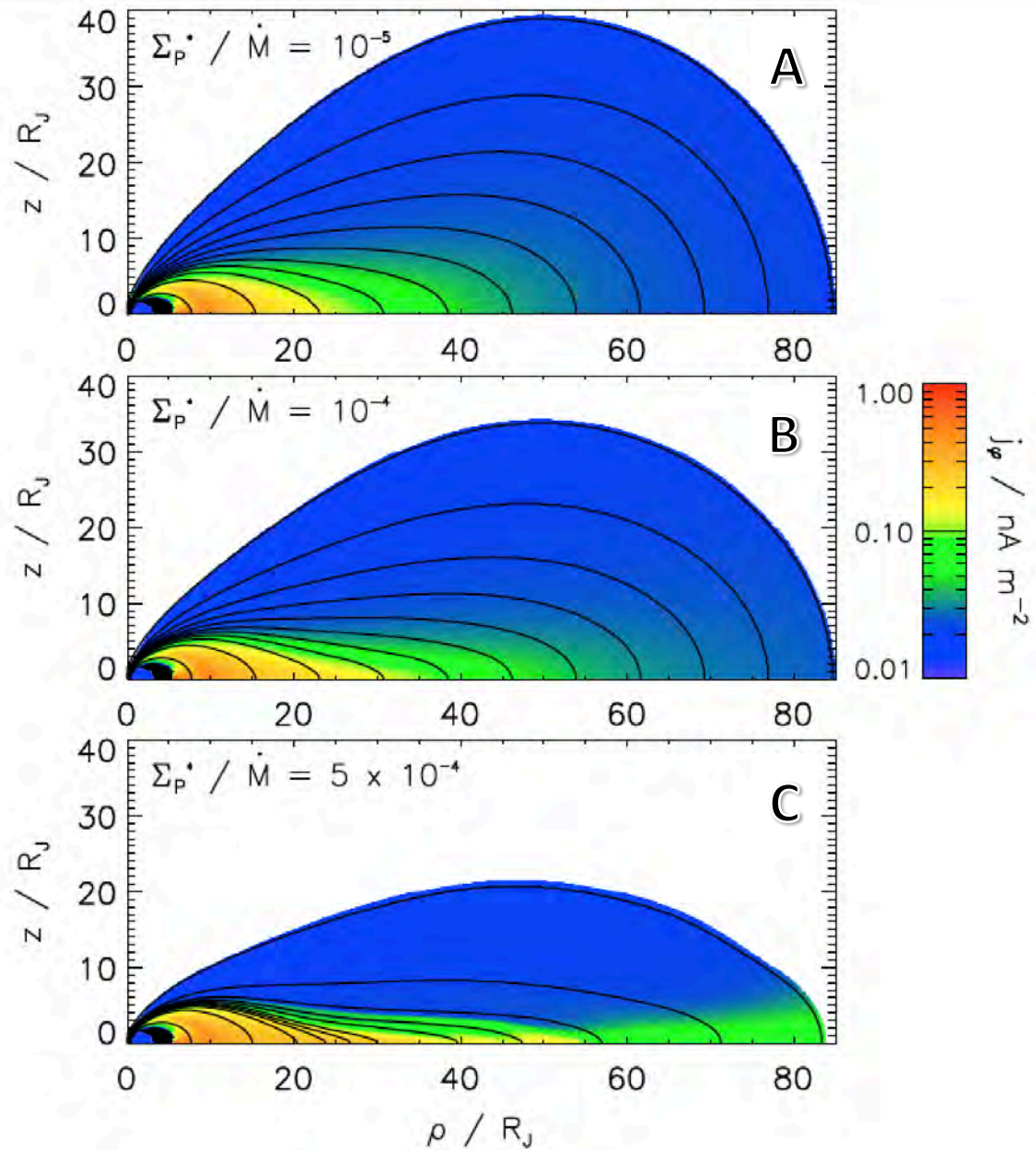


Figure 29: Magnetic field and current sheet structures computed using three values of the quantity (Σ_p^*/\dot{M}) , (A) 10^{-5} , (B) 10^{-4} , and (C) 5×10^{-4} mho s kg^{-1} . The black lines indicate magnetic field lines, and the colors indicate the azimuthal current density \mathbf{j}_ψ (in nA m^{-2}). From Nichols (2011).

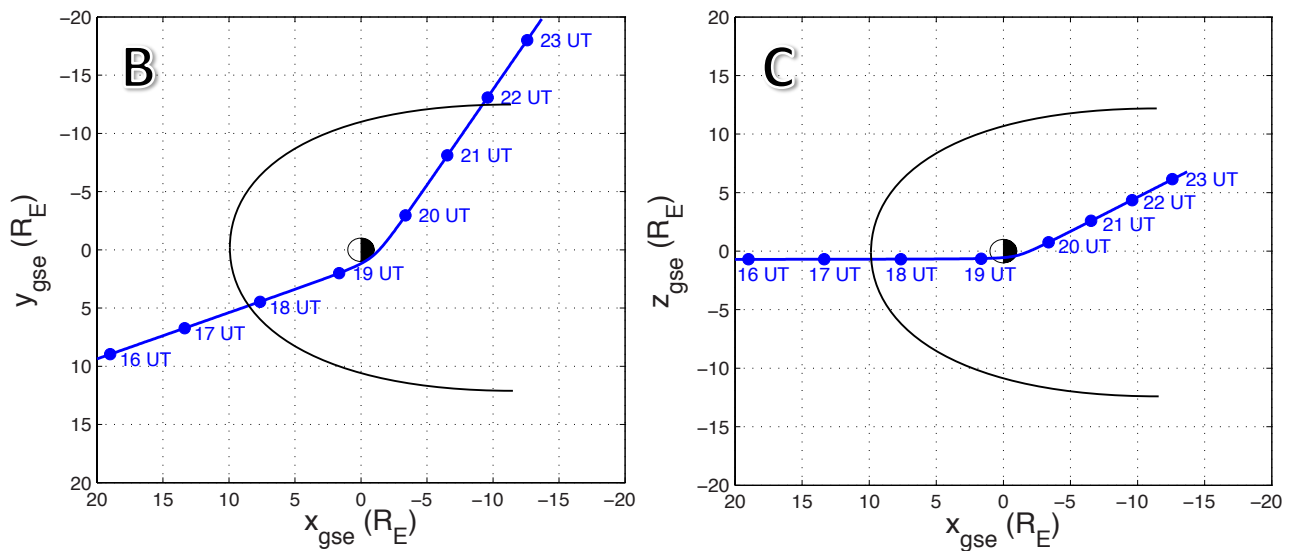
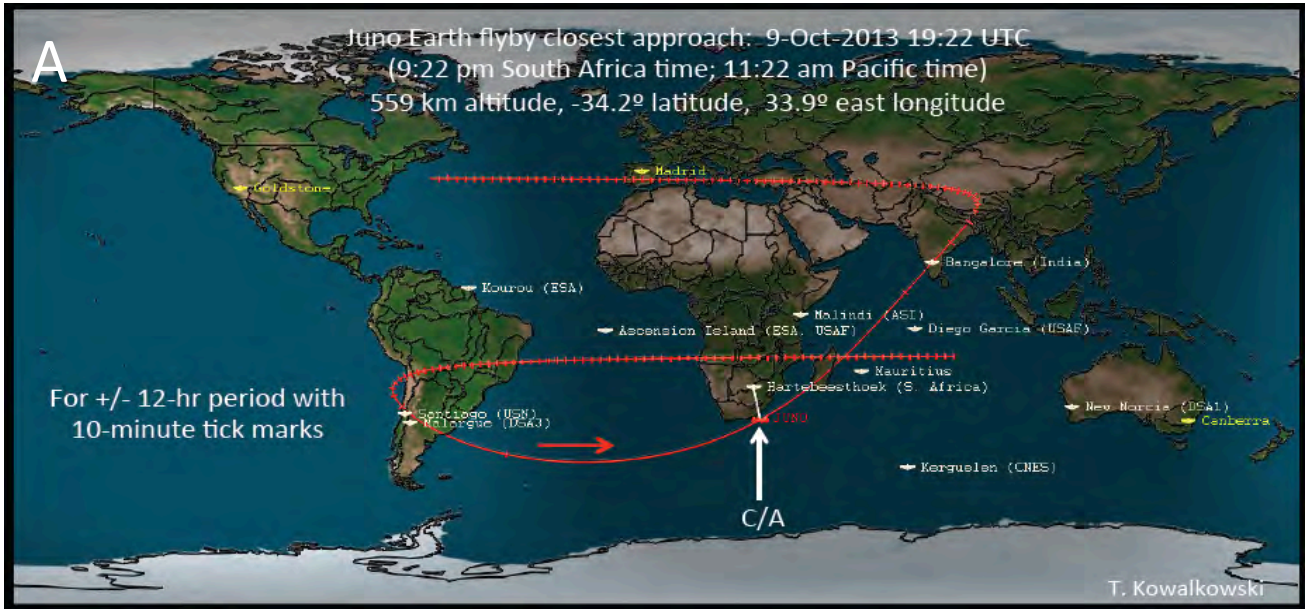


Figure 30: Juno flyby of Earth on October 9, 2013. *Top*: The orbit of *Juno* projected onto the Earth within plus or minus 12 hours of closest approach. *Bottom*: The orbit of *Juno* with markers each hour in Earth solar-ecliptic (GSE) coordinates during passage through the Earth's magnetosphere, in (B) the X-Y plane and (C) the Z-X plane. A nominal average magnetopause boundary with a sub-solar distance of $10 R_E$ is shown to illustrate the brief time spent within the magnetosphere. The location of the sub-solar magnetopause could vary between $6-14 R_E$ dependent on solar wind dynamic pressure at the time of the flyby.

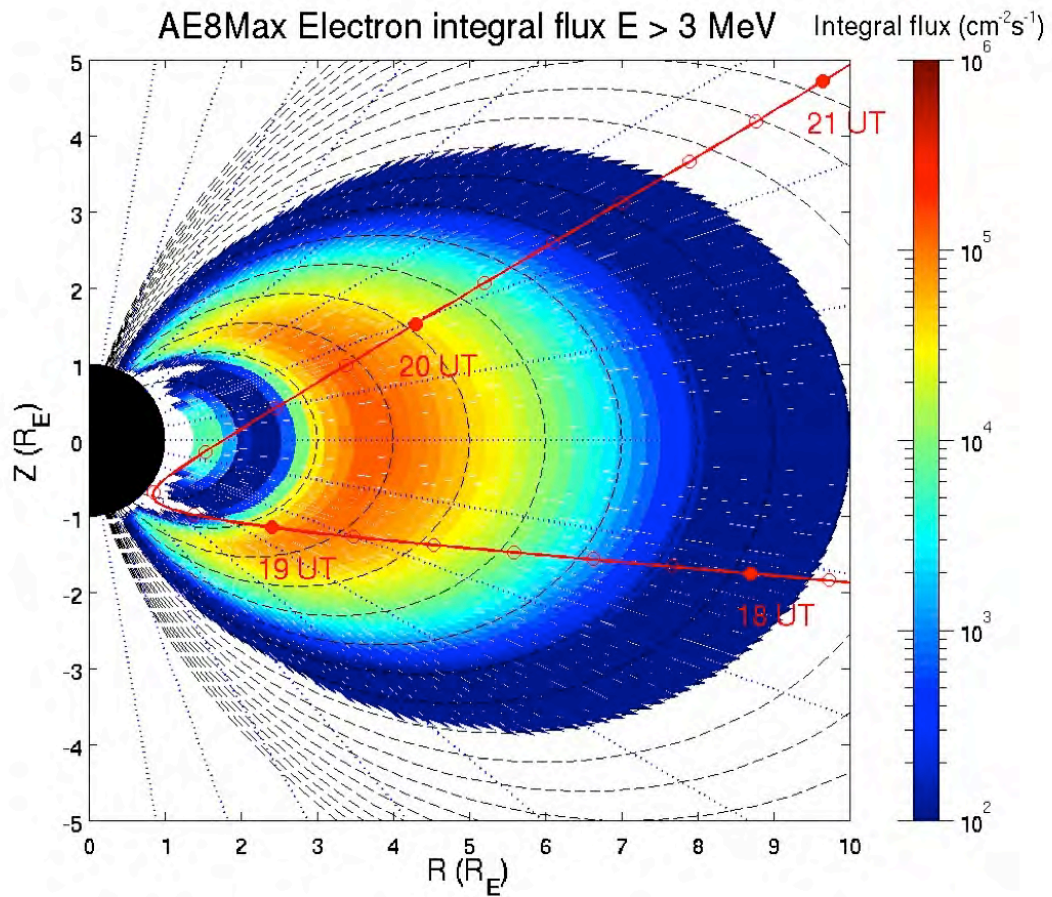


Figure 31: The orbit of *Juno* through the Earth's energetic electron radiation belts (with time markers every 10 minutes) shown in Earth magnetic (GSM) coordinates using the AE8 radiation model. *Juno* will pass through the highly dynamic outer radiation belt between 18:40 - 19:00 UT (dayside) and again on the nightside between 19:45 - 20:10 UT. It will also pass through the inner electron belt and the extremely energetic ion radiation belt around 19:30 UT.

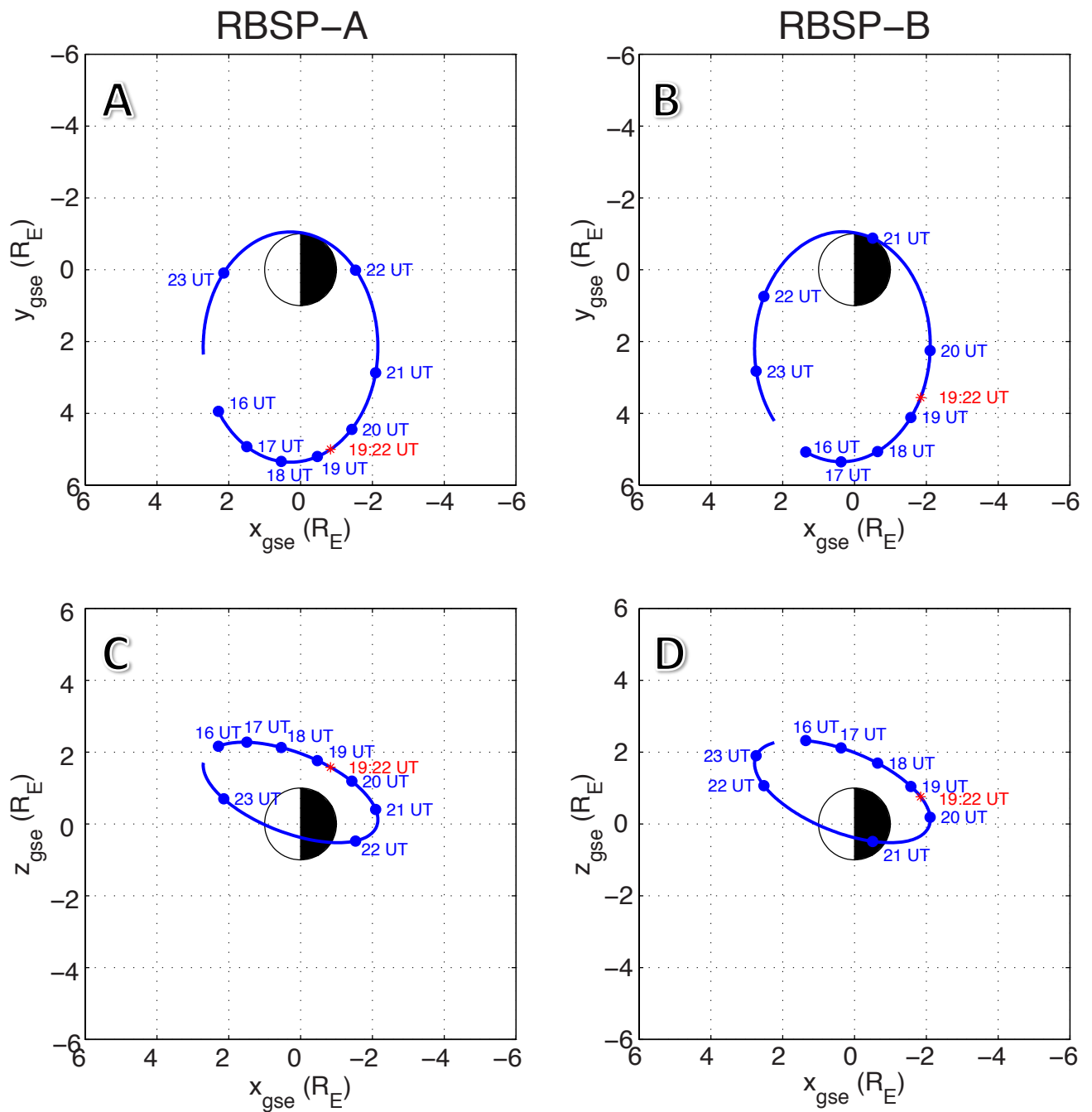


Figure 32: The orbits of the two *Van Allen Probes* within ± 3 hours of closest approach of the *Juno* spacecraft to the Earth (at the time shown in red). A & B are looking down on the ecliptic plane. C & D are looking from the dusk terminator.